



Eidgenössische Technische Hochschule Zürich
Swiss Federal Institute of Technology Zurich



Investigation of scale-up and techno-economic potential of VPSA technology for single cycle H₂ and CO₂ purification

Energy department
Master's Degree in Energy and Nuclear Engineering
Master Thesis

Beatrice Cordiano

September 2, 2019

Examiner:

Prof. Dr. Massimo Santarelli

Supervision:

Prof. Dr. Marco Mazzotti

Dr. Mijndert van der Spek

Anne Streb

Submitted on September 2, 2019 to the Department of Energy at Politecnico di Torino in partial fulfillment of the requirements of the Department of Mechanical and Process Engineering at ETH Zurich.

Abstract

This study investigates the potential of a Vacuum Pressure Swing Adsorption (VPSA) process that produces high purity streams of H_2 and CO_2 , with high recovery for both, starting from syngas (mainly hydrogen, carbon dioxide and impurities such as methane, carbon monoxide and nitrogen).

The goal of the work is twofold: on the one hand, the scale-up of the VPSA technology is investigated for single cycle H_2 and CO_2 purification processes to test its effect on technical performances; on the other hand, the scaled process is evaluated from an economic perspective. Concerning the technology scale-up, the analysis starts from a process which is currently operated at the lab-pilot scale and whose key performance indicators are well defined. However, going from laboratory to commercial scale implies a series of technical challenges, including longer step times, larger volumes, lower overall velocities. A method based on a simplified process model complemented with detailed process simulations is applied to perform the upscaling of (i) a simple Skarstrom cycle, (ii) a simplified VPSA cycle, and (iii) a complete VPSA cycle for hydrogen production and CO_2 capture. The techno-economic assessment of the underlying processes is carried out based on a bottom-up approach, which leads to the definition of the technology development cycle. The costs will initially increase until the first (demonstration/ commercial) plant is built (FOAK, First Of A Kind): here both technological and scientific developments play an important role and have to be carefully considered. A reduction of the overall costs will then occur due to learning pathways and replication effects, until the features of the so-called N-th of a kind (NOAK) plant will be finally achieved.

Acknowledgements

Eccoci qui.

Finalmente ho raggiunto questo traguardo importante, traguardo scalato, traguardo sofferto, traguardo che ha chiesto tanto e che, cosa più importante, ha dato altrettanto. Ora, a percorso concluso, mi fermo e mi guardo indietro con cuore contento e leggero, e ripenso a quante persone ho incontrato in questi anni di università: a chi c'è sempre stato, a chi è passato e ha lasciato qualcosa, a chi invece ho scoperto all'improvviso.

Vorrei come prima cosa ringraziare la mia famiglia, che sempre mi ha sostenuto e motivato, che ha creduto in me e che mi è stata vicina in ogni decisione. Grazie mamma per avermi insegnato a lanciarmi sempre in ciò che mi piace, a prendere al volo le opportunità e a circondarmi di persone vere. Grazie a te, papà, per avermi trasmesso la costanza, la fermezza degli ideali e per avermi fatto capire che ogni tanto bisogna lasciarsi aiutare. Grazie Sandrina per essere stata la mia confidente, la mia supporter e per esser sempre stata pronta a condividere pensieri ed emozioni.

Vorrei ringraziare Andrea, un po' per tutto: per avermi motivata, per avermi dato la forza di affrontare le difficoltà, per avermi insegnato che le emozioni forti vanno condivise e per aver ripulato la mia idea di distanza.

Ringrazio Giuli, Lelli, Tea ed Ele, amiche storiche, per esserci sempre state, per avermi accompagnata dalla quarta ginnasio ad oggi in tutto il percorso scolastico e, per fortuna, anche in quello non scolastico. E' bello sapere di poter contare su di voi e di sapere che sarete sempre "casa".

Un anno fa partivo per Zurigo, felice di cambiare aria, un po' spaventata di cosa mi aspettasse, motivata a fare ricerca su qualcosa in cui credevo e in cui oggi credo ancora più fermamente. Sono stati sette mesi intensi, faticosi e bellissimi. E' stata una boccata di aria fresca, di quella frizzante che si respira la mattina in montagna.

Lì ho conosciuto mille persone. Ho riscoperto Anni, amica di una vita. Grazie a te, che mi hai insegnato cos'è la leggerezza e che mi sei stata affianco in ogni momento. Voglio ringraziare Rami e Davide, due punti di riferimento, due amici con la A maiuscola. Un ringraziamento va a tutti i ragazzi del laboratorio, ognuno dei quali mi ha lasciato un po' di se stesso: a Stewie e Paolo, che mi hanno sostenuta con le loro idee, a Mijndert e Anne, supervisors precisi e da cui ho imparato molto.

Vorrei infine ringraziare Marco, che stimo e ammiro, persona fondamentale senza cui non si sarebbe potuta realizzare questa incredibile esperienza: grazie innanzitutto per avermi dato l'opportunità di lavorare a questo progetto in un ambiente stimolante come l'ETH, grazie per avermi insegnato a non accontentarmi e a cercare sempre più a fondo, per avermi trasmesso la passione per la ricerca e per

avermi fatto capire che ogni cosa va osservata con attenzione fino al più piccolo dettaglio. Grazie a te e Mietta, per essere stati ed essere tuttora famiglia. Grazie a tutti voi che siete qui oggi. Dage, come direbbe Ramona!

Beatrice

Contents

1	Introduction	1
1.1	Global warming and the 2 °C target	1
1.2	The role of Hydrogen in enabling a low-carbon economy	4
1.3	Research goal	5
1.3.1	Hydrogen production by Steam Methane Reformer (SMR)	6
1.3.2	State-of-the-art technologies for CO ₂ separation	7
1.4	Vacuum Pressure Swing Adsorption technology	10
1.4.1	VPSA cycle	10
1.4.2	Performance requirements	13
1.5	Adsorbent selection	14
2	Technical analysis of Pressure Swing Adsorption processes	17
2.1	Existing scale-up methodologies	17
2.1.1	Equilibrium theory	17
2.1.2	A methodology proposed by Rota and Wankat	22
2.2	Developed scale-up method for a simple PSA	25
2.2.1	Equilibrium theory based constraints	25
2.2.2	Towards non-linear isotherms: Henry’s coefficient limitations	27
2.2.3	FAST: full physical mathematical modelling	32
2.2.4	Skarstrom cycle scale-up	38
2.3	Simple VPSA	38
2.3.1	Equilibrium theory based constraints	40
2.3.2	FAST: full physical mathematical modelling	45
2.3.3	Technical scale-up challenges	48
2.4	Full VPSA	53
3	Design and sizing of a VPSA plant	58
3.1	Overdesign and safety margins	60
3.2	Adsorption column design	62
3.3	Intermediate storage tanks design	65
3.4	Waste buffer tank design	71
3.5	Piping and valves system design	72
3.6	Vacuum pumps design	75

4	Economic analysis of low TRL vacuum pressure swing adsorption technology based plant	76
4.1	Exponent method versus factoring approach	76
4.2	Uncertainties in CCS cost estimate	78
4.3	Cost estimate	79
5	Conclusions and outlooks	84

List of Figures

1.1	Observed global temperature change and modeled responses to stylized anthropogenic emission and forcing pathways [1].	1
1.2	Time series of annual emission according to scenarios and modeling simulation in IPCC AR5 [2].	2
1.3	Elegancy project - Enabling a low-carbon economy via Hydrogen and Carbon Capture and Storage [4].	4
1.4	Elegancy project - work breakdown structure [4].	5
1.5	Base Case – SMR hydrogen production without carbon capture, where CWR and CWS are the heated and the cooled water respectively and HT is the High Temperature water gas shift reactor [7].	6
1.6	Main steps for a typical hydrogen production process from natural gas through steam reforming including three different location where the CO ₂ could be captured [6].	7
1.7	Comparison of the different solutions for CO ₂ capture in terms of carbon dioxide avoided and capital costs [5].	9
1.8	Comparison of the different solutions for CO ₂ capture in terms of cost per carbon dioxide avoided and levelized cost of hydrogen [5].	9
1.9	Base cycle for a VPSA technology.	12
1.10	Single component adsorption isotherms at 35 °C for zeolite 13X [5].	16
2.1	Skarstrom cycle.	18
2.2	PSA unit. Operating modus 1 and 2 show the half cycles composed of the pressurization and feed step, and the blowdown and purge steps, respectively [8].	18
2.3	Section of a PSA column [8].	19
2.4	Solute movement theory for PSA (dotted broken lines between points 0 and z ₁ and z ₂ and z ₃ indicate that the exact path is not known) [8].	21
2.5	Typical profiles of column length, particle diameter and adsorbent productivity ratios as a function of the cycle time ratio.	25
2.6	Equilibrium theory constraints for linear isotherm and Skarstrom cycle.	27

2.7	Adsorption isotherms on pelletized zeolite 13X: (a) CO ₂ , (b) CO, (c) N ₂ , (d) CH ₄ (circle, T = 293 K; up pointing triangle, T = 308 K; square, T = 323 K; black symbol, Park et al. [10]; green symbol, T = 323 K, Cavenati et al. [13]; red symbol, T = 323 K, Wang et al. [12]; blue symbol, T = 293 K, Park et al. [11]; spaced n-dash lines with single dot, Langmuir model; spaced n-dash lines with double dot, Sips model; straight lines, temperature-dependent Sips model). (For interpretation of the references to colour in this figure legend, the reader is referred to the web version of [10].) . . .	28
2.8	Langmuir and Sips adsorption isotherms and relative error with respect to experimental data.	29
2.9	Different linearizations of Sips adsorption isotherm.	30
2.10	Operating window for different linearizations: linearization 1 (left), linearization 2 (right)	31
2.11	Results of full physical model applied to a simple Skarstrom cycle	34
2.12	Temperature profiles within the adsorption bed for different recycle ratios (0.2, 0.7, 0.85).	35
2.13	Recoveries and productivities for hydrogen purities higher than 99.9%, Skarstrom cycle.	36
2.14	Purities and productivities for different value of m_{feed} , Skarstrom cycle.	37
2.15	Simple Vacuum Pressure Swing Adsorption unit.	39
2.16	Equilibrium theory constraints for linear isotherm and simple Vacuum Pressure Swing Adsorption cycle.	43
2.17	Operating envelope for a simple Vacuum Pressure Swing Adsorption cycle	44
2.18	Results of full physical model applied to a simple VPSA cycle	45
2.19	Integration of analytical constraints and full physical model results	46
2.20	Products purities, productivities and recoveries for a simple VPSA	47
2.21	Dimensionless concentration profiles for old and new configurations	49
2.22	Pressure profiles for old and new configurations	51
2.23	Results of full physical model applied to a simple VPSA cycle	54
2.24	Optimization results and reference starting point for the full VPSA upscaling.	55
2.25	Key performance indicators for a full VPSA	56
3.1	10 columns scheduling.	59
3.2	16 columns scheduling.	59
3.3	P&ID of a 10 columns adsorption plant for hydrogen production and carbon capture.	61
3.4	Adsorption vessel internals. [15]	64
3.5	Graphic representation of the streams entering and exiting the intermediate storage tanks.	65

3.6	Hydrogen intermediate storage tank, case with 10 columns.	67
3.7	Carbon dioxide intermediate storage tank, case with 10 columns. . .	68
3.8	Molar flowrate inside the storage tank, case with 16 columns. . . .	69
3.9	Number of moles inside the storage tank, case with 16 columns. . .	70
3.10	P&ID of one adsorption column.	72
3.11	Columns and trains disposition top view.	73
4.1	Typical capital cost trend of a new technology. White arrows show the direct and indirect/hybrid approaches to estimate the NOAK capital costs of a new technology.[18]	77
4.2	Capital cost estimate (CAPEX) levels and their elements.[21] . . .	79
4.3	Bare erected cost composition.	80
4.4	Capital cost trend from TRL 3-4 to TRL 8.	83

List of Tables

1.1	Sips isotherm parameters for $T=308$ K, average heats of adsorption and LDF coefficients for CO_2 , CO , N_2 , CH_4 and H_2 on zeolite 13X [6], [10].	15
2.1	Bed properties and process input data for simulations	30
2.2	Minimum column length dependence on the chosen linearization	31
2.3	Input data for the modeling of a simple Skarstrom cycle	33
2.4	Skarstrom cycle scale-up, $m_{\text{feed}}=2.97$, $m_{\text{purge}}=4.09$	38
2.5	Scale-up inconsistencies.	48
2.6	Scale-up results when longer blowdown times are set.	51
2.7	Most relevant inputs to simulations of simple VPSA cycle.	52
2.8	Scale-up results when longer blowdown times are set and the particle size d_p is changed accordingly.	53
2.9	Full VPSA feed stream composition	53
2.10	Scale-up results for a full cycle VPSA.	57
3.1	Considered plant configurations.	58
3.2	Adsorbent bed diameter assuming a single train.	63
3.3	Different configurations for the economic assessment	64
3.4	Design of the two intermediate storage tanks, 10 columns scheduling.	71
3.5	Design of the two intermediate storage tanks, 16 columns scheduling.	71
3.6	Design of the waste buffer tank.	71
3.7	Piping lengths (* "All pipes " includes all the listed lines except from the pressure equalization line)	74
3.8	Piping diameters.	74
3.9	Number of ball valves.	74
3.10	Vacuum pumps design. (* This flowrate already includes a margin of 20%, as explained in the paragraph dedicated to overdesign and safety margins)	75
4.1	Bare erected cost.	80
4.2	AACE Guidelines for process contingency. [21]	81
4.3	Engineering, procurement and construction cost.	81
4.4	Learning curve key points.	82
4.5	Adsorbent material and feed stream comparison.	83

Chapter 1

Introduction

1.1 Global warming and the 2 °C target

Socio-economic growth and anthropogenic greenhouse gas emissions seem to be the main factors leading to a substantial increase in pre-industrial temperatures and to severe climate change. Carbon dioxide concentrations in the atmosphere are unprecedented, CO₂ being one of the most relevant greenhouse gases, that intensively contributes to climate change impacting on natural and human systems. A limitation of global warming is clearly needed to avoid irreversible impacts and long-lasting changes on ecosystems; to this end, global warming should be limited to below 2 °C.

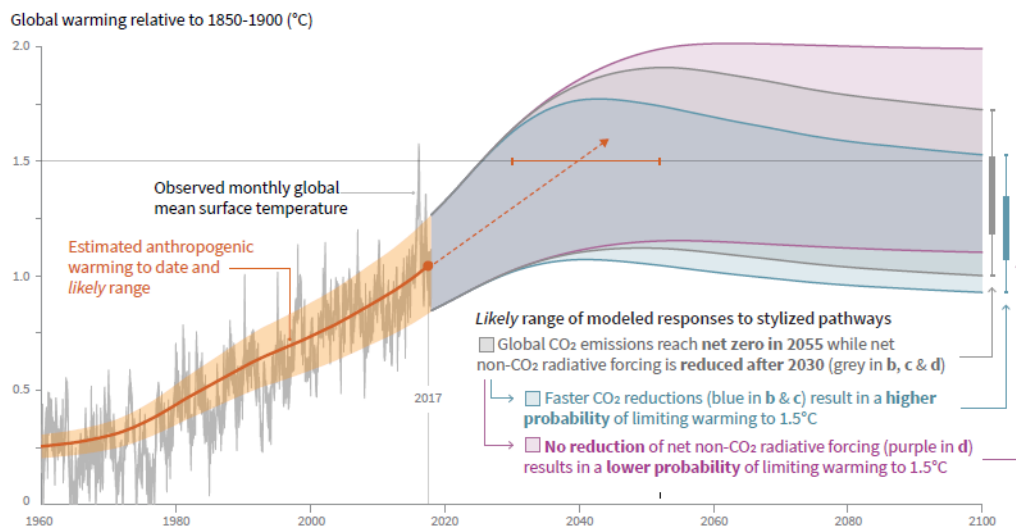


Figure 1.1: Observed global temperature change and modeled responses to stylized anthropogenic emission and forcing pathways [1].

CO₂ emissions derive both from point sources (fossil fuel power plants) and distributed sources (transport and heating). Being quantitatively much higher than the uptakes, they lead to an overall CO₂-positive balance, as shown in Figure 1.1. The same information can be depicted in terms of global emissions instead of temperature; that allows for a better understanding of the possible climate scenarios adopted by the IPCC for climate modeling and research.

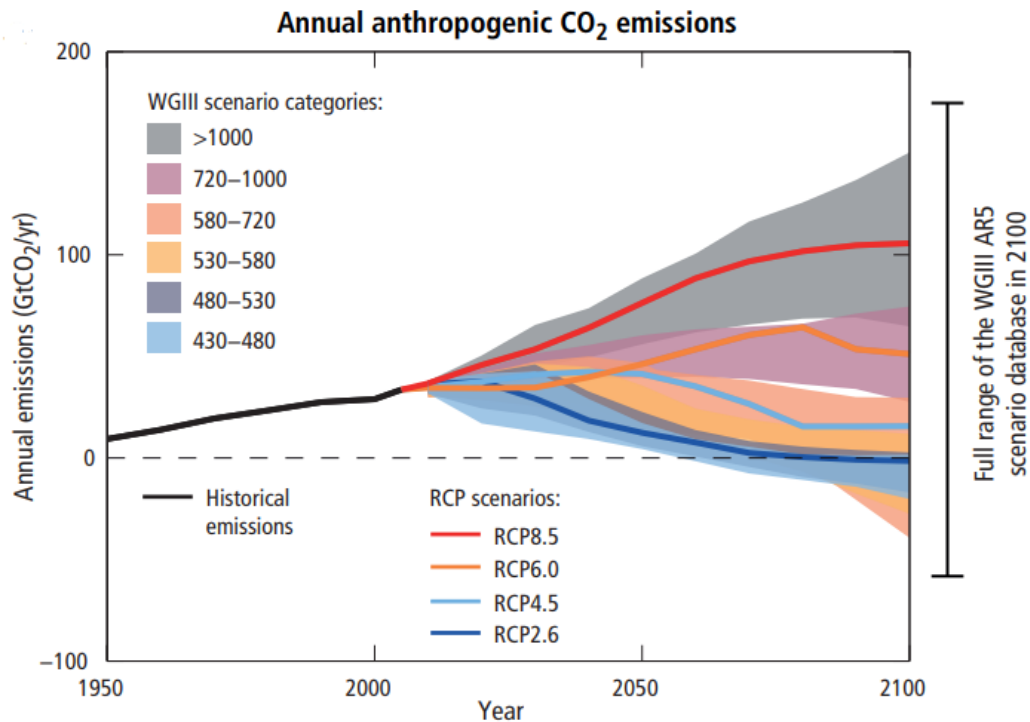


Figure 1.2: Time series of annual emission according to scenarios and modeling simulation in IPCC AR5 [2].

Figure 1.2 shows four representative concentration pathways (RCPs) on the basis of the amount of greenhouse gases emitted in the years to come: RCP 2.6, RCP 4.5, RCP 6.0, RCP 8.5.

The different pathways have been obtained through Integrated Assessment Models (IAMs) and are now used to assess impacts and adaptation measures.

IPCC has provided these projections including a possible stringent scenario aiming to keep global warming below 2 °C with respect to pre-industrial temperature levels, two intermediate trends and one characterized by very high anthropogenic emissions. All baseline scenarios do not foresee efforts to constrain emissions and therefore lead to pathways ranging from RCP 6.0 and RCP 8.5. The latest one is the worst scenario and depicts a future in which no policy changes are

endorsed to reduce greenhouse gases emissions and thus a heavy reliance on fossil fuels together with a high energy intensity will lead to a tripling of CO₂ emissions by 2100. In RCP 6.0 an emissions peak between 2050 and 2100 and a subsequent decline to 25% above today's level, whose causes are represented by stable methane emissions, by an intermediate energy intensity and an increasing use of croplands, are expected. RCP 4.5 is consistent with a future marked by a lower use of croplands and grasslands and a reduced energy intensity, coupled with stringent climate policies which support reforestation programs. Lastly, an increase of bio-energy production, a further decrease in energy intensity and a declining use of oil will lead to a possible low emissions scenario represented by RCP 2.6.

Finding a solution for the avoidance of the net CO₂-positive balance has become a cutting edge challenge for the scientific world and integrating carbon capture and storage (CCS) and carbon capture and utilization (CCU) to already existing power plants seems to play a significant role among the extended possible solutions.

To achieve a low-carbon economy and to limit and contain CO₂ emissions, a transition from fossil fuels to alternative energy sources is needed. Both carbon capture and storage and hydrogen based systems are foreseen to contribute to the deep decarbonization of our economies.

CCS is considered a viable and effective option to lower anthropogenic CO₂ emissions from industries and from heat and electricity generation via fossil fuels; it is thus referred to as an essential component in the vast majority of IPCC scenarios and as a 'bridge' technology for the mid-term mitigation options, long-term solutions being characterised by CCU rather than CCS. Keeping the rise in global temperature within the limits set by the Paris Agreement is expected to be very difficult without it.

CCS has to face three major challenges: first of all, electricity generated with CCS is more expensive than without, therefore the Levelised Cost of Electricity (LCOE) will rise; the second challenge is related to the legal perspective since carbon capture, transportation and injection are regulated by standard industrial norms and long-term storage and the associated liability requires new regulations; last but not least, not only the public perception due to the lack of understanding invisible processes like CO₂ storage and delayed benefit of climate protection but also the perception of conflict between CCS and renewables considerably burden the enhancement of this solution.

As mentioned before, anthropogenic CO₂ emissions strongly depend on both socio-economic development and climate policy; in addition, policy ambitions, technology readiness and deployment are largely detached at the moment. Moreover, reducing plant emissions regrettably comes with a price, which is represented by lower plant efficiency and higher electricity costs. Extensive studies are now under way in order to minimize these drawbacks and assess more efficient technologies in order to safeguard the environment from severe climate change and

reach the CO₂-neutral target [2].

A further progress can be reached by accomplishing a CO₂-negative scenario integrating Direct Air Capture (DAC) or bio-energy production equipped with a carbon capture technology (BECCS). This study goes, though, beyond the scope of the thesis and therefore it will not be taken into account in the following work.

1.2 The role of Hydrogen in enabling a low-carbon economy

The Elegancy project - Enabling a low-carbon economy via Hydrogen and Carbon Capture and Storage - is carried out by five European countries (UK, Switzerland, Norway, Germany and Netherlands) and has the primary objective to fast-track the decarbonization of Europe's energy system by exploiting the joint action of these two technologies [4].

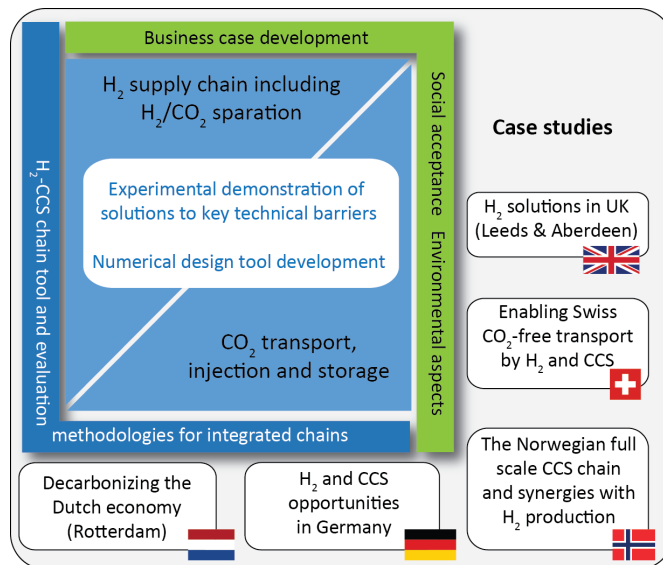


Figure 1.3: Elegancy project - Enabling a low-carbon economy via Hydrogen and Carbon Capture and Storage [4].

Among the multiple objectives are: the development of new carbon capture technologies for hydrogen production from natural gas and biogas, the assessment of their techno-economic-environmental performance and the implementation of a chain tool for the optimal planning of hydrogen networks with CCS. The overall project aims at undertaking country specific case studies to understand how the combination of hydrogen with CCS could play a role in different sectors.

1.3 Research goal

This master thesis will direct particular attention to the WP1, whose aim is to face a major challenge, namely the decarbonization of the transport sector by means of a deep insight into the integration of hydrogen production within the hydrogen supply chain.

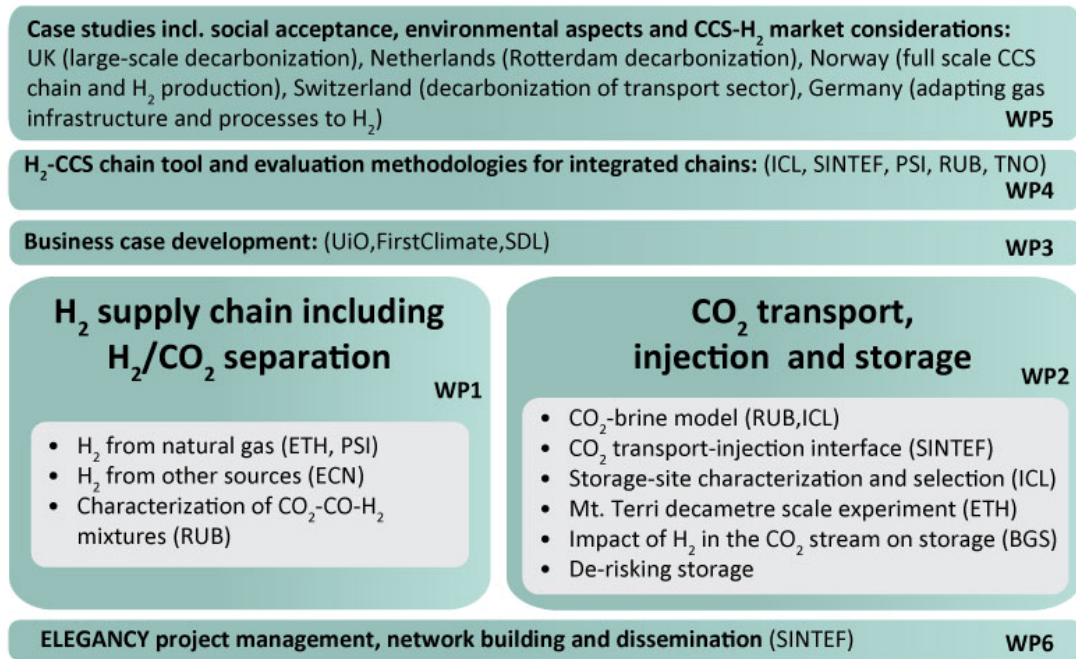


Figure 1.4: Elegancy project - work breakdown structure [4].

The following paragraphs focus on the state-of-the-art technologies for hydrogen production and on the connected limitations, thus showing the need of moving towards more cutting edge processes such as the Vacuum Pressure Swing Adsorption, which might help reduce plant's complexity and costs. The goal of the research is therefore represented by the development and the scale-up of the VPSA technology from TRL 4 to TRL 9 (from lab to future, commercial scale), as well as the performance potential's assessment by means of a techno-economic analysis which will include existing economic uncertainties and that will be provided to WP3, WP4 and WP5 as input for their models, as shown in the work breakdown structure in Figure 1.4.

Coupling CCS with hydrogen production becomes a promising solution to meet the targets set by the Paris Agreement. Furthermore, hydrogen is already used for many purposes, namely oil refining, ammonia and methanol production, and it could play a fundamental role in future energy systems enhancing a deep decarbonization of transport, industry and space heating sectors.

However, the production of H₂ is mainly performed through the conversion of fos-

sil fuels via natural gas reforming or coal gasification followed by water gas shift reactions. These processes are very emission intensive [6]. Therefore, to be viable in a carbon constrained world, the hydrogen should have little associated CO₂ emissions and thus be referred to as "blue" (if originated from the combination of fossil fuels and CCS) or "green" (if generated via electrolysis and renewable energy sources) hydrogen.

1.3.1 Hydrogen production by Steam Methane Reformer (SMR)

In the search of a large scale H₂ production from fossil fuels, the leading technology is currently represented by the steam methane reforming (SMR) plant shown in the image below.

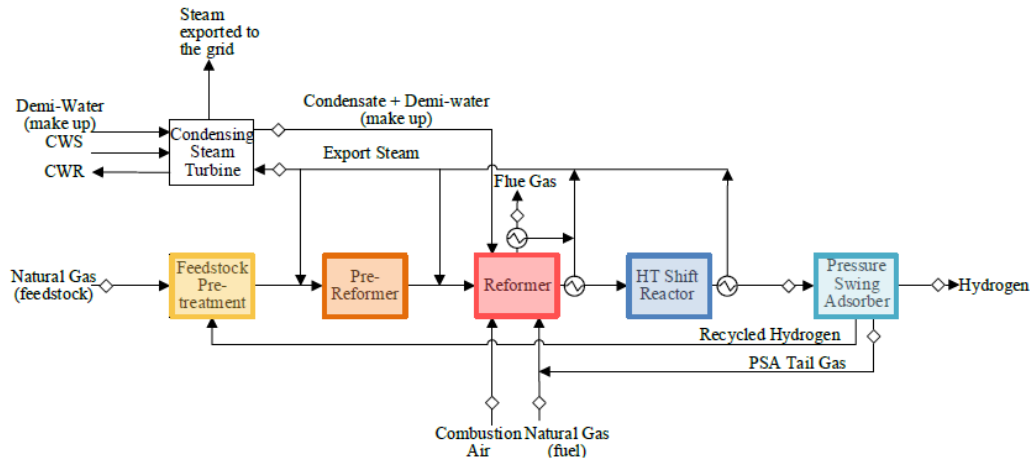


Figure 1.5: Base Case – SMR hydrogen production without carbon capture, where CWR and CWS are the heated and the cooled water respectively and HT is the High Temperature water gas shift reactor [7].

The whole plant consists of three major units, namely a steam reformer, a water-gas shift and a hydrogen purification unit, which fulfill three fundamental process tasks.

As depicted in the graph, the stream of natural gas entering the plant undergoes a pre-treatment aiming to a removal of any sulphur and chlorine present in the feedstock: this step is essential to prevent any poisoning of the catalysts of the downstream processes.

The clean stream is then mixed with process steam and pre-reformed in an adiabatic reactor to convert any light hydrocarbons, mainly C²⁺ and olefins, before being fed in the reformer itself as syngas. The composition of the syngas feed-stream consists mostly of CO₂, H₂, CO, H₂O and residual CH₄ and N₂. The first major step is accomplished within the reformer and has the purpose to convert

methane and superheated steam into hydrogen and carbon monoxide, according to the following endothermic (206 kJ/mol) chemical reaction:



The required energy is provided in form of high temperature (>900 °C) heat by an external furnace combusting a mixture of natural gas, tail gas and pre-heated air. The syngas exiting the reformer is then cooled and fed into the high temperature (>300 °C) shift (HTS) reactor, in which almost all the CO is converted into hydrogen and carbon dioxide making the total H₂ yield rise and the CO concentration drop to 3%.



Adding a low temperature shift (LT-WGS) reactor, higher CO conversion can be achieved, carbon monoxide concentration can fall below 0.5% and the hydrogen content can be increased by around 3 mol%. The third major step consists in purifying the cooled shifted gas in a pressure swing adsorption (PSA) unit, therefore obtaining a very high purity (99.9%) hydrogen product and a tail gas stream consisting of CO₂, CO, CH₄, H₂, N₂ and other impurities [6].

1.3.2 State-of-the-art technologies for CO₂ separation

Currently, the steam methane reformer (SMR) is the leading technology for hydrogen production from natural gas or light hydrocarbons. Although SMR based plants have reached efficiencies able to reduce carbon dioxide emissions down to nearly 10% above its theoretical minimum, a further decrease of emissions from hydrogen production would only be possible by integrating CCS [7].

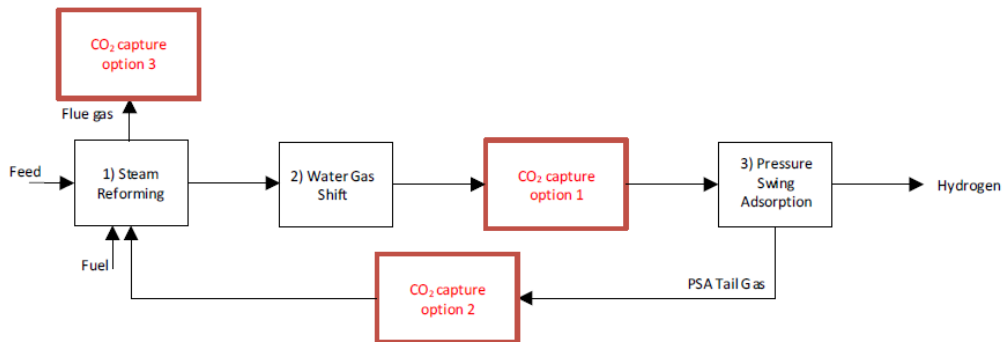


Figure 1.6: Main steps for a typical hydrogen production process from natural gas through steam reforming including three different location where the CO₂ could be captured [6].

Several strategies have been developed to stem greenhouse gases emissions capturing CO₂ from fossil fuel fired power plants: post-combustion, oxy-combustion and pre-combustion capture are the major ones.

Carbon dioxide can be captured at three different locations during the process (see Figure 1.6): after the WGS at intermediate concentration and high pressure (option 1), from the PSA tail gas at high concentration but lower pressure (option 2) e.g. using MDEA or from the flue gas exiting the steam reformer at very low pressure and intermediate concentration (option 3), e.g. using MEA.

In the following graphs a comparison between the aforementioned alternatives for CO₂ capture integration within a hydrogen production plant is shown: the parameters of main interest, namely the amount of CO₂ avoided and the total capital cost as well as the cost per CO₂ avoided and the levelized cost of hydrogen (which we want to be as low as possible), are plotted. In the base case, the cost per CO₂ avoided goes to zero since we do not have any carbon dioxide capture, hence the only aspect we can look at and compare is the capital cost of the plant. In order to capture CO₂ further equipment is required, which guarantees an increase of the percentage of avoided carbon at the expenses of a rise in the total capital cost.

Concerning the ‘pre PSA’ capture option, it shows a comparable amount of carbon captured with respect to the ‘post PSA’ solution: a recovery of 52-53% is achieved due to furnace’s emissions. This solution is easy to implement thanks to the high pressure, moreover it is clearly cost-competitive compared to the other capture options. For these reasons, it seems to be the most promising option from an economic’s perspective if we are willing to accept the limits related to the capture rates.

It is worth noting that in PSA the main contribute to energy requirements is caused by the need of compressing the outlet stream at very high pressures, namely 110 bar, in order to guarantee safe transportation and storage. Furthermore, it is useful to evaluate where the limits of the PSA process arise for the separation of hydrogen and carbon dioxide.

Carbon capture process is driven by performance specifications concerning CO₂ purity and recovery, namely 96% and 90% respectively [6], which do not necessarily lead to optimal economic performance. In fact, to achieve these targets, good alternatives imply the presence of a second adsorption unit or membranes leading to a higher complexity of the plant and thus to additional capital and operational costs.

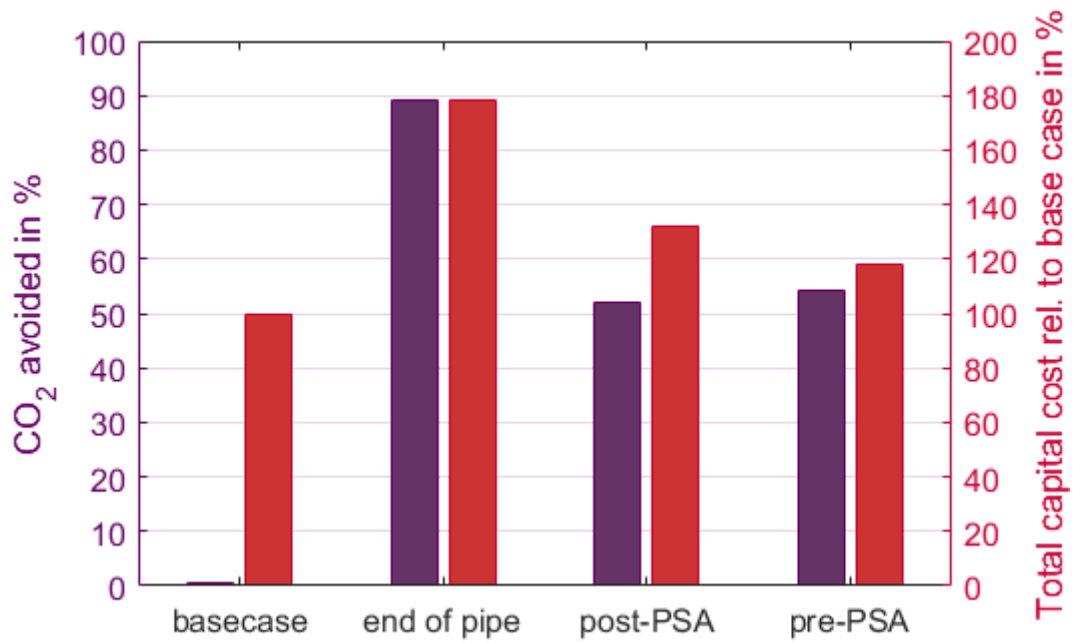


Figure 1.7: Comparison of the different solutions for CO₂ capture in terms of carbon dioxide avoided and capital costs [5].

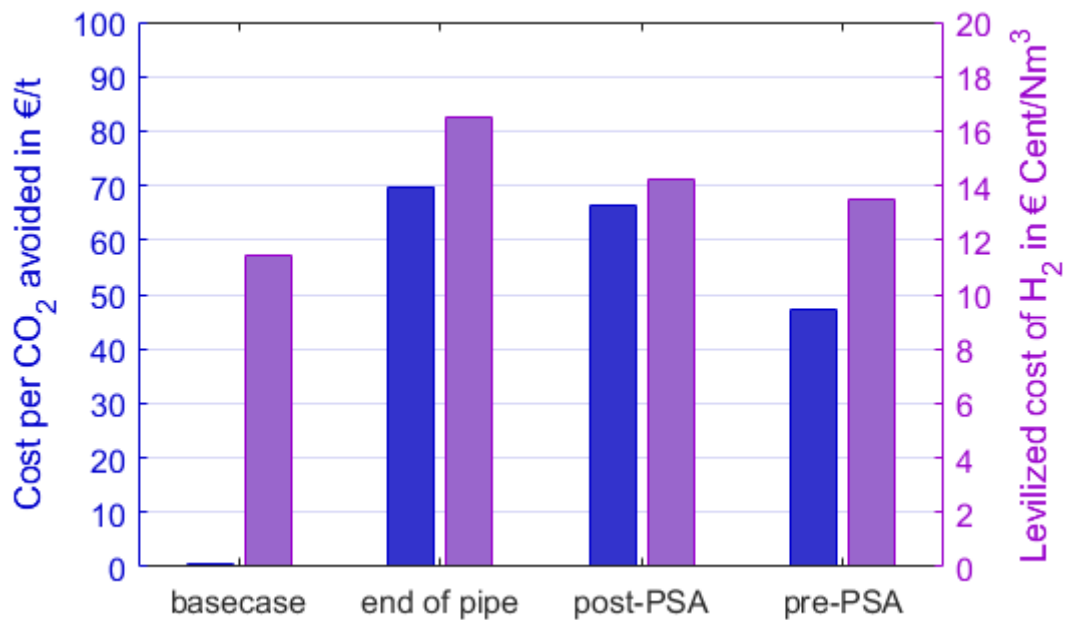


Figure 1.8: Comparison of the different solutions for CO₂ capture in terms of cost per carbon dioxide avoided and levelized cost of hydrogen [5].

1.4 Vacuum Pressure Swing Adsorption technology

The aforementioned state-of-the-art ways to integrate carbon capture within an hydrogen production cycle inevitably lead to high plant complexities.

Vacuum Pressure Swing Adsorption (VPSA) technology might represent an alternative to burden the high costs deriving from additional features needed to fulfill the key performance indicators' requirements for both hydrogen and carbon dioxide. In VPSA systems, hydrogen purification and CO₂ separation are implemented within a single adsorption cycle allowing to avoid any additional separation stage.

The VPSA technology has been so far only tested and modelled at lab scale, reason why this project aims at giving an answer to the following research question: " How can the technology be scaled up to future, commercial sizes and how will its technical and economic performances be affected? ".

1.4.1 VPSA cycle

Figure 1.9 shows a possible configuration of a VPSA cycle, fed with a multicomponent stream, which allows the production of high purity hydrogen and CO₂ with high recoveries. The feed is composed of the two aforementioned components plus impurities like carbon monoxide, methane and nitrogen. Starting from the left, four main characteristic steps are encountered, namely the pressurization (Press) , the adsorption (Ads), the blowdown (BD) and the purge (P), which are interspersed with as many pressurization steps (PE) as necessary to increase the performance and to ensure continuous feed and production.

First of all, the column is pressurized with a high purity H₂ split stream that follows a top-to-bottom direction and cleans the column top end. During the high pressure adsorption (around 25 bar), the column is fed with the multicomponent stream from the bottom. During this step high purity hydrogen is produced and all the impurities are retained within the column. The adsorbent at the column inlet becomes saturated with impurities, which propagate through the column as the step goes on. The adsorption step is stopped before the leading impurity front reaches the column top. A split stream of the pure product is used to perform a pressurization from the top (Press) and another part is used for the subsequent purges (LPtoHP, LPtoW3).

The pressure within the column is then decreased by means of three PE steps in which the column is directly connected with a second, low pressure column. The outflow has a high content of hydrogen and same impurities and is used to co-currently re-pressurize another column after the light purge (LP) step.

The column then undergoes an intermediate blowdown step to ambient pressure, to obtain the most favorable conditions for the purge with heavy product (CO₂).

The outlet consists of hydrogen, impurities and little to no CO₂.

Since the VPSA is designed to co-produce high purity CO₂, a bottom-to-top purge with a carbon dioxide-rich stream (HP) is required to further increase the CO₂ content within the column and therefore the purity of the CO₂ product that can be withdrawn subsequently. A recirculated stream of high purity CO₂ from the next two steps is fed to the bottom of the column: it replaces the void gas and pushes the impurities towards the top end of the column. The outlet stream (waste 2) is composed mainly of impurities with little carbon dioxide, because of the difference in front velocity.

It is worth noting that longer purge times lead to higher losses in CO₂.

After the heavy purge step, carbon dioxide is withdrawn at high purity: drawing a vacuum from the bottom of the column becomes of remarkable importance to enable the CO₂ production and to improve the process' cyclic capacity. A split stream of the CO₂ product is used, as mentioned before, to purge the column in the previous step. The BD-vac step is followed by two counter-current light product purges, with the goal to clean the column top end by removing CO₂ and impurities thereby increasing hydrogen purity and to recover additional carbon dioxide. The column is repressurized in a series of pressure equalization steps using part of the hydrogen product and finally is ready to restart the cycle.

To summarize: in order to fulfill all the separation requirements, three main cycle characteristics are necessary:

- a purge with the heavy product
- a vacuum for carbon dioxide withdrawal
- a waste stream with high impurities but very low H₂ and CO₂ contents

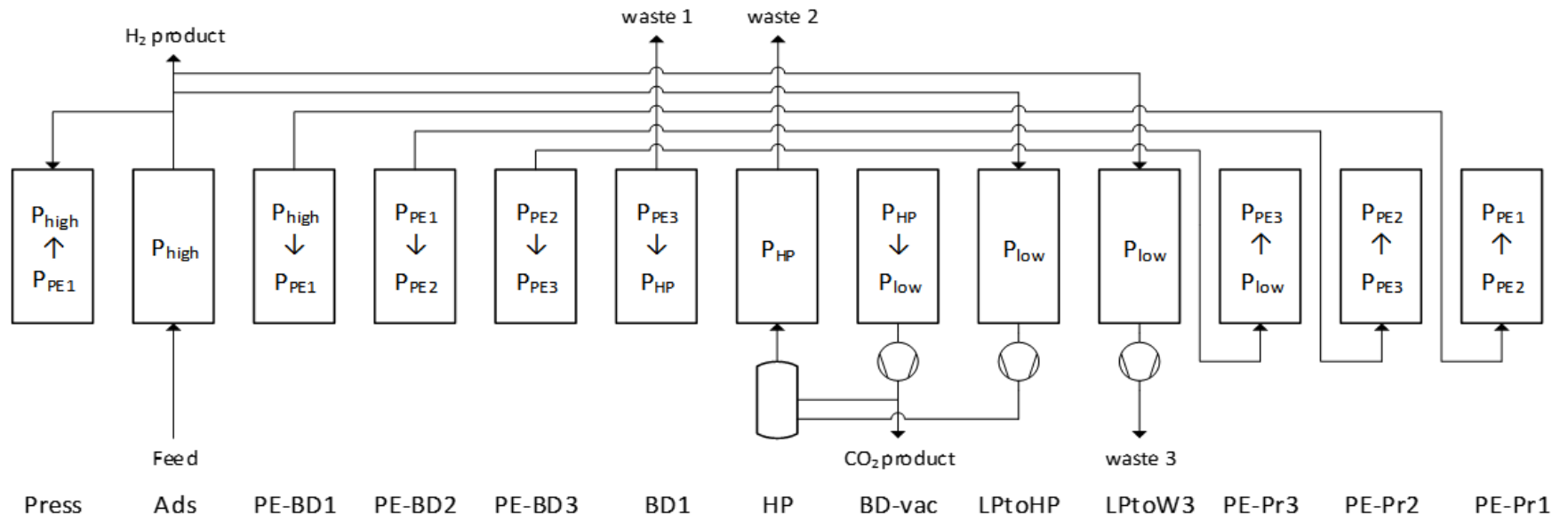


Figure 1.9: Base cycle for a VPSA technology.

1.4.2 Performance requirements

The main difference between PSA and VPSA is represented by the presence of a vacuum pump, which is a component of fundamental importance in order to provide sub-atmospheric pressure for the CO₂ withdrawal, and two storage tanks allowing for different time of the steps.

The energy required for the vacuum pump has to be taken into consideration for evaluating the cycle performance. The specific energy consumption (e) accounts for the electric energy consumption per unit mass of CO₂ produced:

$$e = \frac{e_{\text{vac}}}{n_{\text{CO}_2, \text{Prod}} M_{\text{w}, \text{CO}_2}} \quad (1.3)$$

where:

- n is the molar amount in mol
- M_{w} is the molar weight

Capital and operational costs are described through another reference parameter, namely the productivity (AP), which is defined as the ratio between the product molar flow and the unit mass of adsorbent (product of the bulk density and the column volume).

$$\text{AP} = \frac{n_{\text{Prod}}}{t_{\text{cycle}} \rho_{\text{b}} V_{\text{col}}} \quad (1.4)$$

where:

- t_{cycle} is the cycle duration
- ρ_{b} is the density of the adsorbent bed
- V_{col} is the volume of the column

Considering both hydrogen and carbon dioxide as products, it is necessary to define the performance parameters that will be considered in this research. Important indicators are typically H₂ and CO₂ purities (Φ) and recoveries (r), which are defined as follows and whose mathematical expressions refer to i as the component of interest.

$$\Phi_i = \frac{n_{i, \text{Prod}_j}}{n_{\text{tot}, \text{Prod}_j}} \quad (1.5)$$

$$r_i = \frac{n_{i, \text{Prod}_j}}{n_{i, \text{Prod}}} \quad (1.6)$$

Hydrogen purity requirement is strongly dependent on the application of interest and the purification process must stick to these constraints: the highest

purities are necessary for PEM fuel cells for automotive purposes (99.97%) and for stationary purposes or industrial fuels (99.90%) [6].

The cycle should guarantee a carbon dioxide recovery higher than 90% and a purity that depends on transportation and storage/utilization and which is typically greater than 96%.

1.5 Adsorbent selection

The selection of a suitable adsorbent is of fundamental importance in the optimization of PSA processes.

To produce high purity H₂ and CO₂ streams, it is necessary to look for an adsorbent material which presents the characteristics listed below:

- the material should present a high selectivity of carbon dioxide and impurities over hydrogen so that during the adsorption step they are retained within the adsorbent material and pure hydrogen can leave the column
- the adsorbent should show a high selectivity of carbon dioxide over the other impurities, the other goal of the process being the production of a pure stream of CO₂. In fact, a strong adsorption of CO₂, an intermediate adsorption of impurities and little to no adsorption of hydrogen are the sought features.
- the material should present high cyclic capacity for CO₂ and impurities, fast mass transfer and low heat of adsorption.
- moreover, it should be commercially available and cost competitive.

Two different single component adsorption isotherms are considered in this work, namely Langmuir and Sips isotherms, both sticking to the same general formula. Precisely, Sips isotherm is described by equation 1.7 while Langmuir's follows equation 1.8 [6]:

$$q_{S,i}^*(P, T, y_j) = q_{S,inf,i}(T) \frac{(b_{S,i}(T)y_i P)^{1/n_{S,i}(T)}}{1 + \sum_{j=1}^N (b_{S,j}(T)y_j P)^{1/n_{S,j}(T)}} \quad (1.7)$$

$$q_{L,i}^*(P, T, y_j) = q_{L,inf,i}(T) \frac{b_{L,i}(T)y_i P}{1 + \sum_{j=1}^N b_{L,j}(T)y_j P} \quad (1.8)$$

Where:

$$b_{S,i}(T) = B_0 \cdot e^{\frac{B_1}{T}}$$

$$q_{S,inf,i}(T) = A_1 + A_2 \cdot T$$

$$n_{S,i}(T) = C_1 + \frac{C_2}{T}$$

And:

- $q_i^*(T)$ is the equilibrium adsorbed phase concentration of component i in mol/kg
- $q_{inf,i}(T)$ is the saturation capacity in mol/kg
- $b_i(T)$ is the affinity coefficient
- $n_i(T)$ is an isotherm parameter which accounts for the inhomogeneity of the adsorbent surface. Unitary if the surface is supposed homogeneous
- p as the pressure
- $A_1, A_2, B_0, B_1, C_1, C_2$ are fitting parameters and are different for the considered component [6]

Table 1.1: Sips isotherm parameters for $T=308$ K, average heats of adsorption and LDF coefficients for CO_2 , CO , N_2 , CH_4 and H_2 on zeolite 13X [6], [10].

Component	$q_{L,inf,i}$	$b_{L,i} \times 10^4$	$q_{S,inf,i}$	$b_{S,i} \times 10^4$	$n_{S,i}$	ΔH_{st}	k_i
	mol/kg	kPa ⁻¹	mol/kg	kPa ⁻¹	-	kJ/mol	1/s
CO_2	5.145	900.7	5.944	595.0	1.839	-37000	0.1
CO	3.032	28.34	3.677	17.79	1.177	-25000	0.7
N_2	3.021	8.887	3.210	7.949	1.024	-19000	1.6
CH_4	4.073	11.98	3.934	12.82	0.983	-19000	0.9
H_2	4.099	0.457	4.332	0.451	0.991	-8050	1.6

Both the isotherm models mentioned before are valuable and accurately describe the experimental data, though Sips isotherms seems to be more interesting in low pressure ranges.

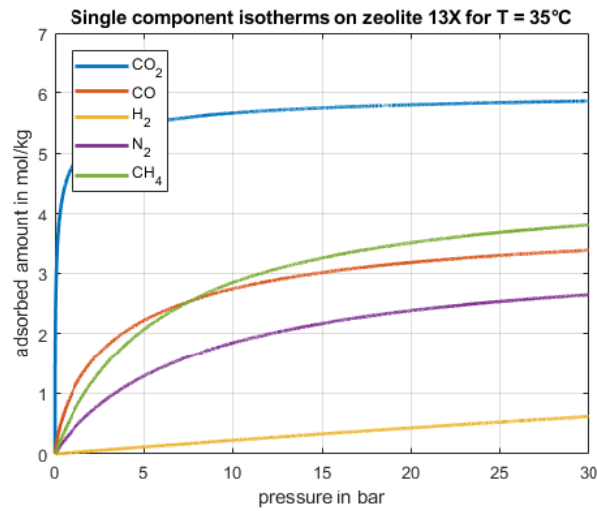


Figure 1.10: Single component adsorption isotherms at 35 °C for zeolite 13X [5].

Chapter 2

Technical analysis of Pressure Swing Adsorption processes

The research project will start from the analysis of the simplest adsorption process and will then move towards more complex cycles and more sophisticated specifications. The goal of the following chapter is to give the reader the fundamentals to understand the idea behind the adopted scale-up methodology.

2.1 Existing scale-up methodologies

Several methods already exist for the upscaling of adsorption technologies. They all fix one or more parameters during the scale-up process. They will be introduced in the following section before introducing the adopted approach.

2.1.1 Equilibrium theory

Equilibrium theory avails itself of partial differential equations and has been already exploited to estimate the movement of the impurities' front during the different steps of a simple Skarstrom cycle (Figure 2.1). To a deeper understanding, here will be reported the operating modes of the two half cycles together with the cycle functional scheme of a single column.

Two columns are needed to have continuous operation. In Figure 2.2 two half cycles are depicted: when the first column is fed by the compressed mixture, part of the product is recycled to the second one as a low pressure purge gas. After the adsorption the first bed is depressurized to atmospheric pressure by means of a blowdown step and the second bed simultaneously undergoes the repressurization.

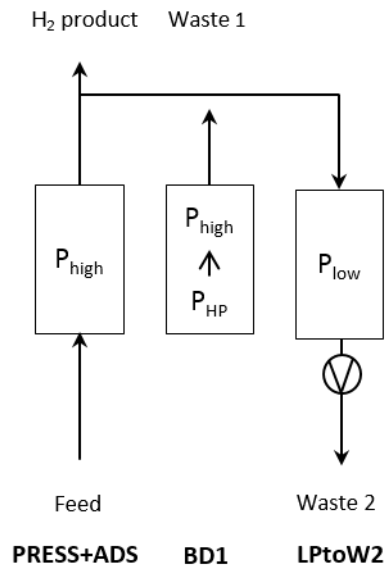


Figure 2.1: Skarstrom cycle.

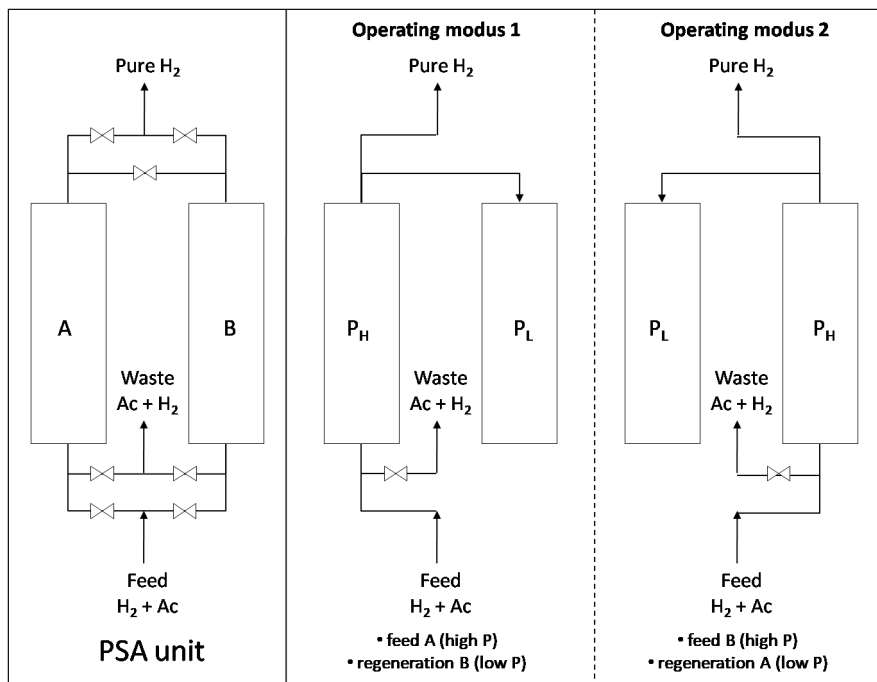


Figure 2.2: PSA unit. Operating modus 1 and 2 show the half cycles composed of the pressurization and feed step, and the blowdown and purge steps, respectively [8].

The assumptions equilibrium theory is based on are the following:

- negligible axial dispersion
- negligible mass transfer resistances
- isothermal behavior
- negligible pressure drop along the column
- ideal gas law
- linear adsorption isotherm

The behavior of a PSA column is very similar to the behavior of a typical chromatographic column, therefore the same equations apply.

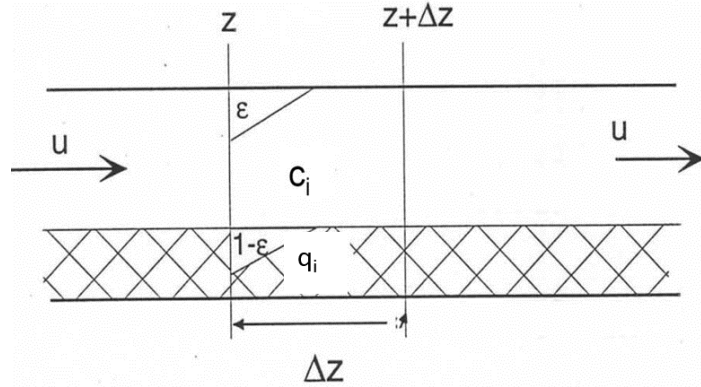


Figure 2.3: Section of a PSA column [8].

For a linear isotherm:

$$(\epsilon + (1 - \epsilon)H_i) \frac{\partial c_i}{\partial t} + \epsilon \frac{\partial(v c_i)}{\partial z} = 0 \quad (2.1)$$

which can be rearranged as:

$$\beta_i \frac{\partial c_i}{\partial t} + \frac{\partial(v c_i)}{\partial z} = 0$$

Where: ϵ is the void fraction, H_i the Henry coefficient of component i , c_i the fluid phase concentration of component i and v_i is the superficial velocity (u in Figure 2.3). Furthermore, $\nu = \frac{1-\epsilon}{\epsilon}$ and $\beta_i = 1 + \nu H_i$.

Assuming ideal gas behavior and considering the feed stream very rich in hydrogen with negligible content in carbon dioxide as impurity, the equation can be written for both components resulting in a system of two partial differential equations.

$$\beta_{CO_2} \frac{\partial(Py_{CO_2})}{\partial t} + \frac{\partial(vPy_{CO_2})}{\partial z} = 0 \quad (2.2)$$

$$\beta_{H_2} \frac{\partial P}{\partial t} + \frac{\partial(vP)}{\partial z} = 0 \quad (2.3)$$

where: $\beta_{CO_2} = 1 + H_{CO_2}$, $\beta_{H_2} = 1$ and y_i is the molar fraction of component i.

Depending on the considered step, the equation will present some peculiarities: during the feed and the purge both the velocity and the pressure are considered constant. In the other two steps, the pressure is time dependent. The expression of the velocity can be derived coupling Equation 2.3 with appropriate boundary conditions.

$$\begin{aligned} \frac{\partial v}{\partial z} &= -\beta_{H_2} \frac{1}{P} \frac{dP}{dt} = -\beta_{H_2} \frac{d(\ln P)}{dP} \\ v &= -\beta_{H_2} \frac{d(\ln P)}{dt} (z - L) \end{aligned} \quad (2.4)$$

Equation 2.2 can be rewritten as

$$\beta_{CO_2} \frac{\partial(\ln y)}{\partial t} + v \frac{\partial(\ln y)}{\partial z} = (\beta_{CO_2} - \beta_{H_2}) \frac{d(\ln P)}{dt}$$

which can be solved using the method of characteristics, from which:

$$\begin{aligned} \frac{dt}{ds} &= \beta_{CO_2} \\ \frac{dz}{ds} &= v = -\beta_{H_2} \frac{d(\ln P)}{dt} (z - L) \\ \frac{d(\ln y)}{ds} &= (\beta_{CO_2} - \beta_{H_2}) \frac{d(\ln P)}{dt} \end{aligned}$$

Combining the first two equations with the expression of the velocity and rearranging it, it is possible to derive the following relationship:

$$\frac{1}{z - L} \frac{d(z - L)}{dt} = \frac{d(\ln(z - L))}{dt} = -\beta \frac{d(\ln P)}{dt} \quad (2.5)$$

where $\beta = \frac{\beta_{H_2}}{\beta_{CO_2}}$ is always higher than 1.

The equation can be integrated between the two pressure levels to obtain the expression of the penetration of the adsorption and desorption fronts within the column, as shown in Figure 2.4.

Pressurization:

$$z_1 = L(1 - r^{-\beta}) \quad (2.6)$$

Blowdown:

$$z_3 = L + (z_2 - L)r^\beta \quad (2.7)$$

where $r = \frac{p_H}{p_L}$.

Concerning the other two phases of the cycle, both the velocity and the pressure contribute to the expression of the coordinates.

Adsorption:

$$z_2 = z_1 + u_{CO_2,ads}t_{ads} \quad (2.8)$$

Purge:

$$z_4 = z_3 + u_{CO_2,purge}t_{purge} \quad (2.9)$$

where

$$u_{CO_2,step} = \frac{u_{step}}{\epsilon + (1 - \epsilon)H_{CO_2}}$$

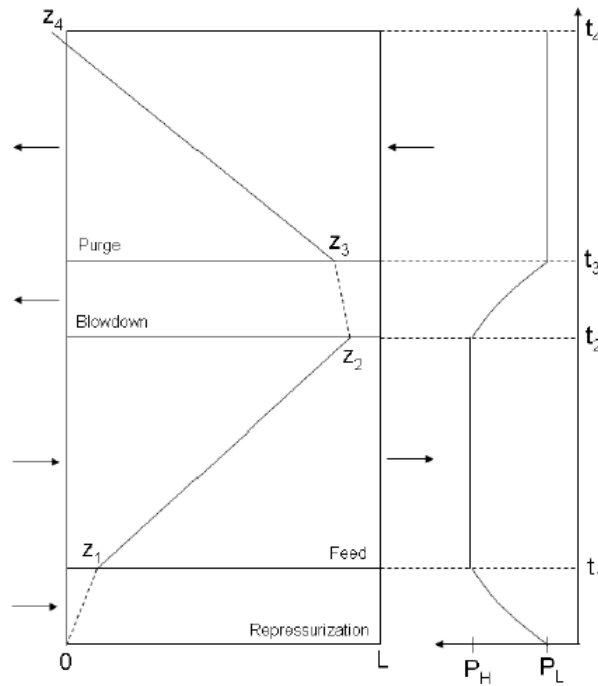


Figure 2.4: Solute movement theory for PSA (dotted broken lines between points 0 and z_1 and z_2 and z_3 indicate that the exact path is not known) [8].

2.1.2 A methodology proposed by Rota and Wankat

A theoretical approach for intensification of PSA processes is presented by Rota and Wankat with the aim of providing simple scaling rules that improve the performance of the plant [9].

They show that for process intensification, it is favourable to shorten the columns and work with smaller adsorbent particles holding constant the pressure drop along the column. Product purity, recovery and adsorbent productivity are investigated making use of suitable reference variables and a dimensionless mathematical model whose solution is constrained to be the same in the new and in the old configuration. This technique allows to derive a set of algebraic equations which relates process characteristics to key performance indicators.

The most important assumptions are:

- Ideal gas law
- Laminar flow
- Negligible axial dispersion
- Negligible radial gradients
- Negligible potential energy
- Negligible irreversible conversion of mechanical to thermal energy
- Constant cross-sectional area and porosity
- Adiabatic columns
- Spherical particles
- Negligible pressure gradient inside the particles

The process is described through mass and energy balance equations, equilibrium isotherms, pressure drop equation and stoichiometric equations, which are made dimensionless dividing every variable by an arbitrary reference variable. The scaling rules that arise from this model are strongly dependent on the mechanism that controls mass and heat transfer; while the latter phenomenon can be neglected, it is not the same for mass transfer. The evaluation of Biot number, which is an indicator of the controlling mechanism, is of fundamental importance to understand whether the resistances are located within the particle or in the external film.

When considering a two columns four steps Skarstrom cycle, the boundary conditions can be written as [9]:

- Pressurization ($n\tau_C \leq \tau < n\tau_C + \tau_1$)

$$\begin{cases} P(\tau, Z = 0) = P_H \\ \bar{c}_i(\tau, Z = 0) = \bar{c}_i \\ \bar{T}(\tau, Z = 0) = \bar{T} \\ U(\tau, Z = 1) = 0 \end{cases}$$

- Adsorption ($n\tau_C + \tau_1 \leq \tau < n\tau_C + \tau_{II}$)

$$\begin{cases} P(\tau, Z = 0) = P_H \\ \bar{c}_i(\tau, Z = 0) = \bar{c}_i \\ \bar{T}(\tau, Z = 0) = \bar{T} \\ U(\tau, Z = 0) = U \end{cases}$$

- Blowdown ($n\tau_C + \tau_{II} \leq \tau < n\tau_C + \tau_{III}$)

$$\begin{cases} P(\tau, Z = 0) = P_L \\ \frac{\partial \bar{c}_i(\tau, Z=1)}{\partial Z} = 0 \\ \frac{\partial \bar{T}(\tau, Z=1)}{\partial Z} = 0 \\ \frac{\partial U(\tau, Z=1)}{\partial Z} = 0 \end{cases}$$

- Purge ($n\tau_C + \tau_{III} \leq \tau < (n+1)\tau_C$)

$$\begin{cases} P(\tau, Z = 0) = P_L \\ \bar{c}_i(\tau, Z = 1) = \bar{c}_i \\ \bar{T}(\tau, Z = 1) = \bar{T} \\ U(\tau, Z = 1) = U \end{cases}$$

where τ_C is the dimensionless cycle time, $\tau_1, \tau_{II}, \tau_{III}$ are the dimensionless end times of pressurization, adsorption and blowdown steps respectively. U is the dimensionless velocity.

Moreover, it is possible to express product purity, recovery and productivity in terms of the aforementioned dimensionless parameters.

$$r = \frac{\int_{\tau_1}^{\tau_{II}} (\bar{c}_i U)_{Z=1} d\tau - \int_{\tau_{III}}^{\tau_C} (\bar{c}_i U)_{Z=1} d\tau}{\int_0^{\tau_{II}} (\bar{c}_i U)_{Z=0} d\tau} \quad (2.10)$$

$$\phi = \frac{\int_{\tau_1}^{\tau_{II}} (\bar{c}_i U)_{Z=1} d\tau - \int_{\tau_{III}}^{\tau_C} (\bar{c}_i U)_{Z=1} d\tau}{\sum_{j=1}^{NC} (\int_{\tau_1}^{\tau_{II}} (\bar{c}_j U)_{Z=1} d\tau - \int_{\tau_{III}}^{\tau_C} (\bar{c}_j U)_{Z=1} d\tau)} \quad (2.11)$$

$$AP = \frac{c_0 u_0 (\int_{\tau_1^{\text{II}}} (\bar{c}_i U)_{Z=1} d\tau - \int_{\tau_{\text{III}}^{\text{C}}} (\bar{c}_i U)_{Z=1} d\tau)}{\tau_C (1 - \epsilon) \rho_P L} \quad (2.12)$$

Being the method proposed for processes' intensification, the idea is to see if it works with the same assumptions but in the opposite direction.

Firstly, an operator ratio R is introduced to compare the old and the new configurations: it is therefore defined as the ratio of any parameter related to the process in the two configurations.

$$R(\alpha) = \frac{\alpha_{\text{NEW}}}{\alpha_{\text{OLD}}}$$

To keep the performances constant, it is sufficient to constrain $R(r)$ and $R(\phi)$ to be equal 1 and see how the productivity behaves when scaling the technology. To this end, all dimensionless profiles must be kept constant, which is possible when all dimensionless groups and all the boundary conditions are equal in both configurations. Not only pressure, temperature and composition of the feed mixture must be the same, but also the pressure drop across the column should not vary, meaning that all physical variables depending on these parameters do not change either.

$$R(q_0) = R(c_0) = R(T_0) = R(p_0) = R(\Delta p) = R(p^j) = R(T^k) = R(c^k_i) = 1$$

$$R(L) = R(u_F) R(t_C) \quad (2.13)$$

$$R(d_p) = R(u_F) R(t_C)^{0.5} \quad (2.14)$$

$$R(AP) = R(t_C)^{-1} \quad (2.15)$$

Moreover, if internal resistances control the adsorption process, another constraint on the feed velocity u_F arises:

$$R(u_F) = 1 \quad (2.16)$$

It is worth noting that, even if purities and recoveries are preserved following these scaling rules, the proposed approach is certainly not promising for our purpose, the adsorption productivity being inversely proportional to the cycle time. In fact, higher column lengths lead to higher cycle times and thereby to lower productivities. The advantage of this method is that it is straightforward and takes into account the importance of mass transfer through the evaluation of the Biot number but it is not a suitable approach for our purposes since it implies a scale-out rather than a scale-up.

Despite the mismatch between the goal of the project and the proposed methodology, the method will be referred to as an integration for other methodologies.

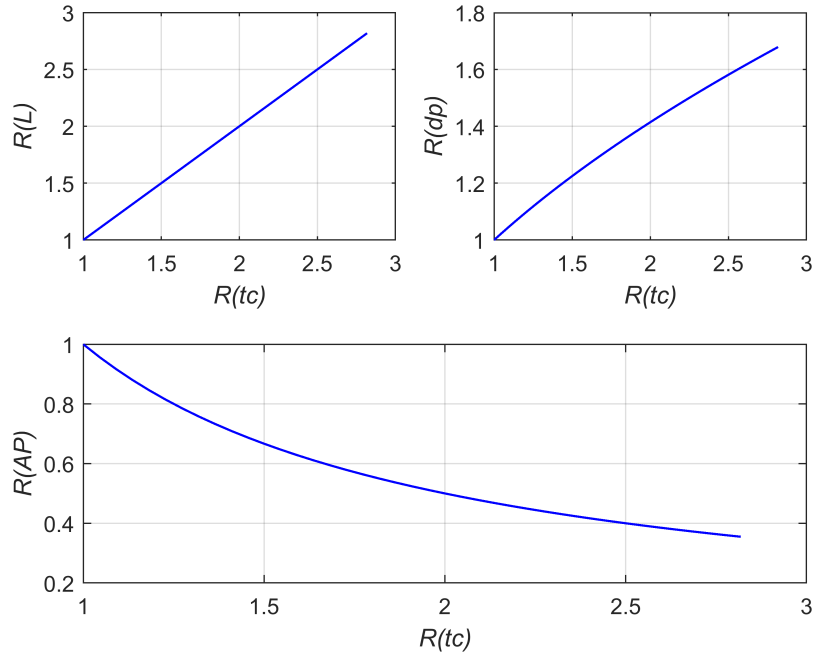


Figure 2.5: Typical profiles of column length, particle diameter and adsorbent productivity ratios as a function of the cycle time ratio.

2.2 Developed scale-up method for a simple PSA

The aforementioned methodologies are fundamental to the comprehension of the upscaling approach and are integrated to develop a new analytical scale-up method leaning on dimensionless number and equilibrium theory.

2.2.1 Equilibrium theory based constraints

Several constraints must be respected to allow for high product purity, in particular the front of the impurities should never overcome the top end of the column so that the breakthrough is avoided. This can be translated in the following mathematical constraint:

$$z_2 < L$$

$$u_{\text{CO}_2, \text{feed}} t_{\text{feed}} < L r^{-\beta}$$

$$\frac{u_{\text{feed}} t_{\text{feed}}}{1 + \nu H_{\text{CO}_2}} < L r^{-\beta}$$

Defining as m the dimensionless ratio between the product of velocity and time and the length of the adsorption bed, the constraint can be expressed as follows:

$$m_{\text{feed}} = \frac{u_{\text{feed}}t_{\text{feed}}}{L} < (1 + \nu H_{\text{CO}_2})r^{-\beta} \quad (2.17)$$

To guarantee a clean column before a new cycle starts, the desorption front has to exit the column at the end of the purge step, therefore:

$$z_4 < 0$$

The relation states that the position of the front at the end of the blowdown step must be smaller than the distance travelled during the step of the purge.

$$\begin{aligned} z_3 &< u_{\text{CO}_2\text{purge}}t_{\text{purge}} \\ u_{\text{feed}}t_{\text{feed}} &< u_{\text{purge}}t_{\text{purge}}r^{-\beta} \end{aligned}$$

Dividing both members by the length, the equation becomes:

$$m_{\text{purge}} > m_{\text{feed}}r^{\beta} \quad (2.18)$$

The last constraint is purely physical and it forces the recycle ratio between the unit undergoing the adsorption step and the other experiencing the purge to be smaller than one.

$$u_{\text{feed}}t_{\text{feed}}r < u_{\text{purge}}t_{\text{purge}}$$

Dividing again by L and multiplying by r^{β} , the expression becomes:

$$m_{\text{purge}} > m_{\text{feed}}r^{\beta}r^{\beta-1} \quad (2.19)$$

A defined region in which it is possible to move respecting the required purities and the physical nature limitations can be found plotting the derived constraints as a function of $m_{\text{feed}}r^{\beta}$. Figure 2.7 clearly shows the mathematical constraints related to the adsorption step (blue), the purge step (red) and the recycle ratio (green) derived for a linear isotherm and a simple Skarstrom cycle.

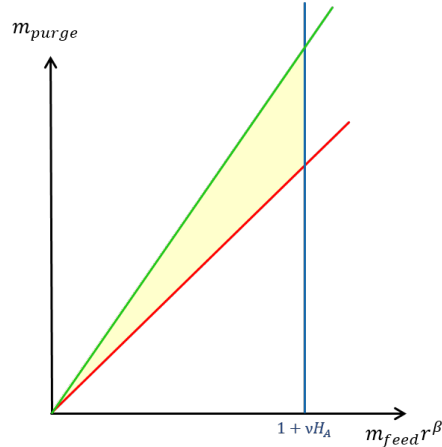


Figure 2.6: Equilibrium theory constraints for linear isotherm and Skarstrom cycle.

2.2.2 Towards non-linear isotherms: Henry's coefficient limitations

As a first approach, non-linear isotherms can be considered to investigate the behavior of the constraints when moving towards more realistic assumptions. When Langmuir and Sips adsorption isotherms are observed, some limitations arise, which are related to Henry's coefficient definition.

Henry's coefficient is defined as the limit of the ratio between the adsorbed amount and the partial pressure as the pressure itself approaches zero.

$$H_i = \lim_{P \rightarrow 0} \frac{q}{P} \quad (2.20)$$

Langmuir proposed an isotherm leaning on a kinetic principle stating that the adsorption and desorption rates are equal, therefore, being q the molar amount of adsorbed gas, P the equilibrium pressure and $q_{m,L}$ and B_L isotherm parameters, the isotherm can be expressed as:

$$q = \frac{q_{m,L} B_L P}{1 + B_L P}$$

It follows that

$$H_{CO_2} = q_{m,L} B_L$$

When evaluating the coefficient it can be noticed that very high values are encountered and that the mathematical constraint previously derived for the adsorption step is pushed towards the x axis positive direction.

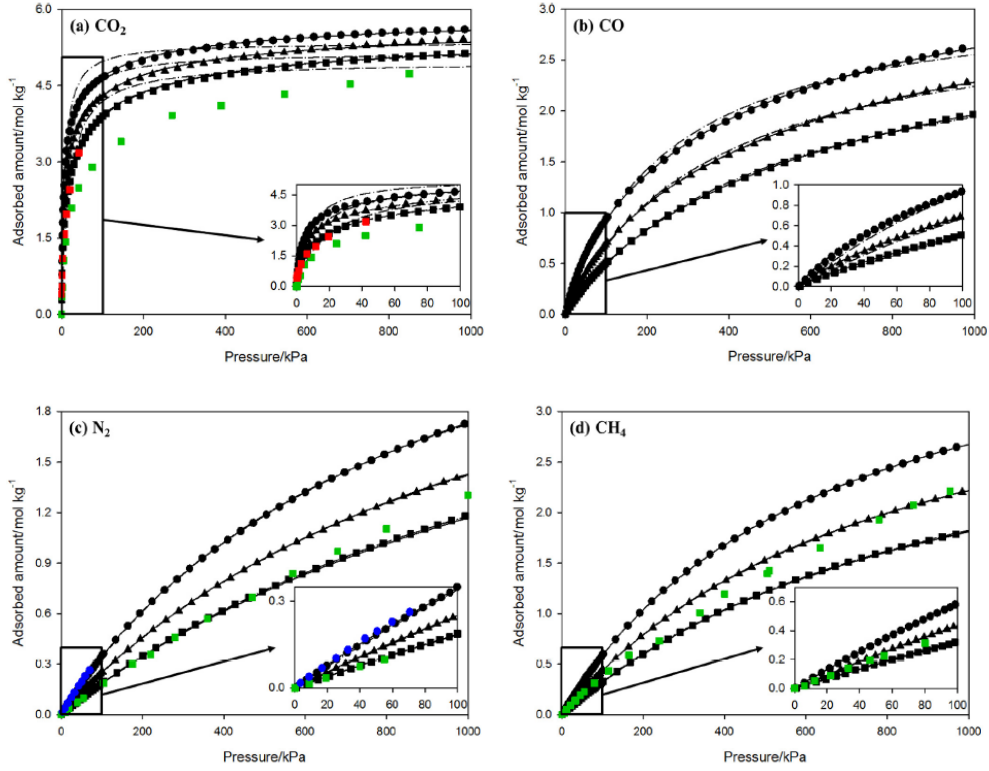


Figure 2.7: Adsorption isotherms on pelletized zeolite 13X: (a) CO₂, (b) CO, (c) N₂, (d) CH₄ (circle, T = 293 K; up pointing triangle, T = 308 K; square, T = 323 K; black symbol, Park et al. [10]; green symbol, T = 323 K, Cavenati et al. [13]; red symbol, T = 323 K, Wang et al. [12]; blue symbol, T = 293 K, Park et al. [11]; spaced n-dash lines with single dot, Langmuir model; spaced n-dash lines with double dot, Sips model; straight lines, temperature-dependent Sips model). (For interpretation of the references to colour in this figure legend, the reader is referred to the web version of [10].)

Concerning Sips isotherm, its mathematical form is the following:

$$q = \frac{q_{m,S}(B_S P)^{1/n}}{(B_S P)^{1/n}}$$

In this case, Henry's coefficient is not univocal anymore since it depends on the value of the isotherm parameter n .

$$H_{\text{CO}_2} = +\infty \text{ if } n > 1$$

$$H_{\text{CO}_2} = B_S P \text{ if } n = 1$$

$$H_{\text{CO}_2} = 0 \text{ if } n < 1$$

This adsorption isotherm, which presents a finite limit when approaching high values of pressure, shows a small relative error with respect to experimental data (see Figure 2.8), thus well describing the empirical adsorption data over rather broad temperature ranges. For this reason it is chosen to run the simulations with the Fortran code.

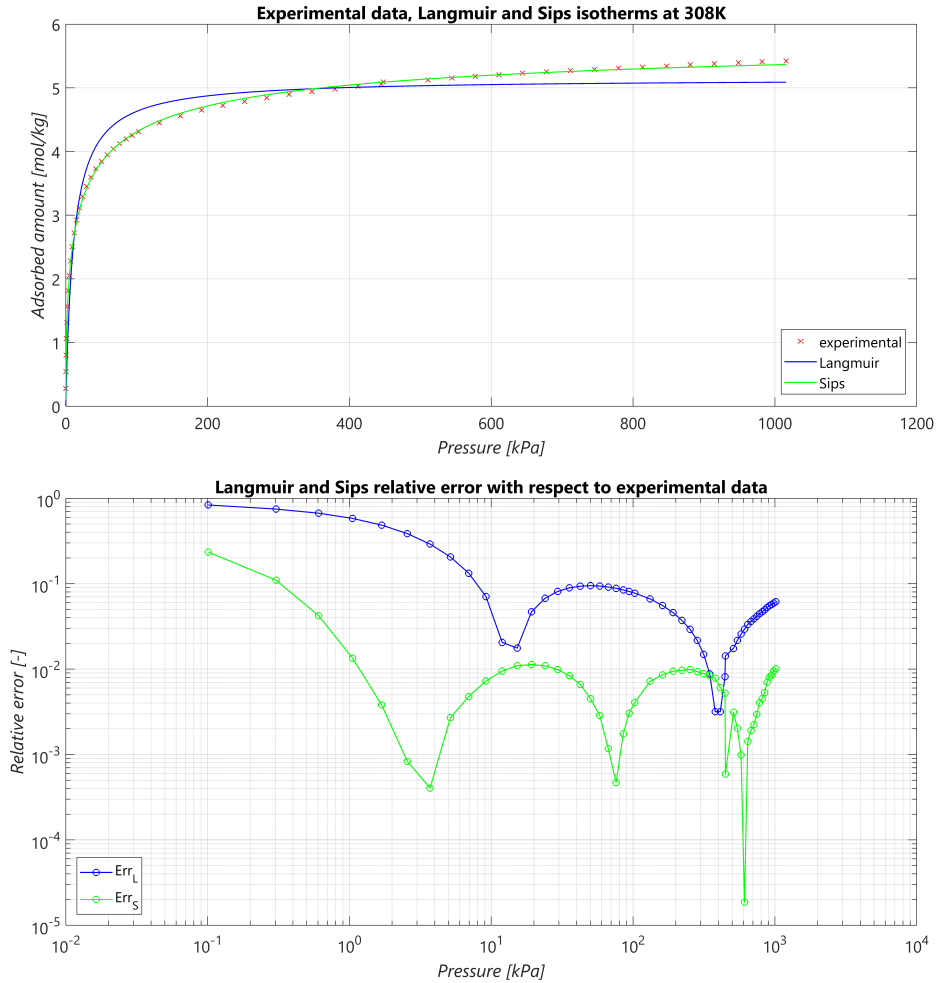


Figure 2.8: Langmuir and Sips adsorption isotherms and relative error with respect to experimental data.

To overcome the problem related to the evaluation of Henry's coefficient and plot the operating triangle on the basis of realistic physical data, a linearization of the adsorption isotherm is thus necessary. In this project, two different linearizations, which are shown in Figure 2.9, are analysed:

- Linearization 1 assures both right adsorbed and desorbed amounts (more complex)
- Linearization 2 guarantees only the proper adsorbed amount (simpler)

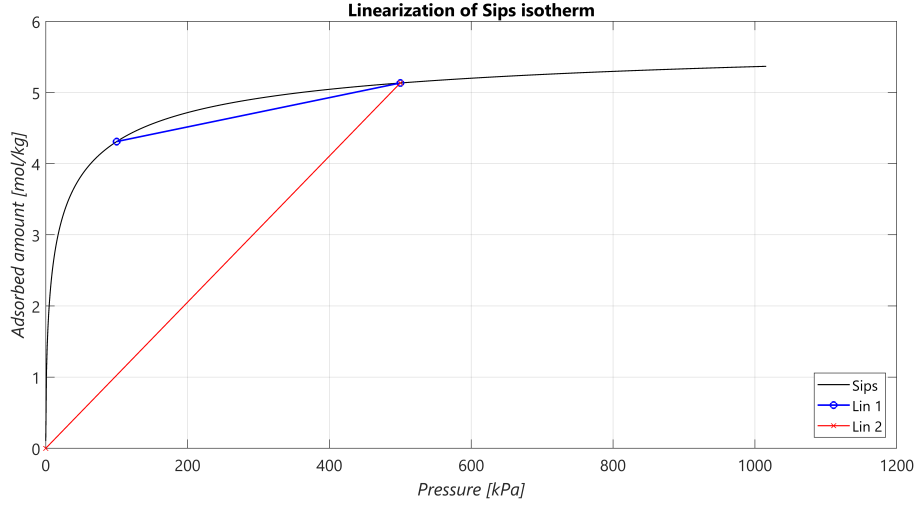


Figure 2.9: Different linearizations of Sips adsorption isotherm.

Table 2.1 gathers the input data of interest used to draw the analytically derived constraints on a real case simulated with Fortran.

Table 2.1: Bed properties and process input data for simulations

Input data	Value	Units
ρ_b	708	kg/m ³
ρ_p	1085	kg/m ³
ρ_s	2359	kg/m ³
ϵ	0.6999	-
ν	0.4288	-
P_H	25	bar
P_L	1	bar
Q_{feed}	5×10^{-5}	m ³ /s

With reference to the constraints, it is possible to derive the minimum column length that assures a pure product and to compare the found results depending on the linearization adopted.

$$L_{\min} = z_1 + \Delta z_2 = L(1 - r^{-\beta}) + u_{\text{CO}_2, \text{ads}} t_{\text{ads}} \quad (2.21)$$

It is evident how choosing the right linearization is not trivial and can lead to very different outputs, the first linearization is more sophisticated and more precise and therefore it allows to calculate realistic lengths of the column. Table 2.2 shows that, increasing the time of the adsorption step, a longer column must be realized to assure product purity.

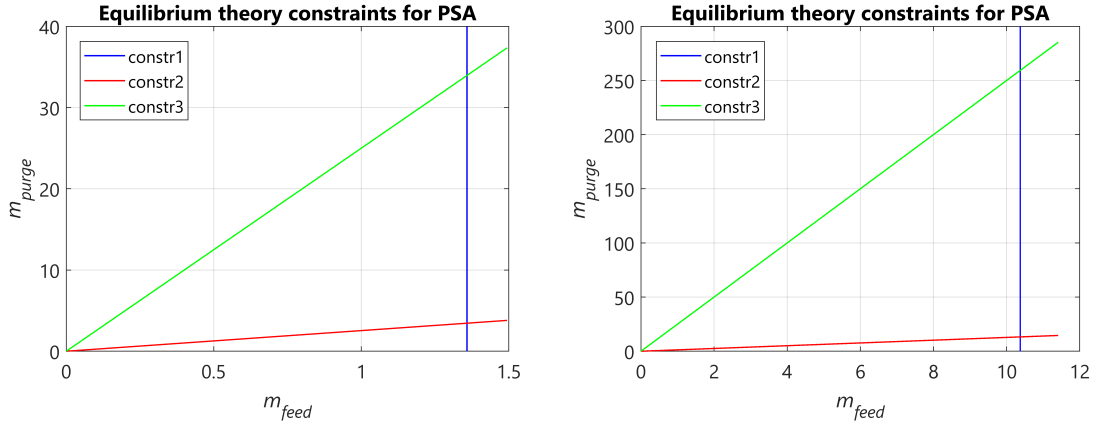


Figure 2.10: Operating window for different linearizations: linearization 1 (left), linearization 2 (right)

Table 2.2: Minimum column length dependence on the chosen linearization

Adsorption time	Linearization 1	Linearization 2
s	m	m
10	1.149	0.369
30	1.993	0.589
60	3.258	0.919
100	4.945	1.359

2.2.3 FAST: full physical mathematical modelling

A Fortran-based Adsorption Simulation Toolbox (FAST) is used to simulate the PSA process within the column during a simple Skarstrom cycle.

The model leans on the following assumptions:

- negligible radial temperature and concentration gradients
- negligible axial diffusion and thermal conductivity along the column wall
- constant heat of adsorption
- thermal equilibrium between the gas and the adsorbent
- pressure drop along the column is described by Ergun equation
- linear driving force (LDF) approximation used to describe mass transfer
- mass transfer coefficient independent from temperature and concentration
- adiabatic conditions

The simplifying assumptions at the basis of the model translate in the following equations:

- component mass balance:

$$\epsilon_t \frac{\partial c_i}{\partial t} + \frac{\partial(uc_i)}{\partial z} + \rho_b \frac{\partial q_i}{\partial t} = 0$$

total mass balance:

$$\epsilon_t \frac{\partial c}{\partial t} + \frac{\partial(uc)}{\partial z} + \rho_b \sum_{i=1}^N \frac{\partial q_i}{\partial t} = 0$$

- mass transfer:

$$\frac{\partial q_i}{\partial t} = k_i(q_i^* - q_i)$$

- energy balance:

$$\frac{(\epsilon_t C_g + \rho_b C_s + \rho_b C_{\text{ads}}) \partial T}{\partial t} - \epsilon_t \frac{\partial p}{\partial t} + u C_g \frac{\partial T}{\partial z} - \rho_b \sum_{i=1}^N -\Delta H_i \frac{\partial q_i}{\partial t} = 0$$

- momentum balance (Ergun equation):

$$\frac{\partial P}{\partial z} = -\frac{150\mu(1 - \epsilon_b)^2}{\epsilon_b^3 d_p^2} u - \frac{1.75(1 - \epsilon_b)\rho}{\epsilon_b^3 d_p} |u|u$$

The Skarstrom cycle is modelled assuming the presence of a single column undergoing the four characteristic steps (pressurization, adsorption or feed, blow-down and purge) swinging between two pressure levels of 25 and 1 bar. Being the adsorption and the purge units connected by a direct recycle, their times are set equal to one another. Furthermore, a Back Pressure Regulator (BPR) is simulated to make the code move to the next step after the desired pressure is reached during the varying pressure steps.

In the table below all the input data for the model are gathered.

Table 2.3: Input data for the modeling of a simple Skarstrom cycle

Parameter	Value	Units
Q_{feed}	5×10^{-5}	m^3/s
P_{feed}	25.8	bar
T_{feed}	308	K
P_{H}	25	bar
P_{L}	1	bar
y_{CO_2}	0.2	-
y_{H_2}	0.8	-
t_{feed}	15-100	s
t_{purge}	15-100	s
RR	10-90	%
L_{bed}	1.2	m

The goal of running simulations moving towards realistic assumptions thus properly describing the behavior of the system is to draw empirically the operating envelope and compare it with the one found analytically.

To move within the plane ($m_{\text{feed}}, m_{\text{purge}}$) two parameters are changed, namely the time of the adsorption step and the recycle ratio connecting the adsorption and the purge.

In Figure 2.11 all the simulated operation conditions are plotted: points in green present hydrogen purity greater than 99.9%. The operating window is strongly dependent on the set performance requirements.

The plot presents few differences with respect to the analytical results: a clear vertical constraint related to the minimum length of the column and therefore to the phenomenon of impurities' breakthrough can still be noticed, moreover the bottom part of the graph shows points with low purities due to low recycle ratios (RR) and thus to insufficient purges.

When moving upwards in the space ($m_{\text{feed}}, m_{\text{purge}}$) overcoming recycle ratios of 80%, product purities reduce again even though the analytical constraint on the recycle ratio can never be reached in reality. Further investigation is performed to understand this unexpected and counterintuitive behavior.

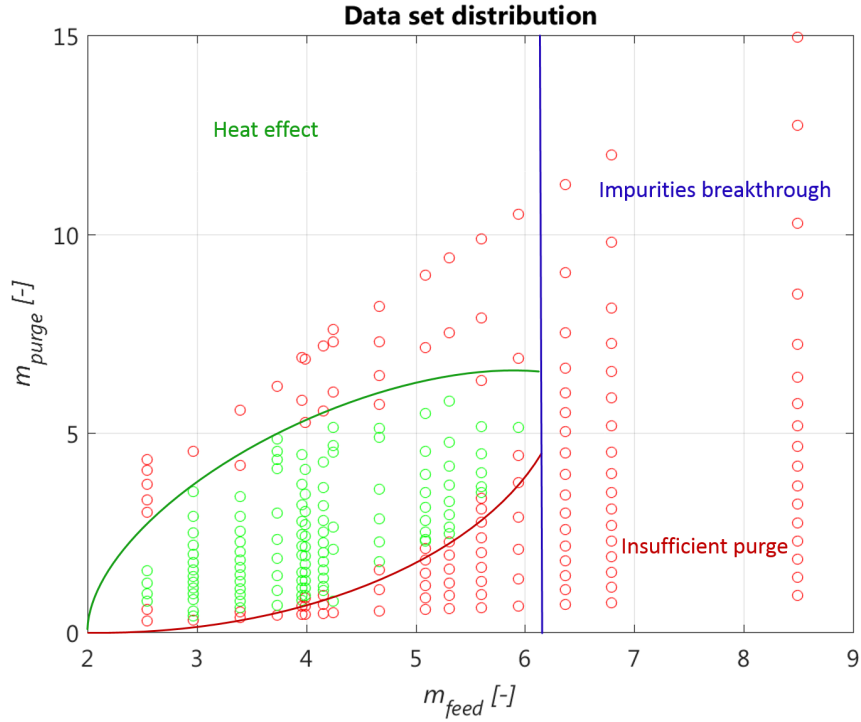


Figure 2.11: Results of full physical model applied to a simple Skarstrom cycle

Concentration, pressure and temperature profiles are analysed to see where the drop in purities might come from and for high recycle ratios very high temperatures are spotted within the column.

To a deeper understanding, an energy balance over the throttling valve connecting the adsorption and the purge units is performed to exclude whether the remarkable difference in temperature might be related to the incorrectness of assuming an isenthalpic expansion.

$$\frac{dE}{dt} = \frac{\Delta v^2}{2} + g\Delta z + \Delta h + \dot{Q} + \dot{W}$$

At steady state, neglecting the change in potential energy, considering adiabatic conditions and no mechanical or electrical work applied, the first principle reduces itself to:

$$\Delta h = -\frac{\Delta v^2}{2}$$

Despite the change in velocity over the valve, a negligible difference in temperature is observed ($1 \cdot 10^{-3}\text{K}$) demonstrating that no artificial energy is added to the system assuming zero temperature drop over the valve. This reasoning leads to the conclusion that, working far from idealities and with the aforementioned assumptions, the convergence is reached at higher temperatures.

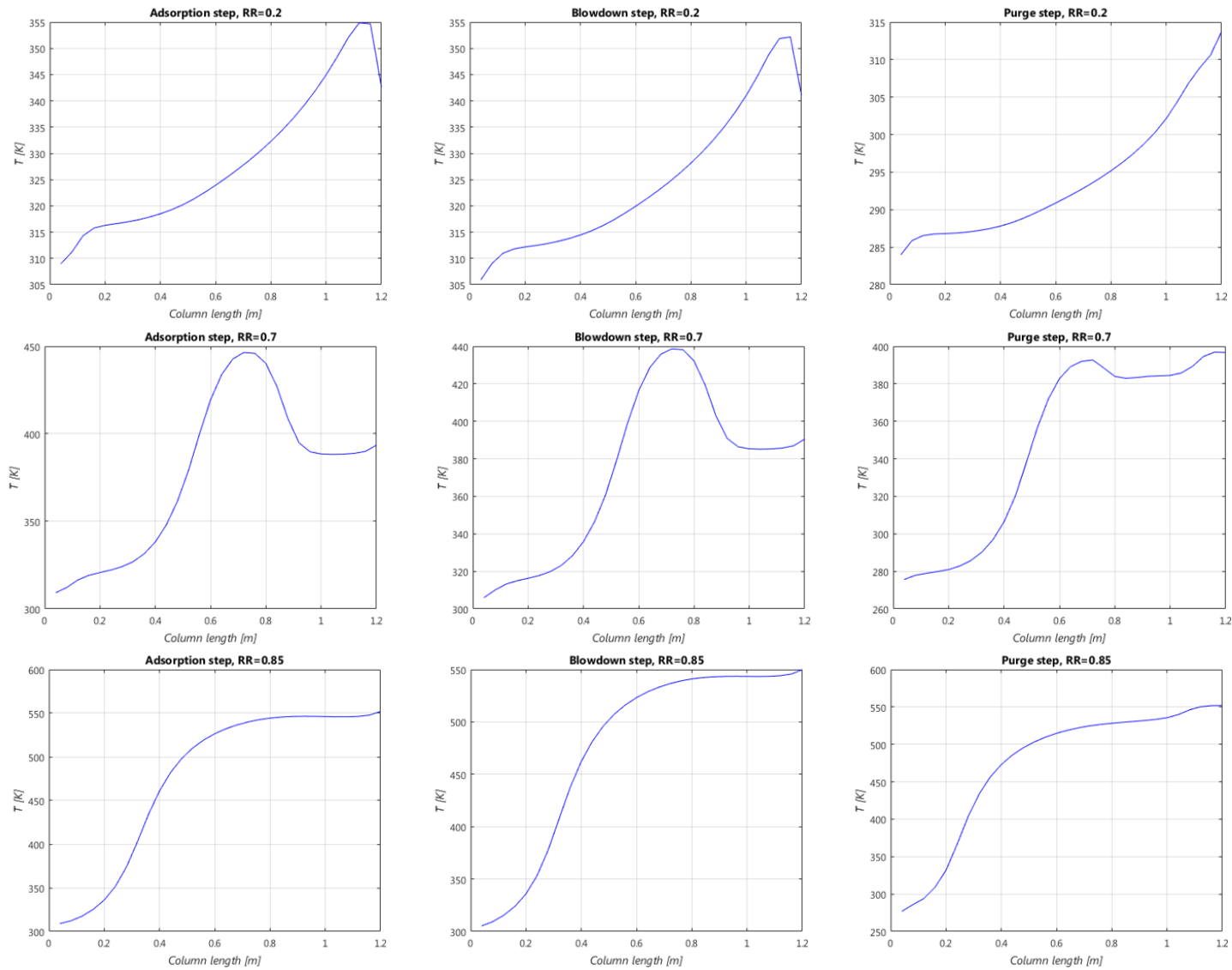


Figure 2.12: Temperature profiles within the adsorption bed for different recycle ratios (0.2, 0.7, 0.85).

As shown in Figure 2.13, both recovery and productivity decrease when increasing the recycled amount. On the other hand, it is expected to spot a grow in these two KPIs when increasing the time of adsorption; this is not evident though in the picture because despite it happens, only the points fulfilling the requirement of 99.9% purity are plotted. This behavior can be better caught in Figure 2.14: as already mentioned, the purity experiences a first increase due to more efficient purges and a secondary decrease. The adsorbent productivity keeps reducing itself following an hyperbolic behavior for higher values of reflux. For a fixed recycled amount instead, longer times of adsorption lead to higher productivities, which do not appear in Figure 2.13 for the reason that only operational points with valuable purities are presented in the graph.

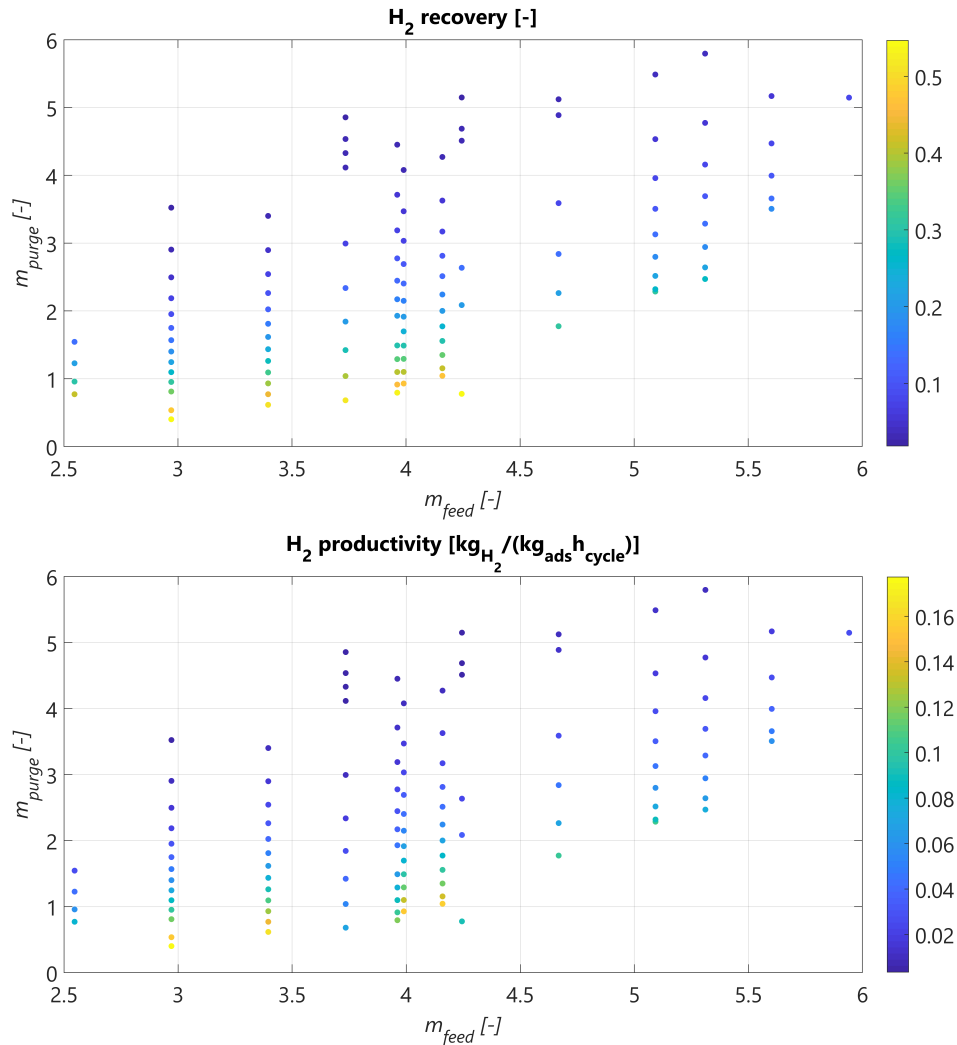


Figure 2.13: Recoveries and productivities for hydrogen purities higher than 99.9%, Skarstrom cycle.

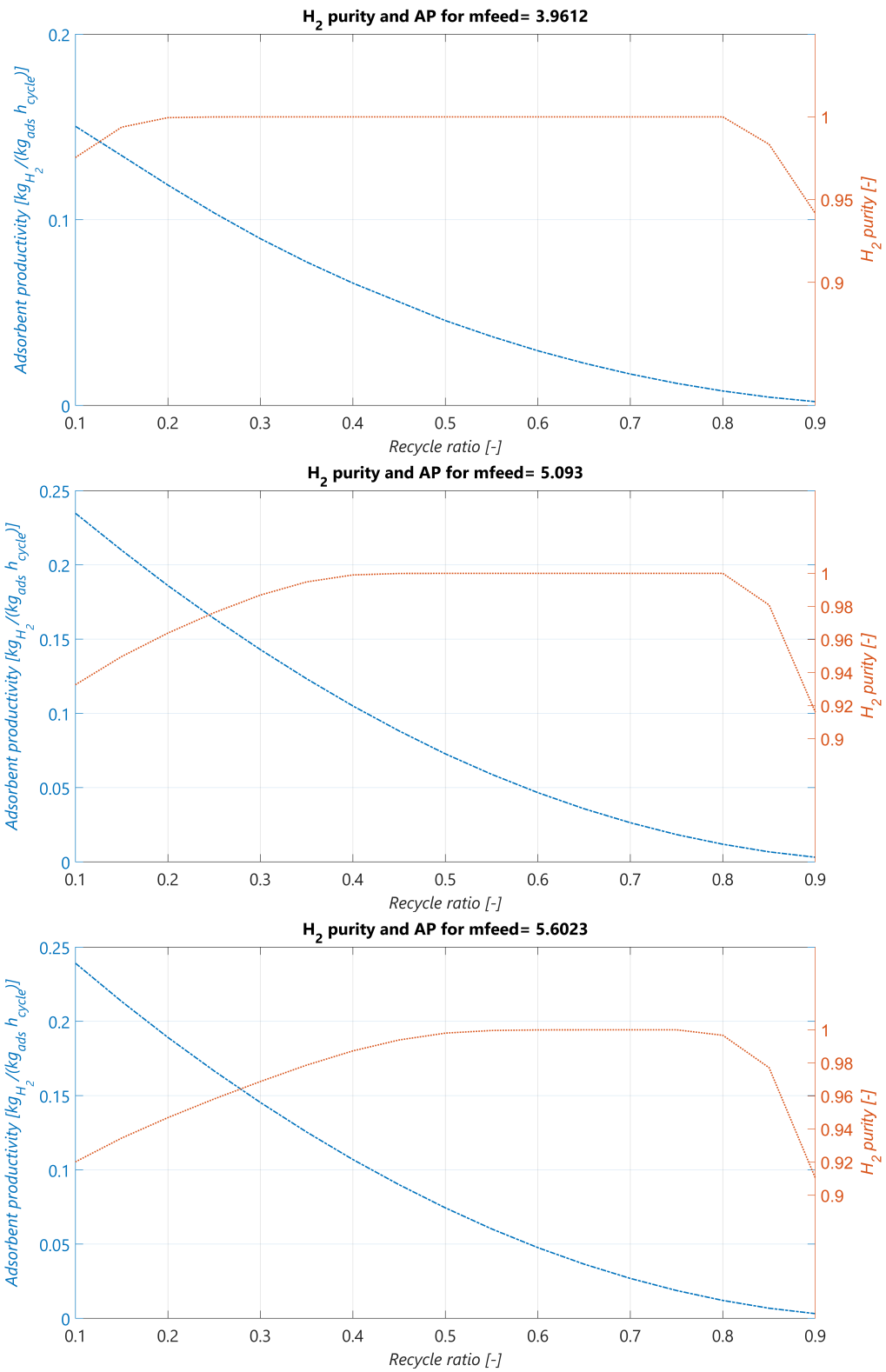


Figure 2.14: Purities and productivities for different value of m_{feed} , Skarstrom cycle.

2.2.4 Skarstrom cycle scale-up

The idea on which this scale-up methodology leans is choosing a promising operational condition and scale the length of the adsorption bed keeping the m dimensionless parameters constant. Being m a function of the velocity of the inlet stream, the time and the length of the column, the goal is that of keeping the residence time constant and vary the feed flowrate proportionally to the length. That allows to stick to fixed m_{feed} and m_{purge} and thus to the same KPIs. An optimal point is chosen and the scale-up methodology is applied; even if the boundaries found with the full physical model are slightly different from the ones derived analytically, it is still possible to scale the technology to higher lengths.

Table 2.4: Skarstrom cycle scale-up, $m_{\text{feed}}=2.97$, $m_{\text{purge}}=4.09$

L_{bed}	Q_{feed}	Φ_{H_2}	AP	r_{H_2}
m	m^3/s	%	$\text{kg}_{\text{H}_2}/(\text{kg}_{\text{ads}}\text{h}_{\text{cycle}})$	%
1.2	5×10^{-5}	99.99	0.177	54.68
1.5	6.25×10^{-5}	99.99	0.177	54.77
2	8.33×10^{-5}	99.99	0.178	55.00
2.5	1.04×10^{-4}	99.99	0.19	55.38

Table 2.4 shows that upscaling the technology is possible even if the constraint found by using the full physical model are not straight as the ones derived analytically. Purities are always fulfilled, productivity and recovery are almost constant and show slightly higher values for longer columns.

2.3 Simple VPSA

A simplified Vacuum Pressure Swing Adsorption (VPSA) is investigated as an intermediate step between the simple PSA experiencing a Skarstrom cycle and the complete and advanced VPSA.

Some differences are taken into account when moving towards the cycle affected by vacuum.

First of all, a multicomponent stream instead of a binary mixture is considered as feed stream. Its composition is characterised by three components, namely 75% hydrogen, 20% carbon dioxide, 5% methane. The latter is chosen as the most significant impurity due to the fact that it is the most adsorbable gas among all the possible impurities that are gathered within a SMR gas. Secondly, an intermediate blowdown and a heavy purge are added to allow impurities to be expelled before the carbon dioxide is withdrawn. A vacuum pump must be integrated for the evacuation of the second product during the second blowdown, in which the vacuum is created inside the column.

The column is first pressurized with the multicomponent inlet feedstream; during the adsorption step, being hydrogen the less adsorbable component, it travels through the column reaching the column top end with high purities. In the second unit (third step), a first blowdown is performed allowing the components considered as impurities for the next steps (methane and hydrogen) to be released until ambient pressure is reached. A purge with the heavy component at ambient pressure is then required to achieve the second goal of the cycle, namely the production of pure CO₂, which implies the need of cleaning the column purging it with a recycled amount of the pure CO₂ product coming out from the next step. The light purge instead is needed for the cleansing of the column from the carbon dioxide retained at the end of the vacuum blowdown; its role is that of pushing the impurity's front towards the bottom end with the aim of satisfying again hydrogen's requirements.

Figure 2.15 shows the steps experienced by one column during the whole cycle; as for the Skarstrom case, two or more columns have to be coupled for a suitable scheduling of the cycle. The first three steps are performed cocurrently, while the last two are countercurrent.

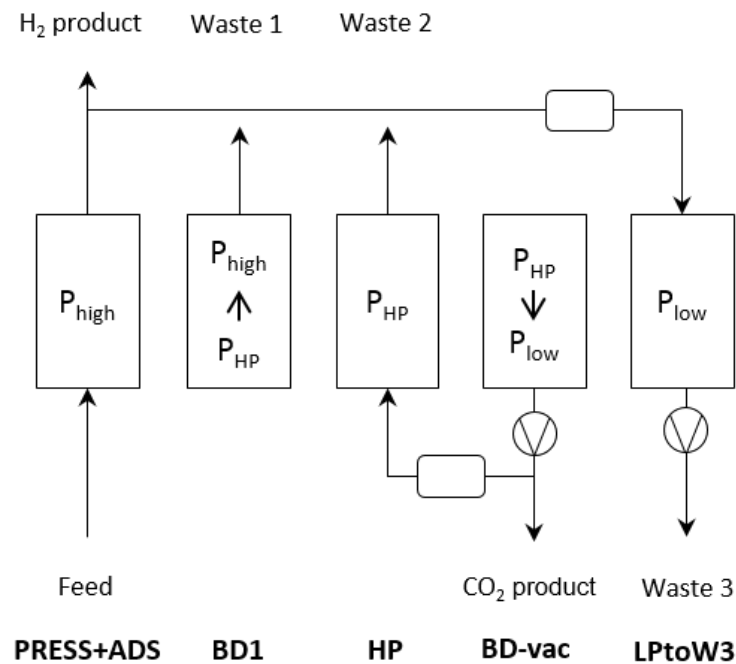


Figure 2.15: Simple Vacuum Pressure Swing Adsorption unit.

Different physical and thermodynamic constraints are derived starting from practical considerations on cycle requirements. As in Equilibrium theory applied to a simple Skarstrom cycle, a set of PDE has to be solved to find the expressions that relates the movement of the impurities' front to partial pressures, Henry's

constant, column length and velocities.

New constraints arise in this case for the reason that not only high hydrogen purity must be guaranteed but also very pure CO₂ has to be produced.

2.3.1 Equilibrium theory based constraints

Equilibrium theory, whose system of partial differential equation expressing the relationship between the adsorbed amount and the partial pressure is the starting point, is applied again to derive the mathematical expression of the coordinate of the impurities' front.

$$\begin{cases} \beta_{H_2} \frac{\partial(Py_{H_2})}{\partial t} + \frac{\partial(vPy_{H_2})}{\partial z} = 0 \\ \beta_{CO_2} \frac{\partial(Py_{CO_2})}{\partial t} + \frac{\partial(vPy_{CO_2})}{\partial z} = 0 \\ \beta_{CH_4} \frac{\partial(Py_{CH_4})}{\partial t} + \frac{\partial(vPy_{CH_4})}{\partial z} = 0 \end{cases}$$

Concerning pressurization and adsorption, the expression of the velocity can be derived assuming $y_{H_2} = 1$ and $y_{CO_2}, y_{CH_4} \ll 1$.

$$v = -\beta_{H_2} \frac{d(\ln P)}{dt} (z - L)$$

$$\beta_i \frac{\partial(\ln P)}{\partial t} + v \frac{\partial(\ln y_i)}{\partial z} = (\beta_{H_2} - \beta_i) \frac{\partial(\ln P)}{\partial t}$$

By means of the method of the characteristics, the partial differential equation can be solved.

$$\frac{dt}{ds} = \beta_i$$

$$\frac{dz}{ds} = v$$

$$\frac{d(\ln y_i)}{\partial z} = (\beta_{H_2} - \beta_i) \frac{\partial(\ln P)}{\partial t}$$

The solution of the system of equations is the following:

$$\ln \left(\frac{z_f - L}{z_i - L} \right) = -\beta' \ln \frac{p_f}{p_i}$$

Where $\beta' = \frac{\beta_{H_2}}{\beta_i}$.

Integrating the equation between known initial conditions ($t = 0, z = 0, p = p_L$), the coordinate of the generic impurity at the end of the pressurization can be expressed as:

$$z_{1,i} = L \left[1 - \left(\frac{p_H}{p_L} \right)^{-\beta'} \right] \quad (2.22)$$

The differential equation related to the adsorption step is slightly different:

$$\beta_i \frac{\partial y}{\partial t} + v \frac{\partial y}{\partial z} = 0$$

$$\frac{dt}{ds} = \beta_i$$

$$\frac{dz}{ds} = v$$

$$\frac{dy_i}{\partial z} = 0$$

$$z_f - z_i = \frac{v}{\beta_i} t$$

$$z_{2,i} = z_{1,i} + \frac{u_{\text{feed}} t_{\text{feed}}}{1 + \nu H_i} \quad (2.23)$$

The expression of the inlet stream velocity during the intermediate blowdown is the following:

$$v = -\beta_{H_2} \frac{d(\ln P)}{dt} z$$

$$\ln \frac{z_f}{z_i} = -\beta' \ln \frac{p_f}{p_i}$$

$$z_{3,i} = z_{2,i} \left(\frac{p_a}{p_H} \right)^{-\beta'} \quad (2.24)$$

From the heavy purge onwards, the assumption of having negligible amounts of carbon dioxide and methane is not valid anymore: the hypothesis of a stream which is constituted mainly from CO₂ is more suitable.

$$z_{4,i} = z_{3,i} + \frac{u_{\text{hp}} t_{\text{hp}}}{1 + \nu H_i} \quad (2.25)$$

On the one hand, the coordinate of the impurities during the heavy purge is not affected by this assumption, on the other hand the position of the front at the end of the vacuum blowdown is.

$$\ln \left(\frac{z_f - L}{z_i - L} \right) = -\beta'' \ln \frac{p_f}{p_i}$$

Where $\beta'' = \frac{\beta_{CO_2}}{\beta_i}$.

Integrating the equation between known initial conditions ($t = t_4, z = z_4, p = p_a$), the coordinate of the generic impurity at the end of the blowdown can be expressed as:

$$z_{5,i} = L + (z_{4,i} - L) \left(\frac{p_L}{p_a} \right)^{-\beta''} \quad (2.26)$$

Eventually, at the end of the last step, namely the light purge, the front's position is:

$$z_{6,i} = z_{5,i} + \frac{u_{lp} t_{lp}}{1 + \nu H_i} \quad (2.27)$$

The first goal of the cycle is that of producing a stream of pure hydrogen, therefore the first boundary of the operating region is related to the most critical component, namely methane, and it is constituted by all the points respecting the following relationship:

$$z_{2,CH_4} \leq L$$

$$m_{\text{feed}} = \frac{u_{\text{feed}} t_{\text{feed}}}{L} \leq (1 + \nu H_{CH_4}) \left(\frac{p_H}{p_L} \right)^{-\beta'} \quad (2.28)$$

Where $\beta' = \frac{\beta_{H_2}}{\beta_{CH_4}}$.

Secondly, the impurities must desorb and exit the column during the light purge (LP) so that the bed is clean and ready for the next cycle. This is translated in the constraint below:

$$z_{6,CO_2} \leq 0$$

$$L + (z_{4,CO_2} - L) \left(\frac{p_L}{p_a} \right)^{\beta''} - \frac{u_{lp} t_{lp}}{(1 + \nu H_{CO_2})} \leq 0$$

Where $\beta'' = \frac{\beta_{CO_2}}{\beta_{CH_4}}$.

$$m_{\text{LP}} \geq (1 + \nu H_{CO_2}) \left[1 + \frac{(z_{4,CO_2} - L)}{L} \left(\frac{p_a}{p_L} \right)^{\beta''} \right] \quad (2.29)$$

Assuming that the carbon dioxide front reaches the column bottom end means assuming that the bed is completely clean at the beginning of the new cycle.

The third constraint is once more related to the reflux between the adsorption and the light purge units:

$$\dot{n}_{\text{feed}} - \dot{n}_{\text{lp}} \geq 0$$

$$\frac{u_{\text{feed}} t_{\text{feed}}}{L} p_H \geq \frac{u_{lp} t_{lp}}{L} p_L$$

$$m_{lp} \leq m_{feed} \frac{p_H}{p_L} \quad (2.30)$$

A fourth boundary has to be respected considering that the cycle is meant to coproduce a pure carbon dioxide stream together with the hydrogen one; therefore the position of the methane front is subject to the following restriction:

$$z_{4,CO_2} \geq L$$

$$\frac{u_{feed} t_{feed}}{L} \left(\frac{p_H}{p_a} \right)^{\beta'''} + \frac{u_{hp} t_{hp}}{L} \geq (1 + \nu H_{CO_2}) \left(\frac{p_a}{p_L} \right)^{-\beta'''}$$

Where $\beta''' = \frac{\beta_{H_2}}{\beta_{CO_2}}$.

$$m_{feed} \left(\frac{p_H}{p_a} \right)^{\beta'''} + m_{hp} \geq (1 + \nu H_{CO_2}) \left[1 + \left(\frac{p_a}{p_L} \right)^{-\beta'''} - \left(\frac{p_a}{p_H} \right)^{-\beta'''} \right] \quad (2.31)$$

This last constraint is applied to carbon dioxide since, if it was applied to the methane's one, the column end would still present a high concentration in CH_4 . Therefore, assuming that CO_2 starts exiting the column at the end of the heavy purge step implies that all the methane has already left the adsorbent bed.

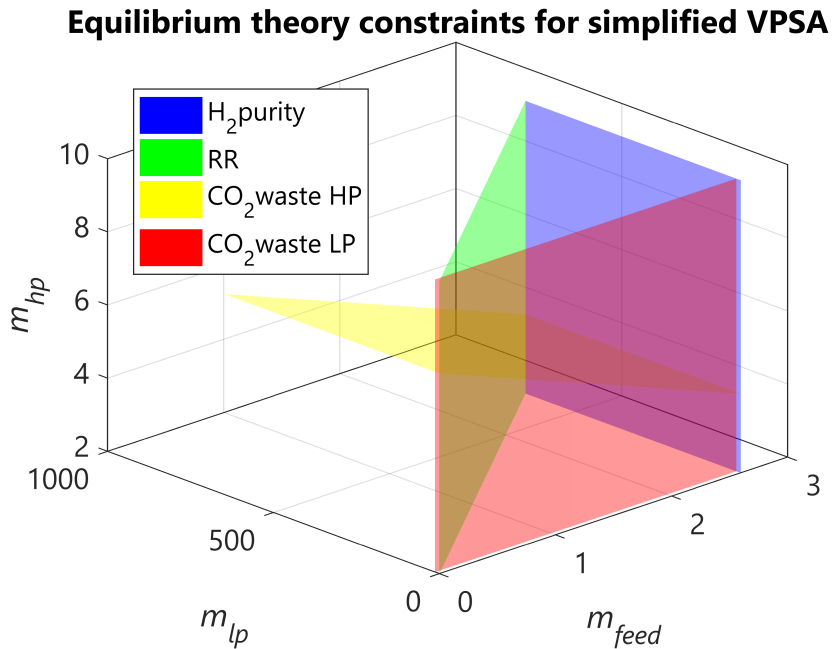


Figure 2.16: Equilibrium theory constraints for linear isotherm and simple Vacuum Pressure Swing Adsorption cycle.

Constraints 2.28, 2.29, 2.30 and 2.31 can be gathered to find the new operating envelope for this intermediate case. Although it is comparable with the one derived for the simple Skarstrom cycle, it presents few differences, among which the more evident is the shape of the domain: two-dimensional before, three-dimensional when vacuum is created. Figure 2.16 shows the four aforementioned boundaries in a three-dimensional space whose axes are represented by three dimensionless parameters m_s concerning the adsorption step (feed), the light purge step (lp) and the heavy purge (hp).

The parallelism between this plot and the one shown in Figure 2.7 is quite evident: even if the considered impurity is changed, the surface depicted in blue is the 3D extension of the blue line related to hydrogen purity for the Skarstrom case, same accounts for the green and the red planes, which concern the physical restriction on the recycle ratio and on the necessary purge respectively. What is new in these boundaries' derivation is the presence of a limitation related to the heavy purge, represented by the tilted yellow plane and accomplishing the need of having a high purity CO_2 stream.

It is worth noting that, in this case, the operating envelope is constituted by a semi-infinite parallelepiped instead of a plane; therefore, analogously to the previous case, points with the most promising operating conditions are enclosed within the three vertical planes and are free to move along the m_{hp} axis as long as they are on top of the yellow surface, as represented in the following graph.

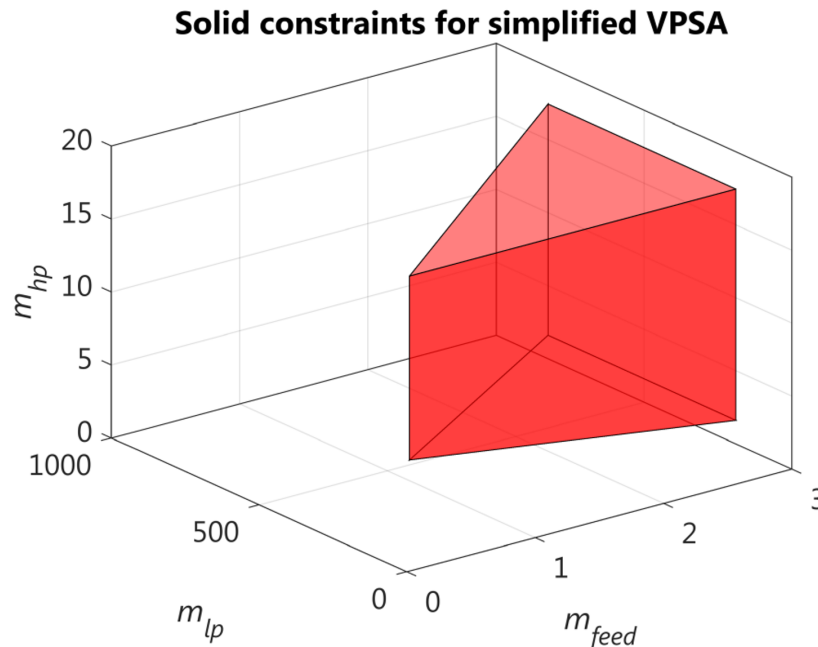


Figure 2.17: Operating envelope for a simple Vacuum Pressure Swing Adsorption cycle

2.3.2 FAST: full physical mathematical modelling

The approach of the technical scale-up is to adopt the methodology implemented for the simplest cycle and adapt it to the case of more complex cycles, starting from the simple VPSA. The full physical model already introduced in the previous chapter is exploited again to check for an analogy between analytical and simulated results. As done for the PSA, the time of the adsorption step is increased to move along the m_{feed} axis and the two recycle ratios are varied to investigate the behavior at higher m_{lp} and m_{hp} . Performing a parametric analysis on these three parameters and fixing desired requirements in terms of purities, new feasible and promising conditions, which are shown in the plot below, are obtained.

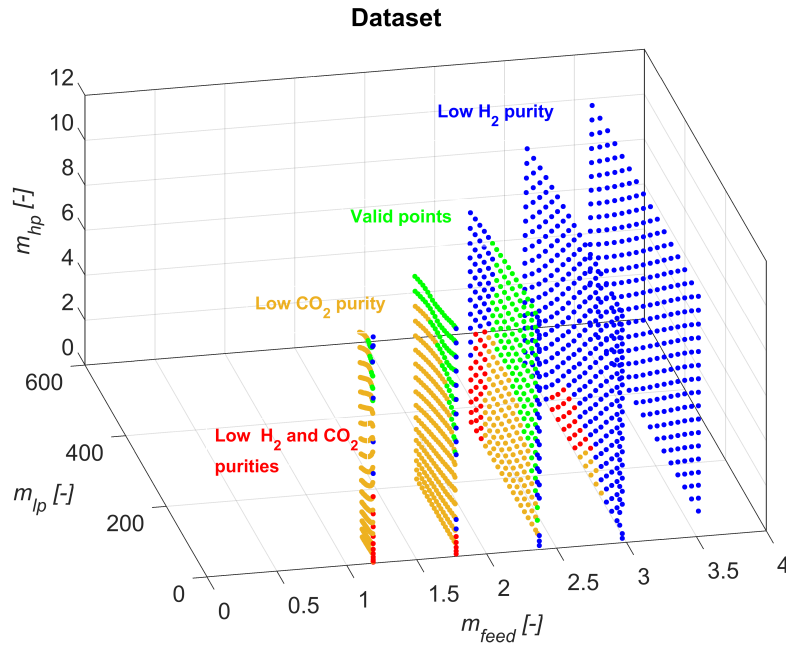


Figure 2.18: Results of full physical model applied to a simple VPSA cycle

Figure 2.18 presents around 6000 simulations in which the time of adsorption is modified from 10 to 100 seconds and the two recycle ratios from 5% to 85%. The green points are the ones for which hydrogen's purity reaches at least 99.5% while carbon dioxide's achieves 94%. Some boundaries can be clearly seen: in the first place, high values of m_{feed} cause the breakthrough of impurities leading to an evident drop in H_2 purity, in the second place, the adsorption bed does not experience a proper cleansing for little recycles, thus triggering the same consequences. Similarly, working with small heavy refluxes leads to insufficient purges

and to low CO₂ purities. Moreover, when increasing the heavy recycle, heat effects plays a role making hydrogen's purity fall.

Figure 2.19 integrates the analytical constraints with the optimal working conditions and clearly highlights the affinity between the mathematical and the physical models. These results present the starting point which to lean on for the analysis of a full and more articulated VPSA cycle that is successfully used in the laboratory.

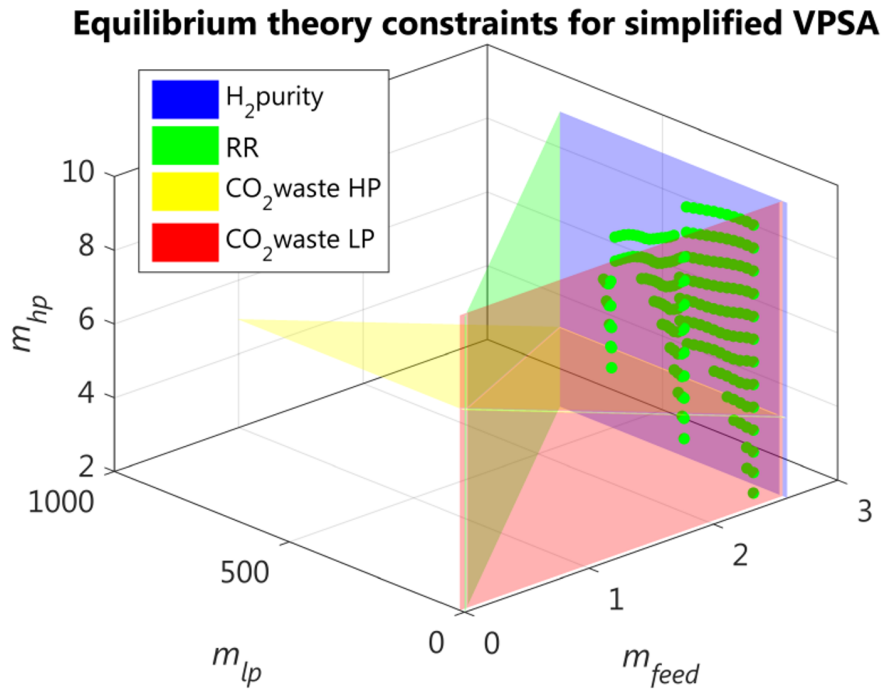


Figure 2.19: Integration of analytical constraints and full physical model results

Investigating the behavior of the key performance indicators when moving inside the feasible volume can be of great interest to understand which, among the several possible configurations, is the optimal one. As highlighted in Figure 2.20, longer adsorption times lead inevitably to opposite purity trends: hydrogen purity falls when the step is longer and impurities travel further and break through, the bed becomes thus more saturated with CO₂ and a purer stream of carbon dioxide is produced during the blowdown. Figure 2.20 shows that both the adsorption time and the light recycle consistently affect hydrogen's productivity and recovery but not carbon dioxide's ones, on the other hand the heavy recycle is representative of CO₂ performance indicators much more than H₂ ones. From the graphs the most promising region where to operate seems to be identified by high values of m_{feed} and low recycles, which lead, once the desired purities are achieved, to the highest productivities and recoveries for both products.

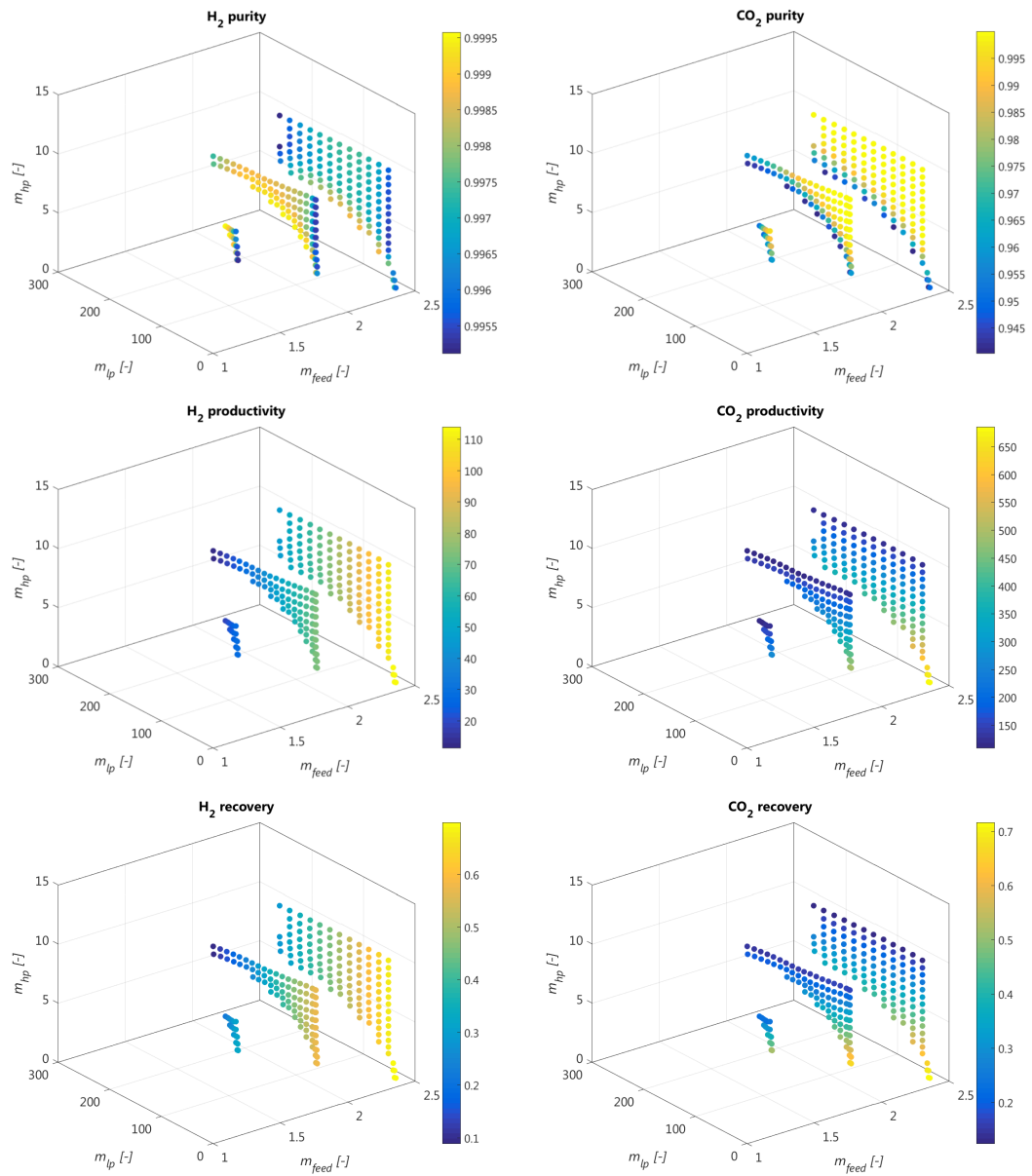


Figure 2.20: Products purities, productivities and recoveries for a simple VPSA

2.3.3 Technical scale-up challenges

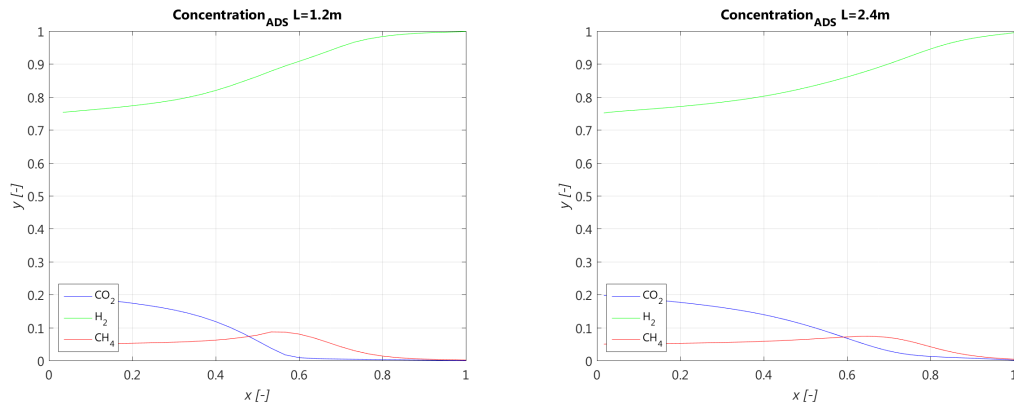
As a first approach, the technology is scaled assuming same operational conditions and therefore keeping the three crucial m dimensionless parameters unvaried: the decision of holding the residence time constant results in the need of changing the column length and the flowrates proportionally. As can be noticed from Table 2.5, some inconsistencies in the key performance indicators of the new and the old configurations are encountered when applying the simplified scale-up method used successfully for the Skarstrom cycle.

Table 2.5: Scale-up inconsistencies.

L_{bed}	Φ_{H_2}	Φ_{CO_2}	AP_{H_2}	AP_{CO_2}	r_{H_2}	r_{CO_2}
m	%	%	$kg_{H_2}/(kg_{ads}h_{cycle})$	$kg_{CO_2}/(kg_{ads}h_{cycle})$	%	%
0.6	99.95	92.30	59.06	252.96	41.02	39.27
1.2	99.93	97.53	54.88	235.08	43.08	31.58
2.4	99.81	99.18	42.77	183.21	45.85	18.48

It is possible to notice how, even controlling the ms it is not straightforward to have a direct control on the performances; the internal profiles are investigated for a deeper understanding. Since the profiles for 0.6 m and 1.2 m differ much less than the ones for 1.2 m and 2.4 m, only the plots of these last two lengths are provided and compared. Scaling up to higher lengths leads to flatter concentration profiles shifted towards the right (Figure 2.21), especially in the heavy purge and vacuum blowdown steps.

It is evident that the simplified approach already used for the PSA upscaling is not valid anymore and that the KPIs cannot be controlled only varying the flowrate proportionally to the bed length: to understand which additional parameter to change, an accurate investigation on the assumptions that differ between equilibrium theory and full physical model must be performed.



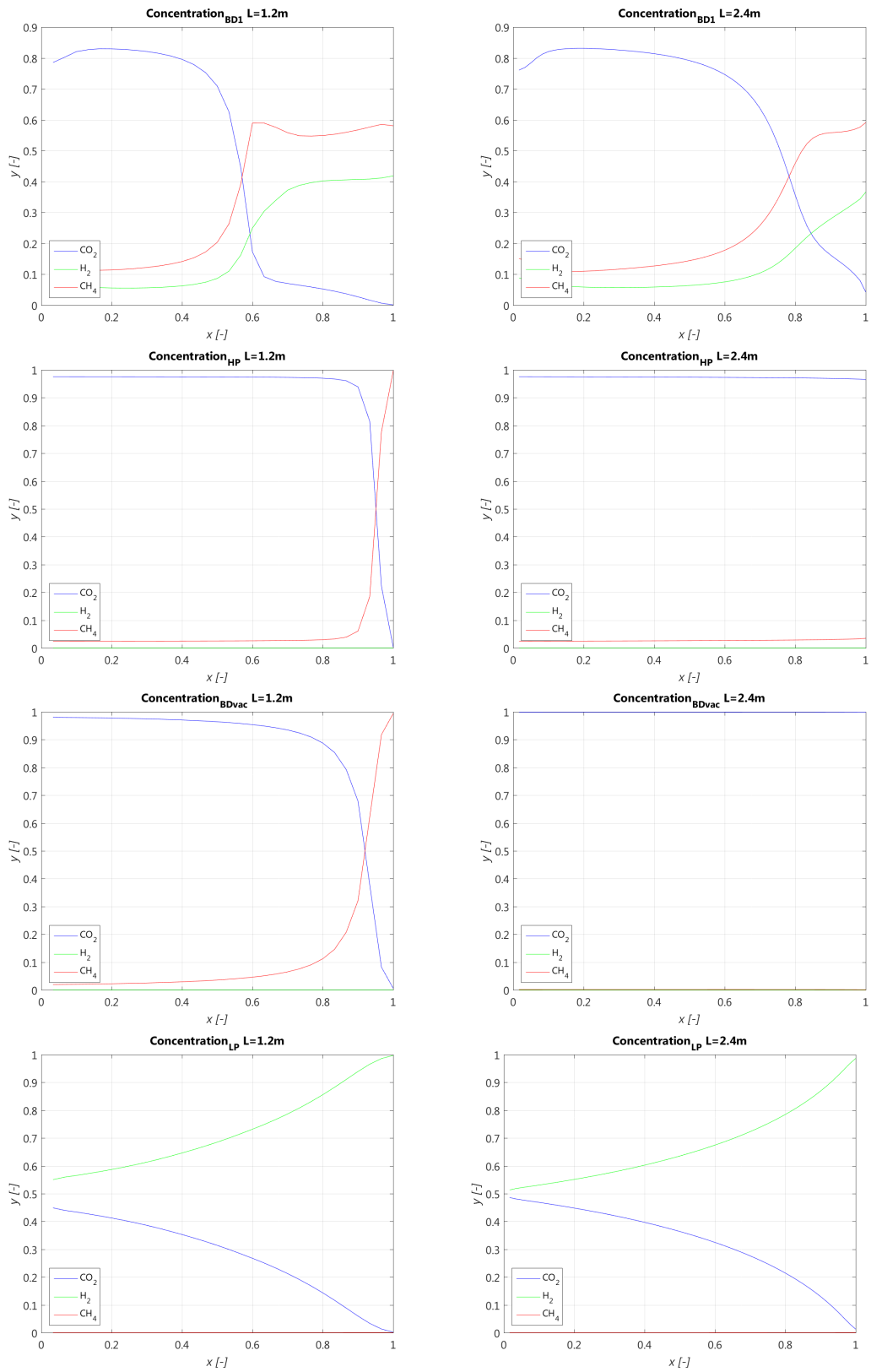
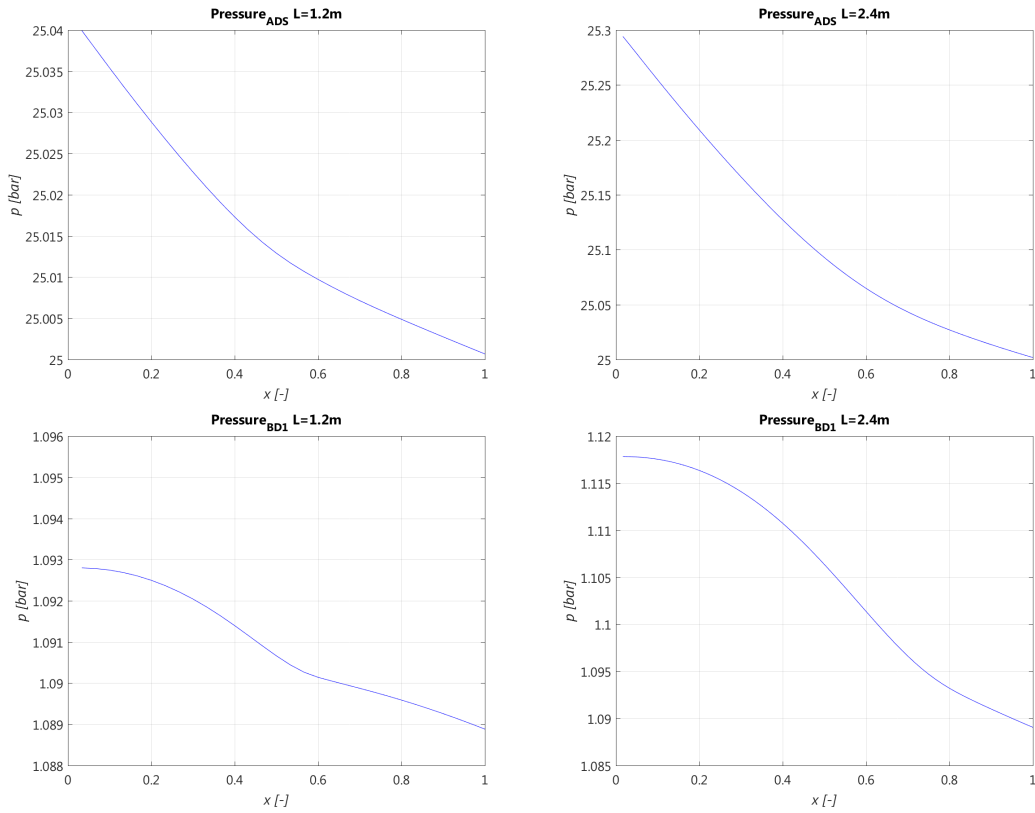


Figure 2.21: Dimensionless concentration profiles for old and new configurations

For every assumption, the dimensionless profiles of concentration, pressure and temperature are examined. On the one hand equilibrium theory provides an analytical solution, on the other hand the full physical model is based on a numerical discretization of the column; the solution of the model doesn't seem to be affected by this issue. Both isothermal and adiabatic behaviors are implemented to check whether the drop in performances might come from this assumption or not. The model is run neglecting mass transfer too to simulate the presence of a linear driving force but the results do not appear to change, therefore mass transfer limitations are discarded as cause for diversity. The linearity of the isotherm is not checked since assuming a non-linear isotherm would make all the analytically derived constraints change completely and therefore the two operating envelopes would not be comparable anymore. A final control is performed on the last different assumption, namely the presence of a pressure drop along the column described by Ergun's equation. Looking in fact at the pressure behavior at steady state depicted in Figure 2.22 it is worth noting that the pressure drop of all the steps in the new configuration is much greater than the one characterising the old configuration. The increase in pressure drop is particularly spotted in the real blowdown and in the light purge steps; it is possible to notice that, during these two phases of the cycle, the difference in pressure along the column almost doubles itself when doubling the length of the adsorbent bed.



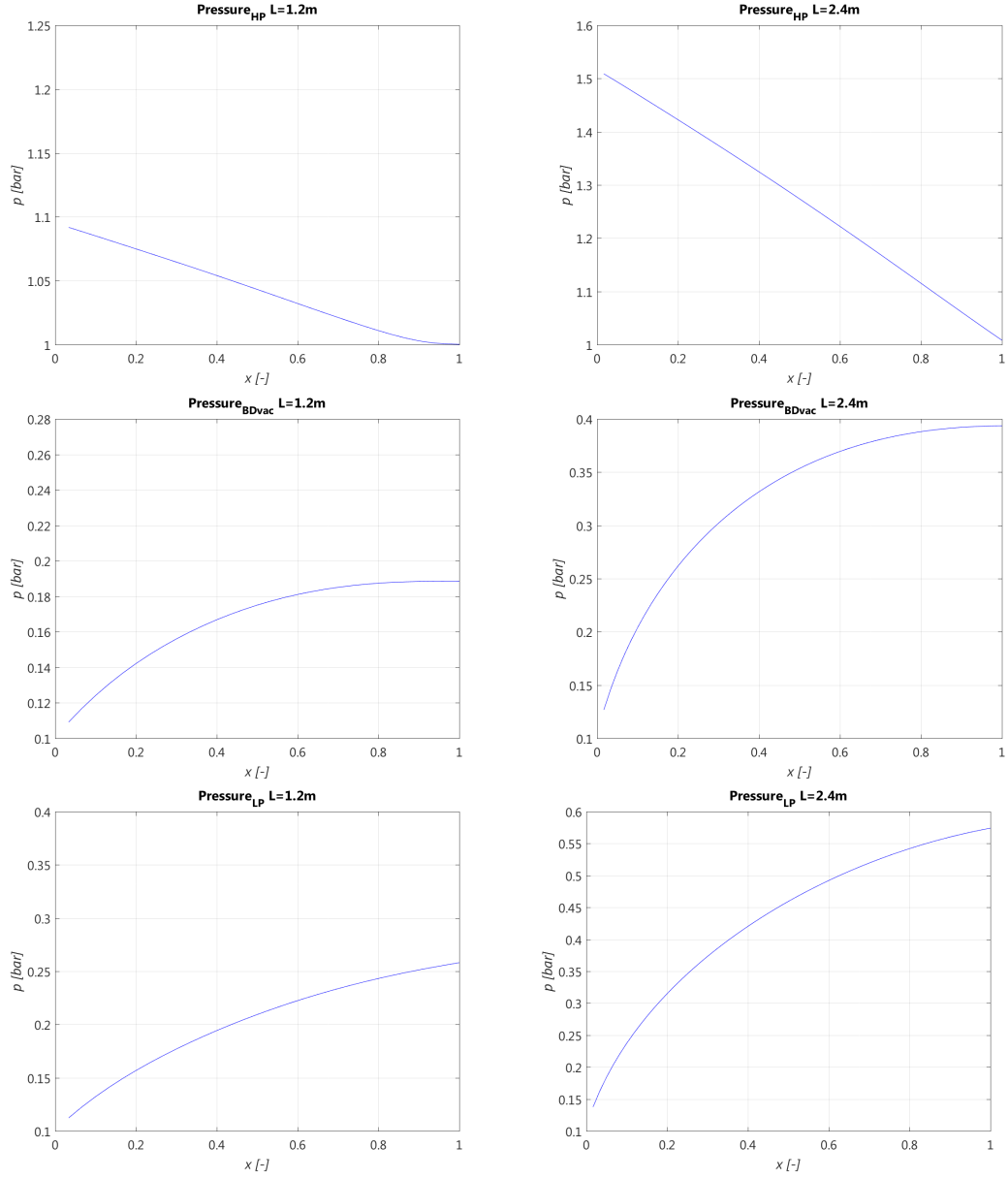


Figure 2.22: Pressure profiles for old and new configurations

Table 2.6: Scale-up results when longer blowdown times are set.

L_{bed}	Φ_{H_2}	Φ_{CO_2}	AP_{H_2}	AP_{CO_2}	r_{H_2}	r_{CO_2}
m	%	%	$kg_{H_2}/(kg_{ads}h_{cycle})$	$kg_{CO_2}/(kg_{ads}h_{cycle})$	%	%
0.6	99.92	92.54	23.80	101.94	40.99	44.70
1.2	99.95	94.97	26.08	111.69	41.93	56.35
2.4	99.84	97.67	28.51	122.12	43.62	68.78

To tackle the problem related to the most critical steps of the cycle, two different approaches are adopted. As a first attempt, longer blowdown times are set: 50 s instead of 20 s for the intermediate blowdown and 150 s rather than 30 s for the vacuum one. Extended times allow the BPR to be reached, making the concentration profiles look more similar, even though not yet equal. In Table 2.6 results extracted from the new simulations are collected, it is clear that an increase of the cycle times constrains all the key performance indicators to look more alike, despite the presence of a residual pressure difference. Since modifying the times of the two blowdown steps does not seem to be enough to reach the exact same performances with the new upscaled technology, Rota and Wankat’s methodology comes into play and the option of changing the adsorbent particle diameter according to their analytical relationships is investigated. In Table 2.7 are listed all the inputs concerning the feed stream and the operational characteristics of the cycle used to run the code with the aforementioned modifications.

Table 2.7: Most relevant inputs to simulations of simple VPSA cycle.

Parameter	Value	Units
H ₂	75	%
CO ₂	20	%
CH ₄	5	%
Q _{feed}	7x10 ⁻⁵	m ³ /s
p _H	25	bar
p _a	1	bar
p _L	0.1	bar
T _{feed}	308	K
p _{feed}	30	bar
t _{press+ads}	15	s
t _{BD1}	50	s
t _{hp}	20	s
t _{BDvac}	200	s
t _{lp}	40	s

It is worth noting that the scale-up method implemented for simple PSA processes is not suitable for more complex cycles such as vacuum integrated cycles; despite these difficulties, very similar performances can be reached with proper adaptations when increasing the dimensions of the apparatus (Table 2.8).

Table 2.8: Scale-up results when longer blowdown times are set and the particle size d_p is changed accordingly.

L_{bed}	d_p	Φ_{H_2}	Φ_{CO_2}	AP_{H_2}	AP_{CO_2}	r_{H_2}	r_{CO_2}
m	m	%	%	$kg_{H_2}/(kg_{ads}h_{cycle})$	$kg_{CO_2}/(kg_{ads}h_{cycle})$	%	%
0.6	0.001	99.95	94.27	30.26	129.59	41.84	53.59
1.2	0.002	99.95	94.56	30.69	131.47	41.98	55.71
2.4	0.004	99.95	95.29	31.91	136.68	42.33	61.02

2.4 Full VPSA

As mentioned in the introduction, the goal of the project is the scale-up of a full Vacuum Pressure Swing Adsorption unit, whose steps are explained in detail in Section 1.4.1. Several differences are implemented in this new cycle: first and foremost the feed composition is extended to five different components, whose concentrations are listed in Table 2.4, secondly three pressure equalization steps operating with a top to bottom configuration are added to increase the performance and to allow for continuous feed operation, eventually the light purge step is splitted into two steps for purity reasons.

Component	Value	Units
H ₂	75.81	%
CO ₂	16.31	%
CH ₄	3.03	%
CO	4.65	%
N ₂	0.2	%
Q _{feed}	2x10 ⁻⁵	m ³ /s

Table 2.9: Full VPSA feed stream composition

Since the mathematical boundaries are obtained starting from physical considerations on the most critical steps of the cycle and being these phases the same in the simple and full VPSA technologies, there is no need to derive again the constraints. It is therefore possible to run directly the Fortran code and compare the simulated results with the operating region already found for the simple VPSA. Same conceptual boundaries are found when using a full physical model, as a consequence, the simulated operating windows of simple and full VPSA present a very similar shape. The system runs into the same drawbacks when overcoming similar limitations, therefore the considerations explained above for the simple cycle are still valid for the comprehension of Figure 2.23.

In the advanced cycle pressurization and adsorption are not gathered in one single unit anymore, they are splitted into different steps instead: unit 1 represents the product pressurization, units 2 to 5 represent the different stages of the adsorption

phase. In this case the parametric analysis is performed varying the time of unit 5, which is the most significant when considering the adsorption step, together with the two recycle ratios, as in the previous case. The overall adsorption time is evaluated summing up all the durations of units 2 to 5.

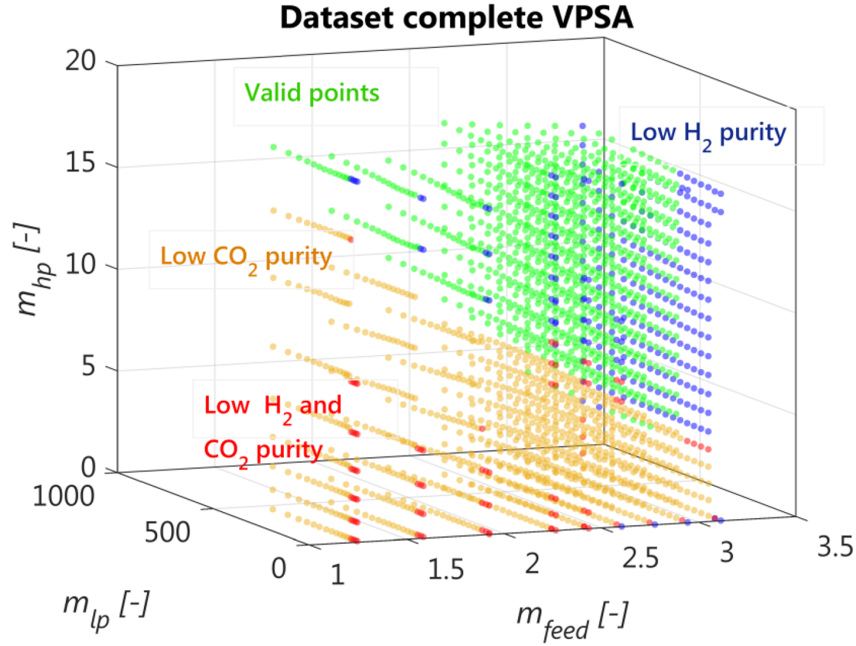


Figure 2.23: Results of full physical model applied to a simple VPSA cycle

The points shown in green represent operating conditions which allow to accomplish at least 99.7% hydrogen purity and 95.5% carbon dioxide's. The validity of the new integrated scale-up method has been already assessed for the intermediate case of the simple VPSA cycle, the idea is thus to replicate the analysis on the full VPSA starting from a point chosen from previous optimizations.

As shown in Figure 2.24, the simulator searches for the optimal cycle moving along a curve in the plane (m_{feed} , m_{lp}). All points are optimal and allow to achieve remarkable performances, therefore, on the basis of purity considerations, one operating condition, represented in the plot by the black star, is selected to apply the scale-up method.

When plotting the KPIs, exact same trends are found (see Figure 2.25) and thus similar considerations can be done.

The most promising operating region appears to be in the bottom-right corner of the plot, thus including all the points with high m_{feed} and low m_{lp} and m_{hp} .

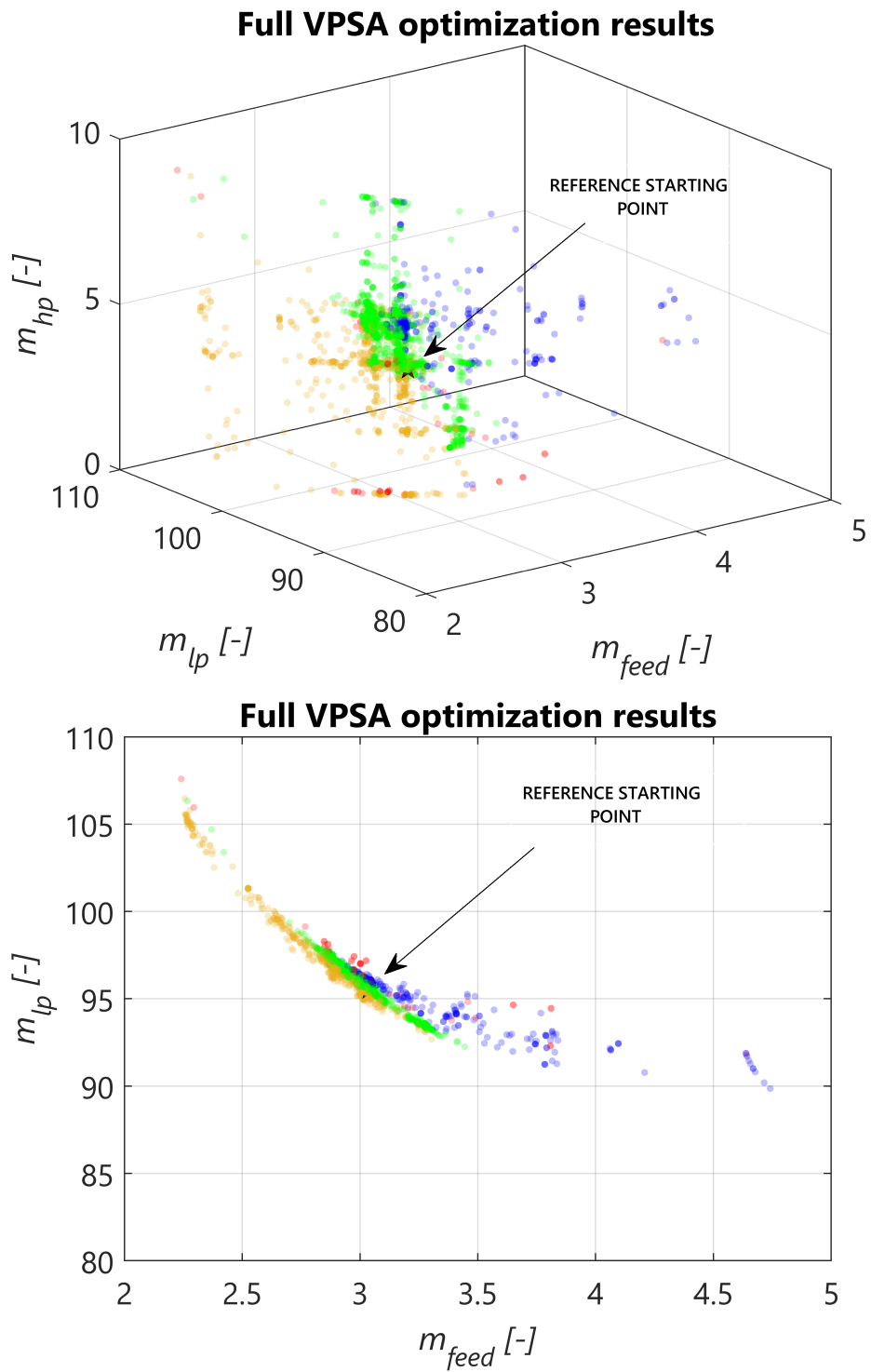


Figure 2.24: Optimization results and reference starting point for the full VPSA upscaling.

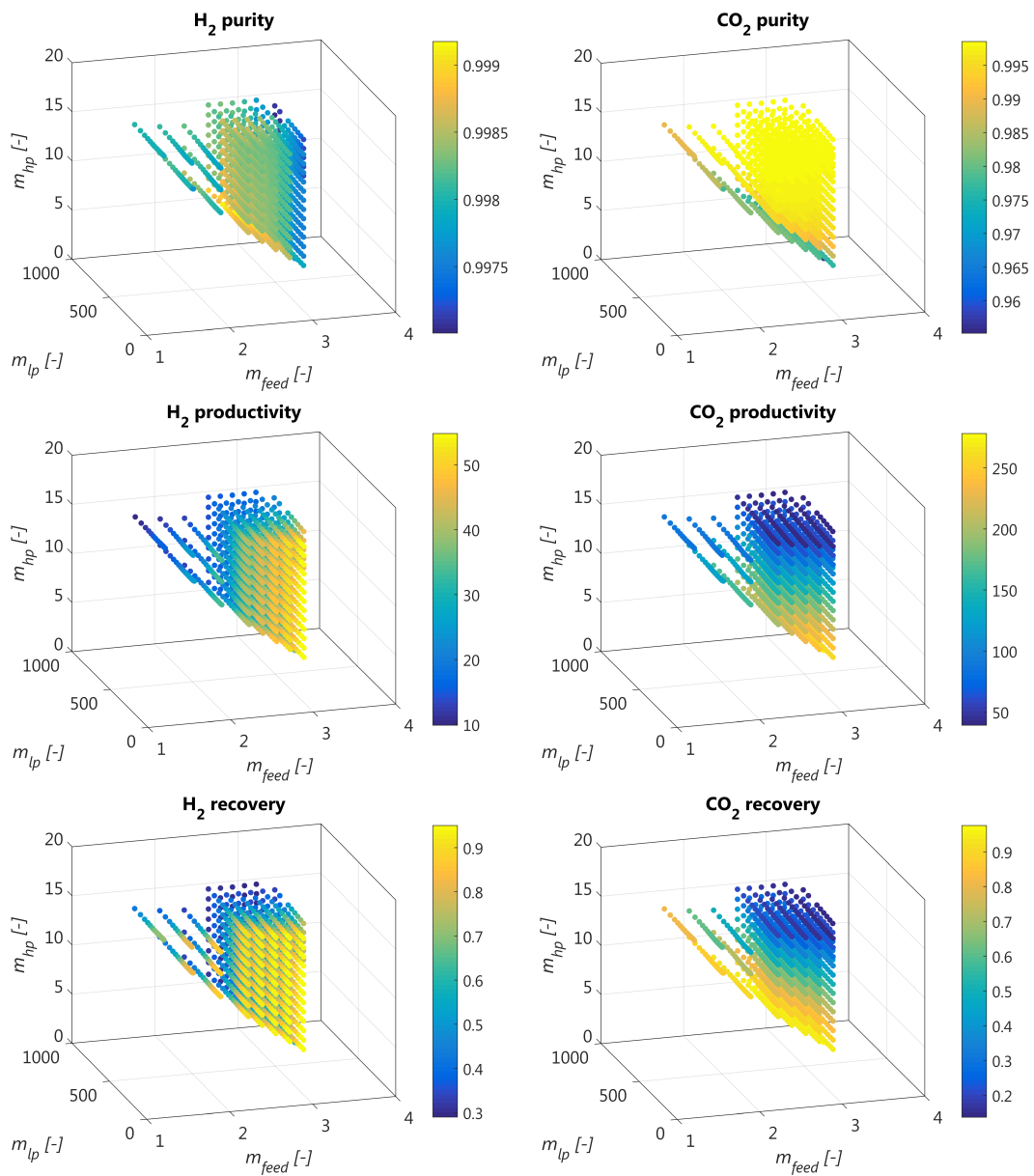


Figure 2.25: Key performance indicators for a full VPSA

Upscaling such an advanced technology with a relatively analytical approach is not trivial: the commercial availability of the adsorbent material must be taken into account when scaling the particle diameter. Since particles with diameters up to 0.005 m are quite common to find and this dimension seems to be the biggest in the market, the choice of using this "maximum size" instead of bigger particles for a bed length of 3.6 m is made. For the same reason the bed is scaled up to three times the original length and longer columns are not investigated. When working with a 3.6 m length bed made of 5 mm adsorbent particles it is possible to notice that hydrogen purity experiences a slight reduction, therefore adsorption time is reduced by 0.5 seconds to counteract this effect.

L_{bed}	d_p	Φ_{H_2}	Φ_{CO_2}	AP_{H_2}	AP_{CO_2}	r_{H_2}	r_{CO_2}
m	m	%	%	$kg_{H_2}/(kg_{ads}h_{cycle})$	$kg_{CO_2}/(kg_{ads}h_{cycle})$	%	%
1.2	0.002	99.978	97.095	36.47	180.37	93.17	97.39
2.4	0.004	99.977	96.766	36.44	180.20	93.17	97.37
3.6	0.005	99.974	96.05	35.98	177.84	93.01	97.17

Table 2.10: Scale-up results for a full cycle VPSA.

The first goal of the project, whose results are presented in Table 2.4, is successfully achieved: a suitable method for the upscaling of pressure swing adsorption units is developed and the columns can be scaled up to typical industrial heights maintaining the same optimal performances achieved by means of optimizations on the cycle of a pilot scale VPSA.

Chapter 3

Design and sizing of a VPSA plant

At the interface of technical and economic evaluations is the equipment listing and sizing. To have a reliable cost estimate it is necessary to accurately evaluate which components might be needed in the commercial plant, how many of them, how many spare and redundant systems, how long has to be the connecting piping system. To this end, Aspen Capital Cost Estimator software is used for the equipment design and subsequently for the cost estimate.

The project takes into consideration four different configurations, considering two different bed lengths and two different schedulings of the cycle, as shown in Table 3.1. The different cases are further explained in the following section.

Table 3.1: Considered plant configurations.

Cases	2.4 m	3.6 m
10 columns	B	A
16 columns	D	C

A VPSA plant is typically characterized by the presence of:

- several adsorption beds gathered in trains, whose number depends on the required hydrogen product and on the scheduling
- intermediate tanks for the storage of H₂ and CO₂, to ensure indirect recycles
- a waste buffer tank
- vacuum pumps for the carbon dioxide withdrawal
- a set of automatically operated valves, to allow for the synchronization of the columns

- a piping system for the transport of the different streams

Column 1	Ads								
Column 2	PE 1	PE 2	PE 3	BD1			HP		
Column 3	HP		BD-vac						
Column 4	BD-vac								
Column 5	BD-vac						LP 1		
Column 6	LP 1								
Column 7	LP 1		LP 2						
Column 8			PE 3						
Column 9		PE 2							
Column 10	PE 1								Press

Figure 3.1: 10 columns scheduling.

Column 1	Ads								
Column 2	Ads								
Column 3	PE 1	PE 2	PE 3	BD1					
Column 4	BD1	HP							
Column 5	HP		BD-vac						
Column 6	BD-vac								
Column 7	BD-vac								
Column 8	BD-vac								
Column 9	BD-vac								
Column 10	BD-vac						LP 1		
Column 11	LP 1								
Column 12	LP 1								
Column 13	LP 1		LP 2						
Column 14			PE 3						
Column 15		PE 2							
Column 16	PE 1								Press

Figure 3.2: 16 columns scheduling.

The synchronization of the adsorption beds is the starting point for the specification of the amount of the foreseen equipment: it is thereby important to have a clear understanding of the two different schedules of the cycle. Figure 3.1 and 3.2 graphically represent how all the adsorption columns are synchronized. The block depicted in Figure 3.1 has a reference time equal to the time of adsorption, moreover idle times are inserted to make the pressure equalization steps match perfectly and to ensure continuous feed to the plant. The block is then repeated ten times, shifting every time the column which undergoes a specific step: in this way, each column experiences a whole cycle. For instance, during the second block, column 2 will perform the adsorption, column 3 will experience the three pressure equalizations, the intermediate blowdown and part of the heavy purge and so on until the complete cycle is performed and the first block is repeated again.

Same accounts when 16 columns are used.

For the sake of simplicity, here the P&ID of the VPSA plant (Figure 3.3) will be presented to give the reader an idea of the plant layout. The design and sizing of all the components will be further explained in the following sections.

3.1 Overdesign and safety margins

As a rule of thumb, for pressure integrity reasons, a vessel must be designed to withstand the maximum pressure to which it is likely to be subjected in operation and at which the relief valves are set [15]. In accordance with the design code, the design pressure is generally set 5% to 10% above the normal operating pressure. In this project, a margin of 10% is conservatively fixed to avoid spurious intervention of the safety systems and face any possible change in operating conditions.

The maximum allowable stress originates from the maximum temperature the material can suffer, the material's strength inevitably dropping when increasing the temperature. A margin of 10°C is applied on the maximum operating temperature (MOT) experienced during the cycle [15].

Moreover, a suitable material must be chosen to ensure a proper fabrication as well as compatibility with the process environment [15]: here, all columns and tanks are designed to be constructed from stainless steel 316 (SS316), whose content in molybdenum improves its resistance to pitting, corrosion and temperature.

Concerning the storages, they are designed to withstand not only an increase in pressure but also any unexpected rise in gas volume due to thermodynamic deviations.

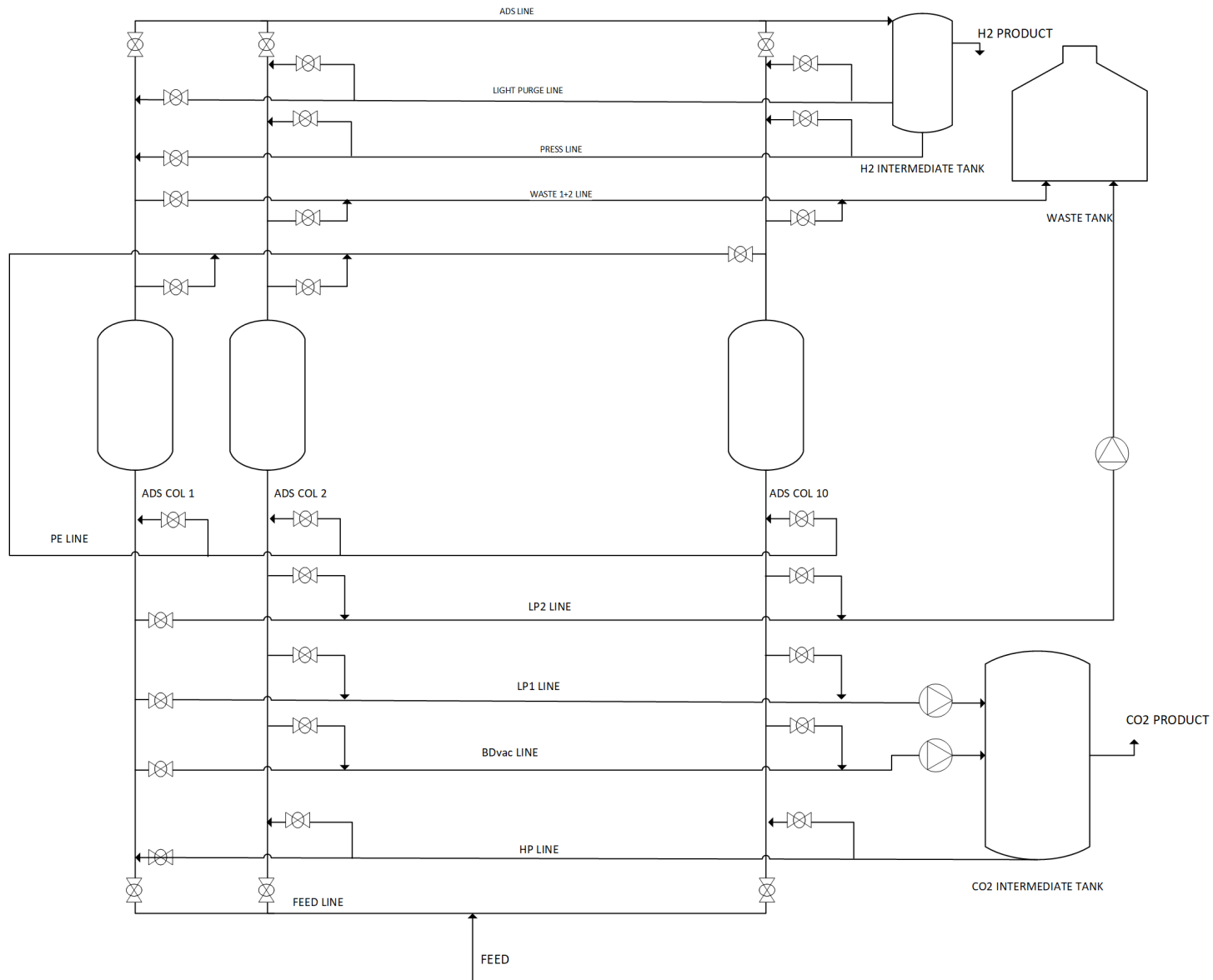


Figure 3.3: P&ID of a 10 columns adsorption plant for hydrogen production and carbon capture.

3.2 Adsorption column design

To allow the plant to process typical industrial flowrates, not only a scale-up is needed but also a scale-out. The former, already performed in the previous chapter, allows to feed a greater amount into the column exploiting velocities of the stream which are very close to the fluidization velocity; the latter instead, plays a role when it is not possible to increase the column height anymore but still consistent flowrates have to be fed.

Generally, the adsorption vessel can be sized as a cylindrical pressure vessel, therefore starting from two lengths of the adsorption bed, namely 2.4 m and 3.6 m, the diameter of the column is increased to fulfill a hydrogen demand of 100000 Nm³/h (8994 kg/h), as retrieved from IEAGHG techno-economic report [14].

The column diameter is determined on the basis of the scheduling of the cycle, that affects the total hydrogen productivity, reducing it with respect to the one obtained with an infinite number of columns.

Two cases are analysed:

- 10 columns, which accomplishes 67% of the ideal productivity and is chosen because it is the minimum number of columns required to work with continuous feed conditions and three pressure equalization steps.
- 16 columns, which is the number of beds in which the feed stream must be split to reach the highest productivity (84% of the ideal one)

In both cases the evaluation is performed as follows, starting from the computation of the amount of hydrogen produced using all the available columns:

$$\dot{m}_{H_2, \text{prod}, \text{tot}, \text{ideal}} = 8994 \frac{\text{kg}}{\text{h}} = 2.4983 \frac{\text{kg}}{\text{s}}$$

$$m_{H_2, \text{prod}, \text{tot}, \text{ideal}} = \dot{m}_{H_2, \text{prod}, \text{tot}, \text{ideal}} t_{\text{ads}} = 190.95 \frac{\text{kg}}{\text{cycle}}$$

Where t_{ads} is the effective production time, sum of units 2 and 5, equal to 76.431 s.

Knowing the amount of hydrogen produced in the plant with no scheduling for a defined length, namely 0.0047 kg/h for a 2.4 m bed length and 0.0067 kg/h for 3.6 m, the actual production can be calculated for the standard bed diameter that is not yet scaled out.

- 2.4 m:

$$m_{H_2, \text{prod}, \text{tot}, 10 \text{ columns}} = m_{H_2, \text{prod}, \text{tot}, \text{ideal}} \cdot \eta_{10 \text{ columns}} = 2.99 \cdot 10^{-3} \frac{\text{kg}}{\text{cycle}}$$

$$m_{H_2, \text{prod}, \text{tot}, 16 \text{ columns}} = m_{H_2, \text{prod}, \text{tot}, \text{ideal}} \cdot \eta_{16 \text{ columns}} = 3.76 \cdot 10^{-3} \frac{\text{kg}}{\text{cycle}}$$

- 3.6 m:

$$m_{H_2, \text{prod, tot, 16 columns}} = m_{H_2, \text{prod, tot, ideal}} \cdot \eta_{16 \text{ columns}} = 4.45 \cdot 10^{-3} \frac{\text{kg}}{\text{cycle}}$$

$$m_{H_2, \text{prod, tot, 16 columns}} = m_{H_2, \text{prod, tot, ideal}} \cdot \eta_{16 \text{ columns}} = 5.60 \cdot 10^{-3} \frac{\text{kg}}{\text{cycle}}$$

Being the produced amount directly proportional to the fed one and being this last one proportional to the column length, once the desired production flowrate is defined, it is possible to evaluate the diameter needed to process the feed-stream. The velocity of the feed must be kept constant when increasing the column diameter to reach the same KPIs.

$$Q_{\text{feed, scaled}} = v \cdot \pi \frac{D_{\text{scaled}}^2}{4}$$

$$Q_{\text{feed, lab}} = v \cdot \pi \frac{D_{\text{lab}}^2}{4}$$

$$\frac{m_{H_2, \text{prod, tot, scaled}}}{m_{H_2, \text{prod, tot, ideal}}} = \frac{Q_{\text{feed, scaled}}}{Q_{\text{feed, lab}}} = \frac{D_{\text{scaled}}^2}{D_{\text{lab}}^2}$$

Therefore

$$D_{\text{scaled}} = D_{\text{lab}}^2 \cdot \sqrt{\frac{m_{H_2, \text{prod, tot, scaled}}}{m_{H_2, \text{prod, tot, ideal}}}}$$

In Table 3.2 the resulting diameters are presented for the four different cases.

Table 3.2: Adsorbent bed diameter assuming a single train.

Cases	2.4 m	3.6 m
10 columns	6.31 [m]	5.14 [m]
16 columns	5.63 [m]	4.59 [m]

The assumption of a minimum aspect ratio L/D of 1, where L is the tangent to tangent height of the column (see Figure 3.4), is made. In reality though, aspect ratios are higher to ensure a more efficient use of the adsorbent.

$$L_{2.4\text{m}} = 2.4 + 0.125 \cdot 2 \cdot 2.4 + 0.4 = 3.4\text{m}$$

$$L_{3.6\text{m}} = 3.6 + 0.125 \cdot 2 \cdot 3.6 + 0.4 = 4.9\text{m}$$

Therefore, when the column diameter is greater than this height, the number of trains N is increased. Since the total processed flowrate and the velocity of the

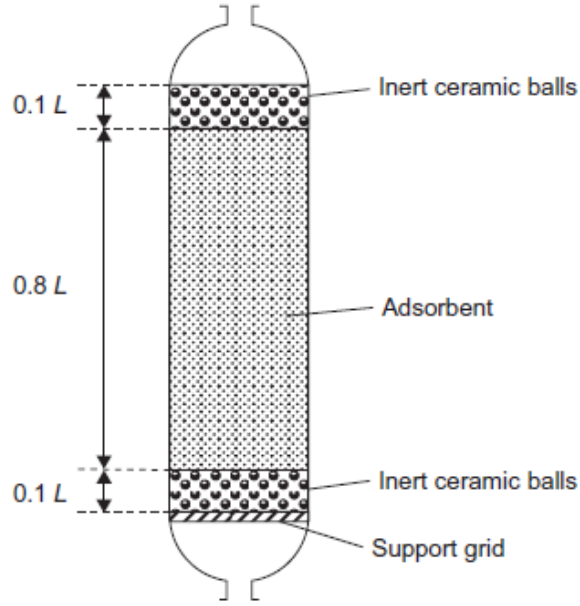


Figure 3.4: Adsorption vessel internals. [15]

inlet stream must be unvaried to obtain the same performances, the new diameter is calculated as:

$$Q_{\text{feed,scaled}} = v \cdot \pi \frac{D_{\text{scaled,1 train}}^2}{4} = N \cdot v \cdot \pi \frac{D_{\text{scaled,N trains}}^2}{4}$$

$$D_{\text{scaled,N trains}} = \frac{D_{\text{scaled,1 train}}}{\sqrt{N}}$$

The head is usually left empty and up to 20% of the volume between the tangent lines of the vessel is packed with inert ceramic balls to ensure a uniform distribution of the flow at the two extremities of the bed and to prevent "fingering" of contaminant through the bed [15].

Four cases are thus taken into consideration for the economic assessment:

Table 3.3: Different configurations for the economic assessment

Case	L_{bed}	Trains	$D_{\text{scaled,N trains}}$	Scheduling
	m	-	m	-
A	3.6	2	3.64	10 columns
B	2.4	5	2.82	10 columns
C	3.6	2	3.24	16 columns
D	2.4	4	2.82	16 columns

3.3 Intermediate storage tanks design

The sizing of the intermediate CO₂ and H₂ storage tanks is closely related to the type of scheduling adopted in the process. The time profiles of the involved units have to be investigated and a mass balance must be performed to evaluate the needed capacity and the initially stored amount of moles.

It is worth noting that all four hypothetical configurations have been sized to produce the same amount of hydrogen, therefore only the scheduling will matter when designing the intermediate storages. This means that once the cycle schedule is selected and the productivity is defined, the column dimensions are not relevant for the definition of the storages' size.

Figure 3.5 reports the inlet and outlet streams characterizing the dynamics of the storage, to properly design the tanks a mass balance has to be performed at each time instant.

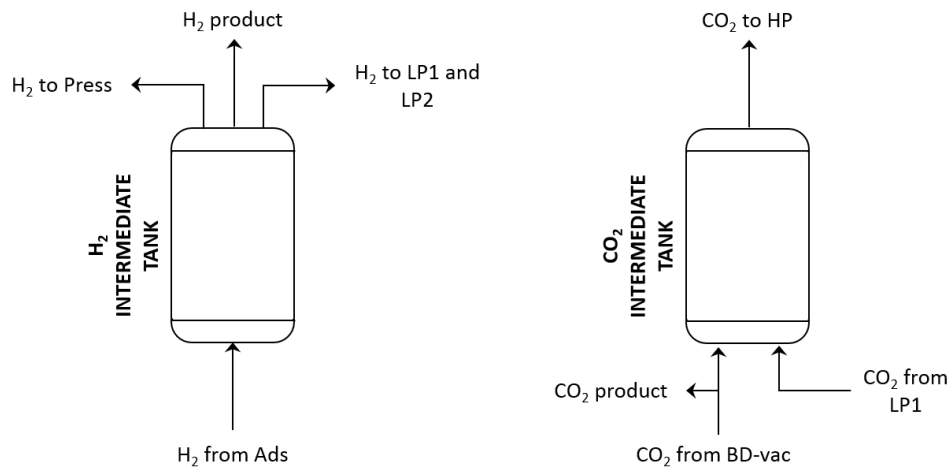


Figure 3.5: Graphic representation of the streams entering and exiting the intermediate storage tanks.

- 10 columns

Plots 3.6 and 3.7 show, for all the columns connected to the tank, the production (pedix "p") and the consumption (pedix "c") in terms of molar flowrate entering and exiting the storage, represented by continuous and dashed lines respectively.

Concerning the hydrogen plot it is possible to notice that it gathers information about the adsorption, pressurization and light purge steps.

For a better understanding, a mass balance over the tank can be identified: H₂ production is almost continuous over the entire adsorption time (units 2 to 5). All the hydrogen exiting the columns at the beginning of the adsorption step (unit 2) is used to pressurize another column when needed;

the amount produced further on (unit 3) is transported to a final tank before being sent to the grid; the stream exiting the columns during unit 4 is entirely used for the light purge; eventually, part of the amount produced during unit 5 is consumed as the actual final product and the rest is recycled back to perform the light purge. It is worth noting that all the products of the adsorption step flow into the intermediate storage tank, where they are retained until they are sent to other tanks or columns. A cumulative of production and demand is represented in yellow and is referred to as the basis for the final design. The hydrogen storage is sized for an average pressure of 25 bar and a temperature of 308 K; as already mentioned in the paragraph related to safety margins, the tank's capacity is increased by 20% of the theoretical stored volume.

Same reasoning applies concerning the carbon dioxide storage, the only difference is that the actual product does not enter the tank but it is split before due to purity reasons. The only consumption is performed by columns 2 and 3 which undergo the heavy purge. The production instead is ensured on the one hand by the recycled amount from the vacuum blowdown (performed by columns 5 to 10), on the other hand by the outlet stream of the first light purge (ensured by columns 10 to 13).

The vessel presents average pressure and temperature of 1 bar and 468.5 K with a final volume of 297.41 m³. The reason why this tank is consistently bigger than the previous one is that the gas is stored at a much lower pressure.

- 16 columns

Being the number of synchronized columns higher than the previous case, graphs 3.8 and 3.9 appear more complicated but the aforementioned considerations still accounts, therefore they can be read in the same way.

If the storages were empty at the beginning of the cycle, they would experience a vacuum after the first seconds, for this reason it is preferable to have already an amount of gas stored when a new cycle starts. This can be seen from the yellow axis in the second plots of Figures 3.6 and 3.7. Concerning the hydrogen storage for a 10 columns scheduling, an initial amount of around 1×10^4 moles is ensured to overcome the aforementioned downsides; same accounts for the CO₂ storage, which requires 1.1×10^4 moles. When assuming a 16 columns scheduling, the moles inside the hydrogen and carbon dioxide storages are 1.35×10^4 and 5.8×10^3 respectively.

Table 3.4 and 3.5 summarize the evaluated design data for the two intermediate storages.

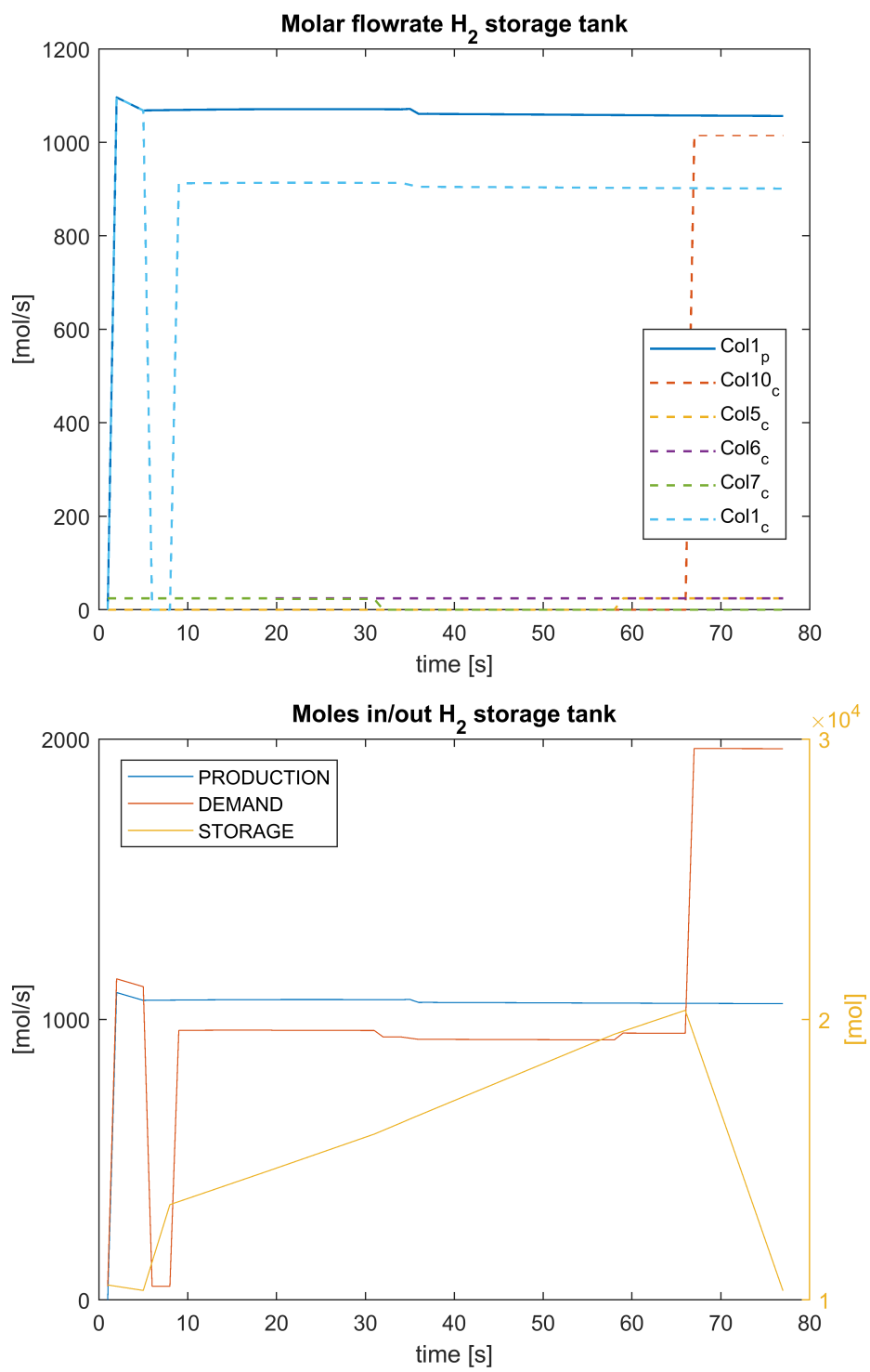


Figure 3.6: Hydrogen intermediate storage tank, case with 10 columns.

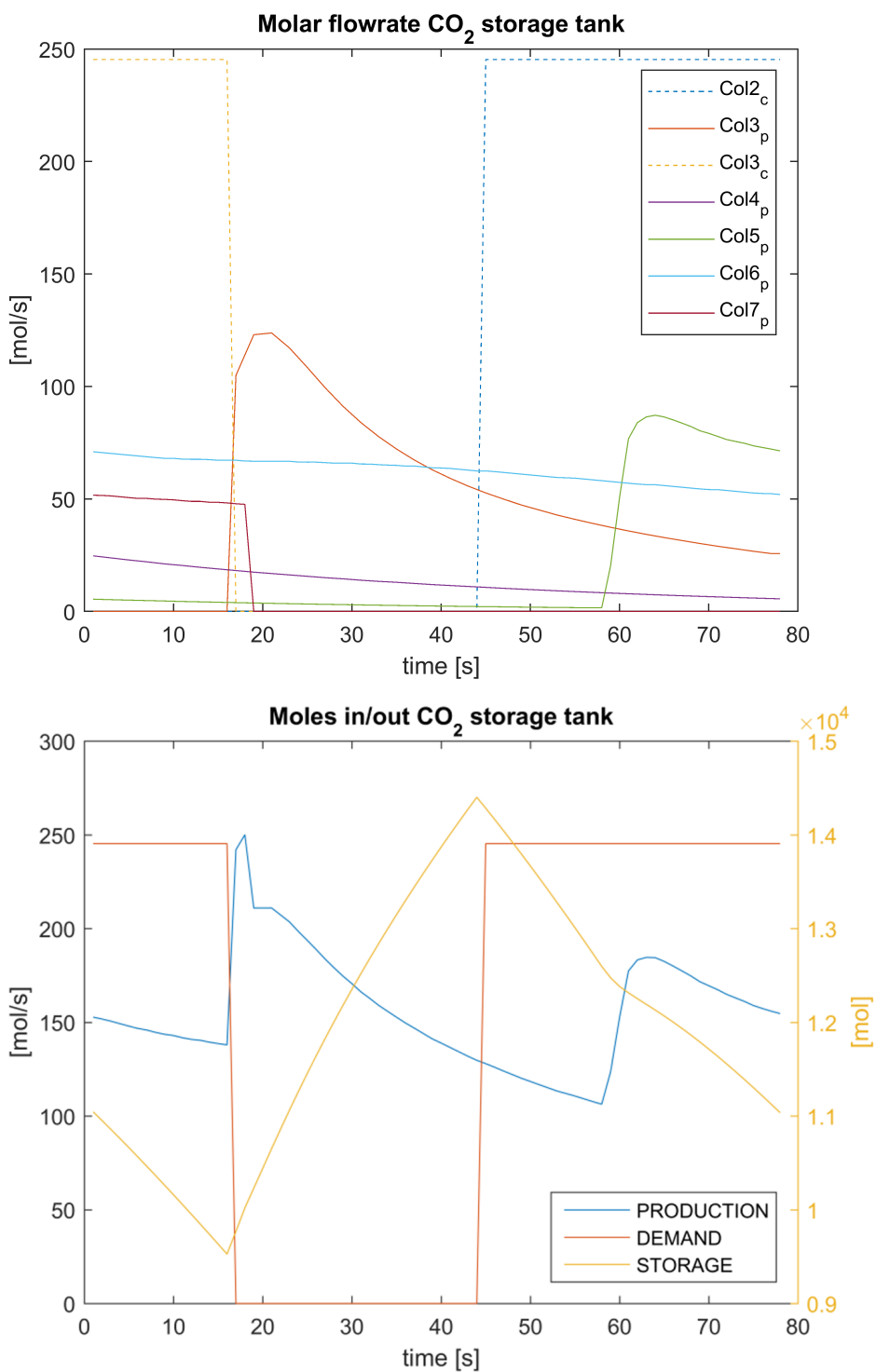


Figure 3.7: Carbon dioxide intermediate storage tank, case with 10 columns.

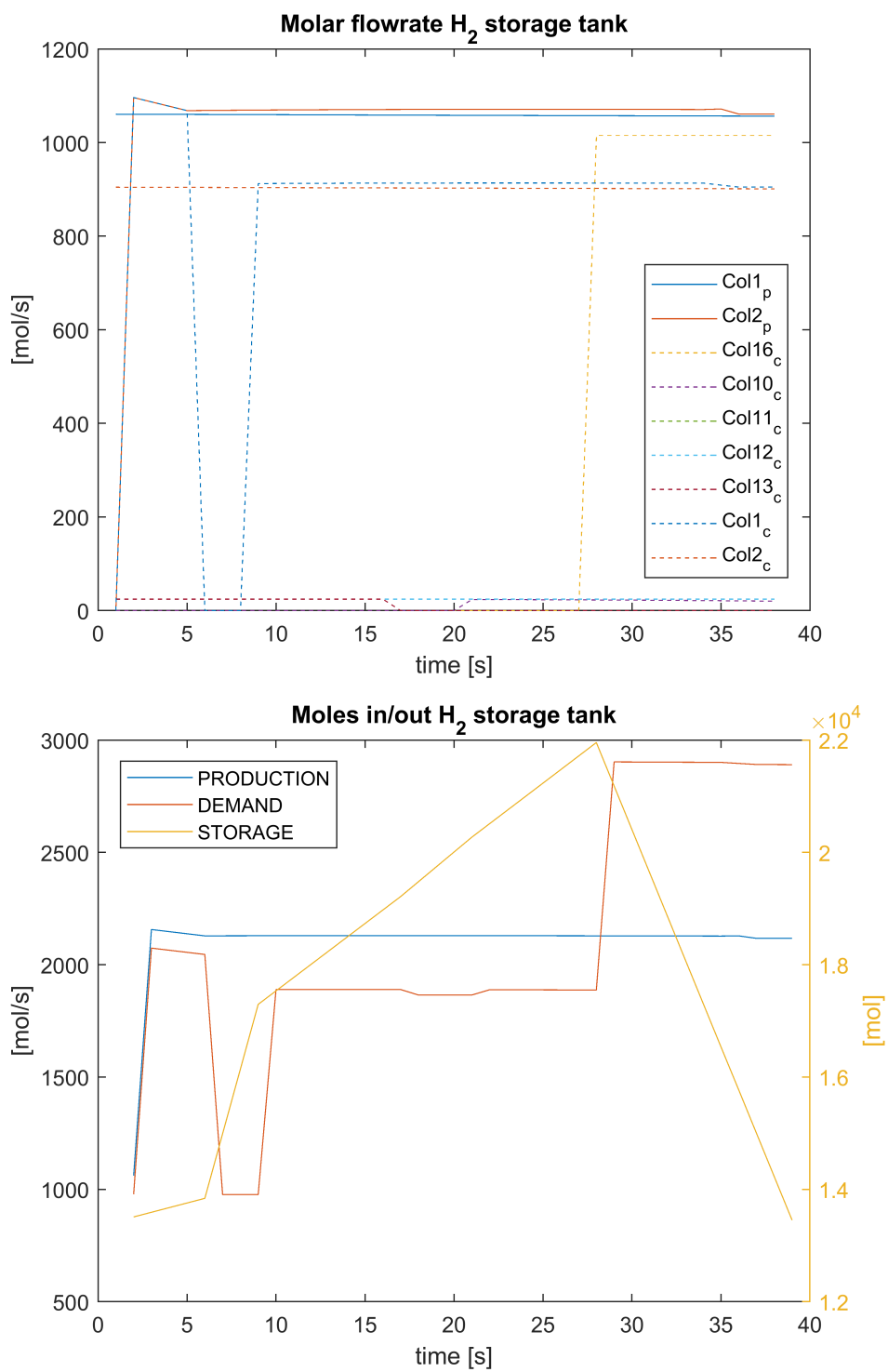


Figure 3.8: Molar flowrate inside the storage tank, case with 16 columns.

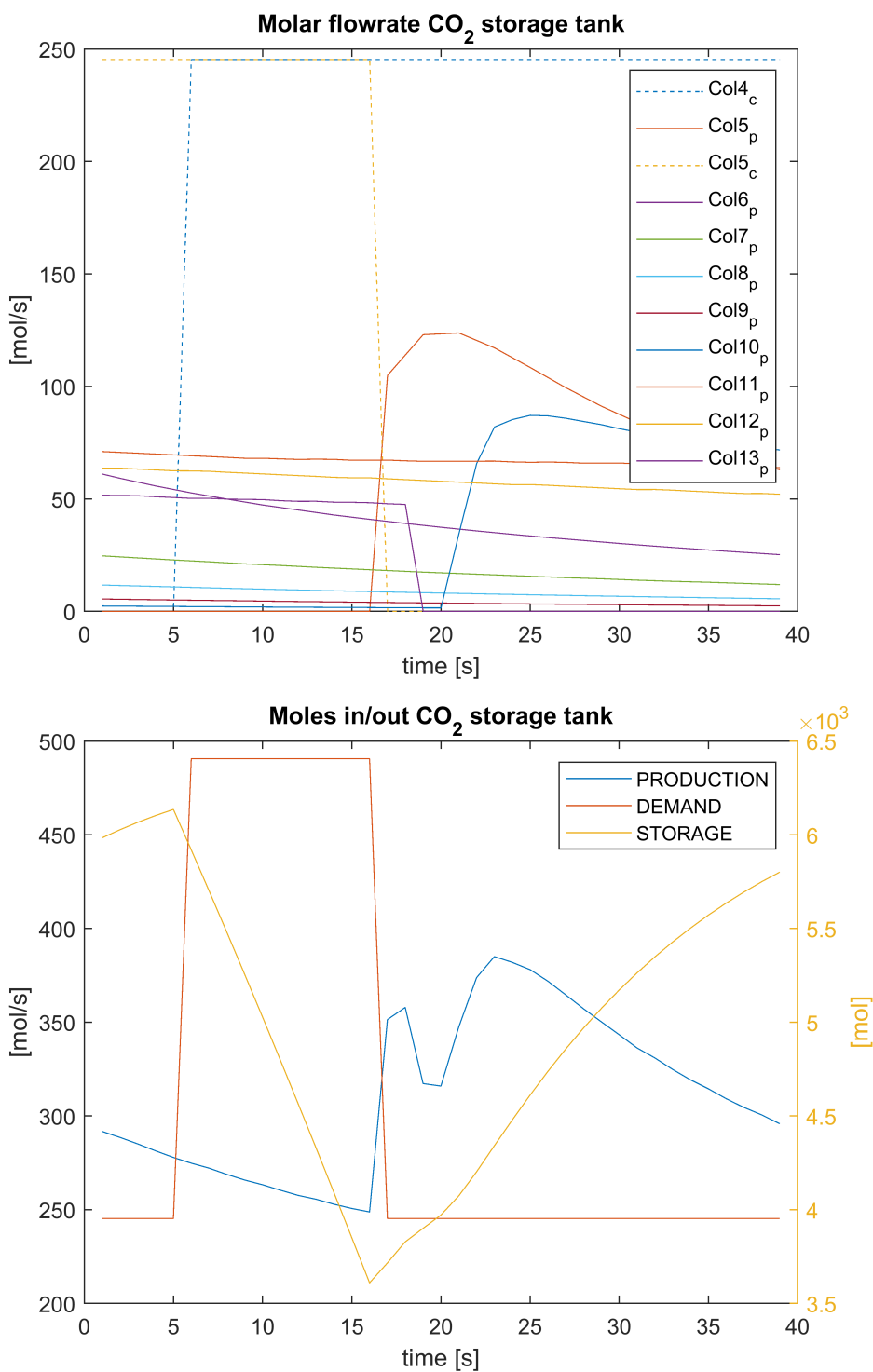


Figure 3.9: Number of moles inside the storage tank, case with 16 columns.

Table 3.4: Design of the two intermediate storage tanks, 10 columns scheduling.

Storage	Volume	Gauge pressure	Vacuum gauge pressure	MOT
-	m ³	kPa	kPa	°C
H ₂	16.47	3385.9	-	45
CO ₂	297.41	44.2	-31.9	222

Table 3.5: Design of the two intermediate storage tanks, 16 columns scheduling.

Storage	Volume	Gauge pressure	Vacuum gauge pressure	MOT
-	m ³	kPa	kPa	°C
H ₂	18.31	3323.4	-	45
CO ₂	193.69	35.0	-27.8	215

3.4 Waste buffer tank design

The design of the waste buffer is performed relying on information provided in the process flow diagram of the Shell Scotford Upgrader expansion 1 for hydrogen manufacturing within the Quest carbon capture and storage project [16].

For a 12 columns plant, a ratio of the volume of the waste tank over the volume of one adsorption column equal to 7.146 is presented. A proportion is applied to evaluate the tank volume for all the four cases, taking into consideration the difference in dimensions and amount of columns. The approach is not really precise but a scaling like this is a good first order approximation of the buffer tank size. The vessels' capacities are represented in Table 3.6:

Table 3.6: Design of the waste buffer tank.

Case	Volume	Gauge pressure	Vacuum gauge pressure	MOT
-	m ³	kPa	kPa	°C
A	607.29	36.5	-63.5	60
B	632.29	35.5	-64.5	60
C	771.28	48.7	-51.3	58
D	807.04	46.9	-53.0	58

3.5 Piping and valves system design

The process flow diagram depicted in Figure 3.3 becomes useful to understand the number of pipes and the corresponding amount of valves needed in the plant. It is worth noting that the number of pipes does not change from one configuration to another: in fact, such piping system is suitable for the matching of all the cycle steps, thus processing all the streams in compliance with the purity requirements. It is nevertheless necessary to properly adapt the dimensions of the connections and the number of valves to the flowrates and to the amount of columns respectively.

The P&ID of the adsorption column given by Aspen Capital Cost Estimator already involves the presence of five pipelines and their corresponding valve system. In Figure 3.10 the inlet and outlet lines related to the adsorption, namely the wet gas feed and the dry product gas lines, are already included; same accounts for the piping concerning the vacuum blowdown product (exhaust regenerant gas) and for the one associated to the hot regenerant gas entering the columns during the light purge. Furthermore, a line for the safety relief system is incorporated too.

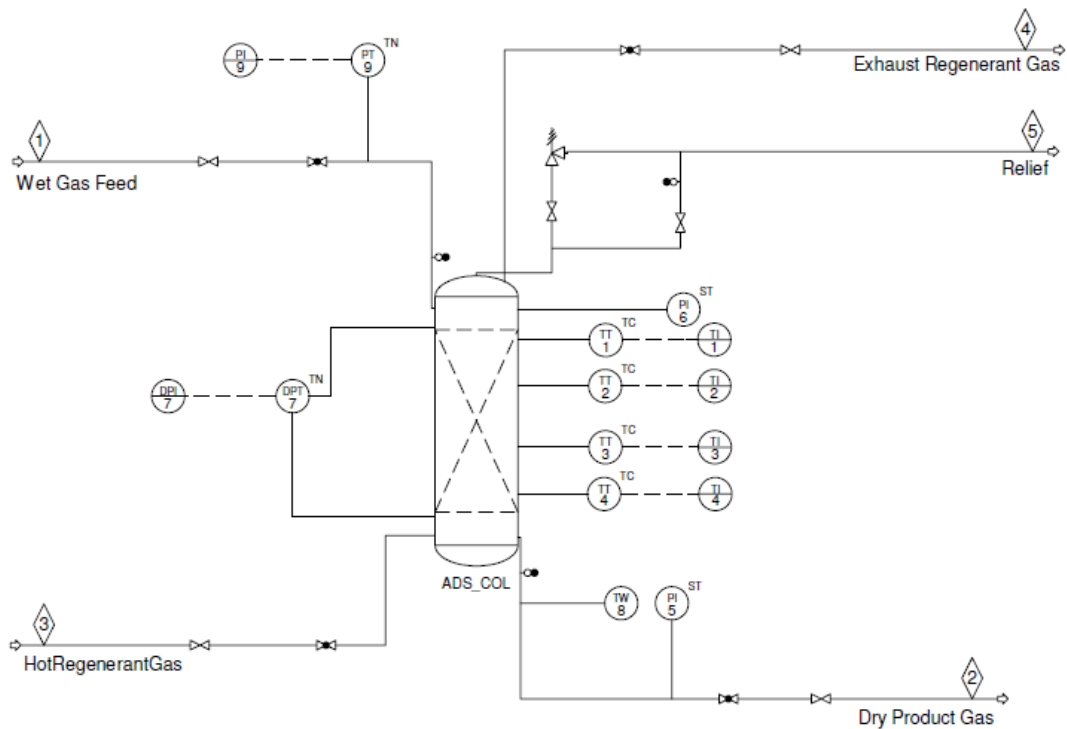


Figure 3.10: P&ID of one adsorption column.

Comparing the two graphs it is possible to spot that the missing connections are represented by:

- the inlet for the heavy purge step (HP in)
- the inlet for the pressurization step (Press in)
- the outlet for the tail gas exiting the intermediate blowdown and the heavy purge steps (Waste₁₊₂ out)
- two outlet lines for the streams coming out from the two light purges (LP₁ out and LP₂ out), which cannot merge within the same pipe due to purity reasons
- a pressure equalization line (PE), whose length will be approximately twice the length of the other pipes due to the fact that the columns need to be connected in a top-to-bottom configuration

The pipes' diameter is sized on the basis of the maximum flowrate passing through the cross section during the cycle evolution; this volumetric flowrate is taken from the simulations' output files and is increased by 20% to account for any possible deviation in pressure and temperature.

Concerning the lines' length, it is approximately evaluated considering that the distances between two columns of the same train and two columns of different trains are assumed to be equal to the column radius and to twice the column diameter respectively, as shown in Figure 3.11.

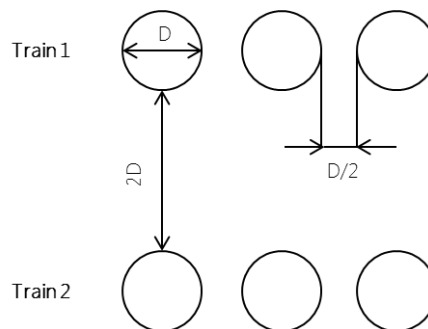


Figure 3.11: Columns and trains disposition top view.

The diameter of the lines is chosen by Aspen Capital Cost Estimator starting from the volumetric input values, which depend only from the considered schedule. Tables 3.7 and collect the design data of the missing piping system.

Table 3.7: Piping lengths (* "All pipes " includes all the listed lines except from the pressure equalization line)

Case	All pipes* length	PE line length
-	m	m
A	127.5	255
B	318.75	637.5
C	181.5	363
D	225.5	451

Table 3.8: Piping diameters.

Scheduling	HP in	LP ₁ out	LP ₂ out	Waste ₁₊₂ out	PE	Press in
-	m	m	m	m	m	m
10 columns	0.3	0.25	0.2	0.3	0.6	0.25
16 columns	0.45	0.35	0.2	0.35	0.6	0.25

Each line must present as many valves as the number of columns connected to it; this comes from the fact that when a column undergoes a specific step of the cycle, only one valve will open ensuring the flowing of the related stream while the others will shut to avoid the mixing of inflows/outflows with very different compositions. The type of valves, namely automatic ball valves, is dictated by the need of having one-way pressure driven valves to avoid backflow. Aspen Capital Cost Estimator already takes into account a bunch of valves governing the pipes included in the P&ID in Figure 3.10. Table 3.9 shows the amount of valves needed for the additional lines for each of the different configurations.

Table 3.9: Number of ball valves.

Case A	Case B	Case C	Case D
121	301	193	385

3.6 Vacuum pumps design

For purity reasons, a vacuum pump is provided for each of the streams exiting the column bottom end, namely the outflows of the vacuum blowdown and the two light purges. For the sake of simplicity, it is assumed that the fluid undergoes an isentropic process when flowing through the vacuum pump. Furthermore, a proportion is applied to estimate the actual mass flowrate accounting for the effect of the cycle schedule and for the number of trains.

$$\frac{\dot{m}_{H_2, \text{prod}, 1 \text{ column}}}{\dot{m}_{H_2, \text{prod}, N \text{ columns}}} = \frac{\dot{m}_{\text{tot}, \text{prod}, i, 1 \text{ column}}}{\dot{m}_{\text{tot}, \text{prod}, i, N \text{ columns}}}$$

Where \dot{m} is the actual mass flowrate, in kg/cycle, i is the considered step, N is the number of columns.

Since Aspen Capital Cost Estimator needs the flowrate expressed in m³/h as an input for the drive power, the evaluated mass flowrate is converted into volume flowrate by means of the density of the gas mixture.

Oil-sealed vacuum pumps seem to be the most suitable pumps for the plant, due to the need of processing very high actual flowrates and working at low ultimate pressure.

Table 3.10: Vacuum pumps design. (* This flowrate already includes a margin of 20%, as explained in the paragraph dedicated to overdesign and safety margins)

Line	Actual gas flowrate*	Drive power	Speed	Pumps
-	m ³ /h	kW	rpm	-
CASE A				
LP ₁	1106.84	18.5	1500	11
LP ₂	752.83	15	1500	1
BD _{vac}	1131.86	22	1500	32
CASE B				
LP ₁	1065.79	18.5	1500	12
LP ₂	733.99	15	1500	1
BD _{vac}	1131.75	22	1500	32
CASE C				
LP ₁	1084.29	22	1500	14
LP ₂	950.30	18.5	1500	1
BD _{vac}	1136.73	18.5	1500	40
CASE D				
LP ₁	1141.63	22	1500	14
LP ₂	917.23	18.5	1500	1
BD _{vac}	1131.48	18.5	1500	40

Chapter 4

Economic analysis of low TRL vacuum pressure swing adsorption technology based plant

Among a wide portfolio of carbon capture technologies, the investigated VPSA seems to be one of the most cutting-edge in terms of technical and environmental performances. Being in the very early stage of development and thus showing a technology readiness level (TRL) of 3-4, its economic performance is still affected by great uncertainties and to be meaningfully compared to an existing wide range of promising technologies it has to be projected to a future commercial stage.[17] A method is presented in this chapter to explain how technological development and deployment can be taken into consideration during an economic assessment. Well-known methods already exist for mature technologies, which are close to the market, and lean on a detailed process description based on mass and energy balances as well as an exhaustive list of equipment. Despite the readiness of these methodologies, they appear not to be suitable when dealing with feasibility studies on low TRLs projects thus leading to consistent uncertainties. The research work focuses on the capital cost estimate, whose core is represented by the evaluation of the investment cost of a Nth of a kind (NOAK) plant.

4.1 Exponent method versus factoring approach

Cost estimates can be splitted in two main categories, namely exponent methods and bottom-up methods. The former group gathers all the methodologies taking advantage of scaling exponents to reliably escalate the assessed cost for a reference equipment to the size of the same equipment in a new study. [17]

$$C = C_{ref} \left(\frac{Q}{Q_{ref}} \right)^n$$

Where C and C_{ref} , Q and Q_{ref} are the cost and the size of the equipment/plant in the new and the reference state respectively and n is the scaling factor. The lacking of information on reference plants is the reason why this method is not appropriate for emerging technologies, thereby bringing to the necessity of exploiting a bottom-up approach whose CAPEX evaluation is based on an accurate equipment list and on purchased equipment costs. The latter group is meant for early stage technologies that are far from commercialisation and whose level of design is simplified and approximate. In this case, the cost climbs over a period stretching from the lab stage (TRL 3-4) to the moment the first large demonstration plant (first of a kind, FOAK) is built (TRL 7-8).

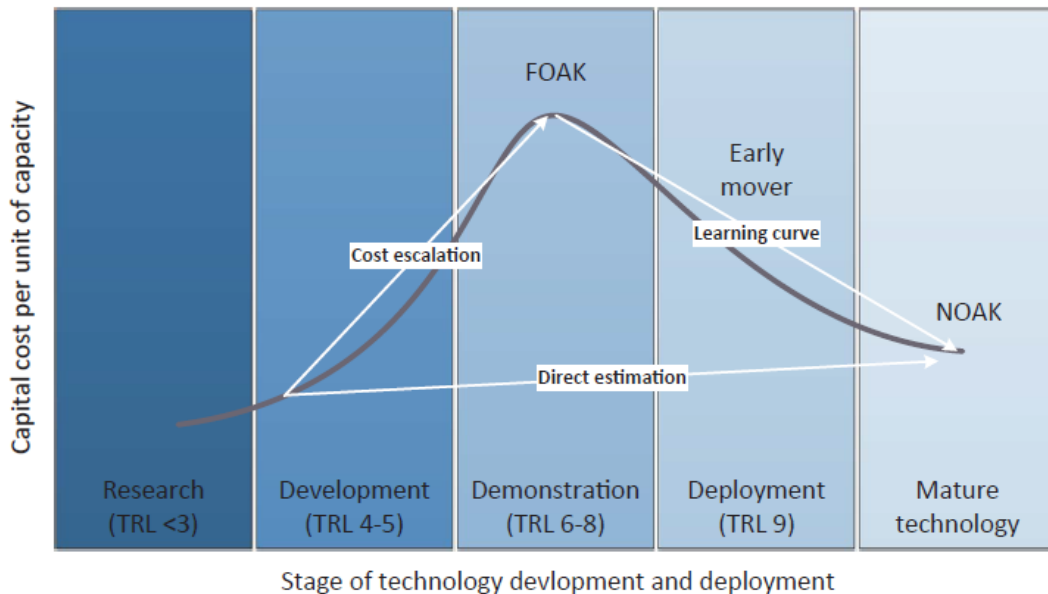


Figure 4.1: Typical capital cost trend of a new technology. White arrows show the direct and indirect/hybrid approaches to estimate the NOAK capital costs of a new technology.[18]

As depicted in Figure 4.1, as the technology development and therefore the detailing of the process increases, unforeseen difficulties can be brought up thus leading to the need of including specific and additional equipment, longer connections, safety systems and so on, thereby escalating the capital costs through the technology development cycle. This causes an increase of the capital cost of the technology. Once the first, large, commercial scale plant is built, the costs start falling due to reproduction and learning effects, until attaining a plateau representative of the NOAK plant's cost.

This indirect method was presented by Rubin [18] and it is articulated in three main steps:

- estimate of the preliminary equipment cost and of the engineering procurement and contracting (EPC) cost
- inclusion of process and project contingencies to arrive at the FOAK total plant cost (TPC)
- exploitation of learning curves to find the NOAK total plant cost

Differently from the direct method, which disregards the learning curve's effect, it accounts for unforeseen cost escalation during the technology scale-up over the several stages of its development, overtaking the challenges of early stages technologies.

4.2 Uncertainties in CCS cost estimate

Significant differences are encountered in technical literature concerning what should and should not be included in the cost estimate of carbon capture technologies. The work follows a clear approach explained by Rubin et al. , who highlight key methodological issues related to terminology, calculation procedures and items inclusion in reporting CCS costs. At the present time, inconsistencies can be highlighted in the way CCS costs are evaluated, to tackle this problem national and international companies and government agencies such as EPRI, DOE/NETL and IAEGHG International Energy Agency Greenhouse Gas Programme have developed guidelines for calculating plant-level capital costs, operational and maintenance (O&M) costs and cost of electricity (COE) and hydrogen (COH). [19] Notwithstanding the ingent amount of published economic estimates, it is worth noting that not many full-scale CCS integrated power plants have been built yet, thereby leading to the lack of public domain data on the actual cost.

Figure 4.2 schematically represents how the capital cost is generally built up. Five levels of cost can be defined, namely the Bare Erected Cost (BEC), the Engineering, Procurement and Construction Cost (EPCC), the Total Plant Cost (TPC), the Total Overnight Cost (TOC) and the Total As-Spent Capital (TASC).

The first item of the pyramid is an overnight cost including the cost of process equipment, on-site facilities and infrastructures needed to run the plant. It does not include EPC services yet and can be estimated using costing softwares, like for instance the Aspen Capital Cost Estimator. When contractor permits and construction management costs such as costs for engineering, procurement and contracting are added, the cost escalates to the level of the EPCC. TPC is obtained taking into account project and process contingencies and it is the starting

point for the evaluation of the final cost, which is not an overnight cost anymore but it considers the escalation in time of the capital expenditure.

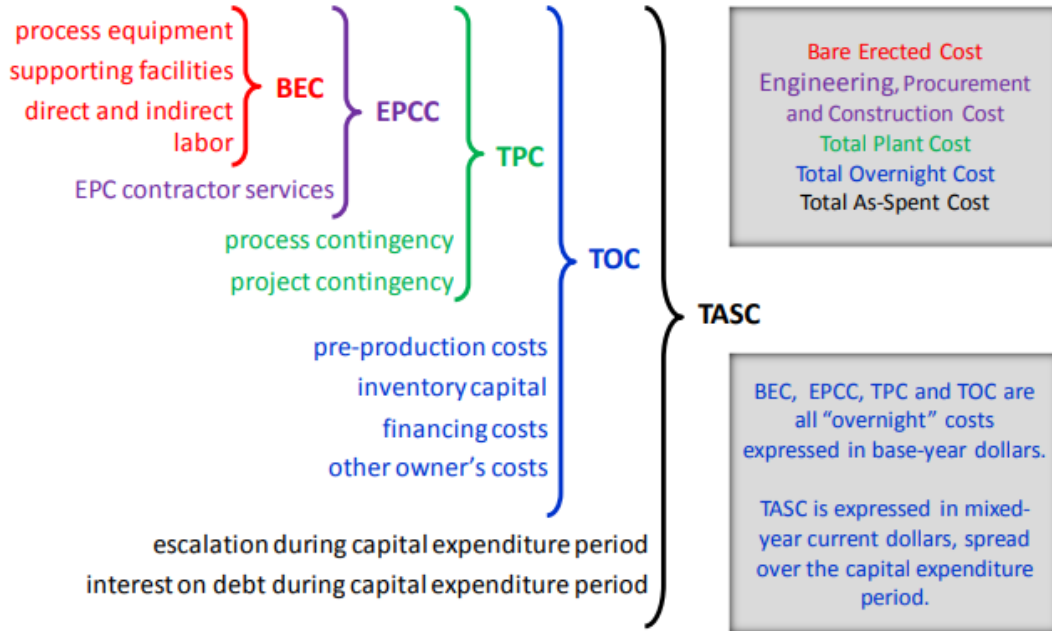


Figure 4.2: Capital cost estimate (CAPEX) levels and their elements.[21]

4.3 Cost estimate

The analysis is implemented on Aspen Capital Cost Estimator, which provides the cost of the process equipment (EC) including instrumentation, piping, civil, electrical items, insulation, structural steel and paint. For all the aforementioned items manpower cost is evaluated and added to the total material cost to reach the Bare Erected Cost (BEC), shown in Table 4.1. EPC contractor services are estimated to be 8 to 10% of BEC [21], a value of 9% is chosen to assess the Engineering, Procurement and Construction Cost of every component (Table 4.3).

$$EPCC = (1 + 0.09) \cdot BEC$$

Once the total EPCC is reached, process and project contingencies are added to scale the cost to the level of the Total Plant Cost. Process contingencies are defined as a percentage of the EPCC, for new concepts with limited data they contribute for more than 40% [21], therefore a value of 50% is used in the study.

Table 4.1: Bare erected cost.

Capture unit equipment	Case A	Case B	Case C	Case D
	kEur 2013	kEur 2013	kEur 2013	kEur 2013
Vessels				
Adsorber columns	14617	23228.8	20244.8	29703
H ₂ intermediate storage	294	294	335	335
CO ₂ intermediate storage	1187	1187	823	823
Waste buffer	1650	1686	1870	1928
Vacuum pumps				
LP ₁	1337	1422	1679	1738
LP ₂	103	103	103	103
BD _{vac}	3951	3951	4957	4939
Valves				
Ball valves	4356	10836	6948	13860
Piping				
HP _{in}	50	126	117	145
LP _{1, out}	40	139	109	135
LP _{2, out}	55	100	57	71
Press _{in}	39	98	56	69
Waste _{1+2, out}	50	126	79	98
PE	229	563	324	400
Total BEC	27951	43850	37707	54353

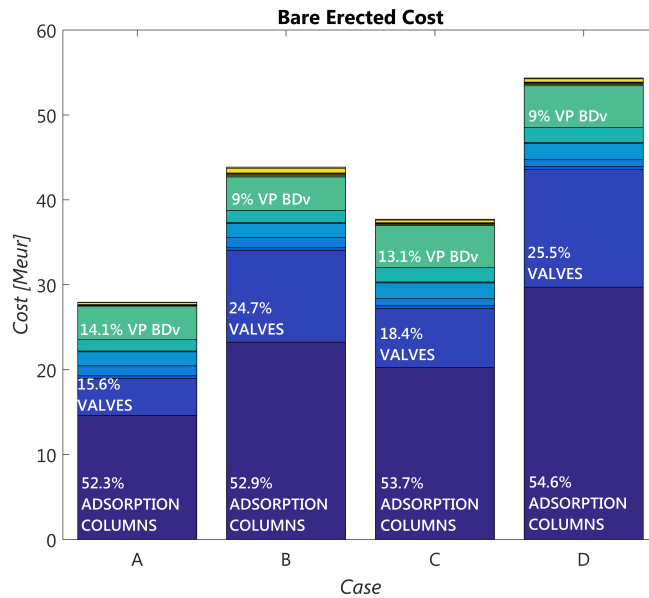


Figure 4.3: Bare erected cost composition.

Table 4.2: AACE Guidelines for process contingency. [21]

Technology status	Process contingency (% of associated process capital)
New concept with limited data	40+
Concept with bench-scale data	30-70
Small pilot plant data	20-35
Full-sized modules have been operated	5-20
Process is used commercially	0-10

Project contingencies are instead added to the total cost which includes already process contingencies and they appear to be 15 to 30% of it [21]; the highest value of the range is selected.

$$\text{TPC} = \text{EPCC} \cdot (1 + 0.5) \cdot (1 + 0.3)$$

Table 4.3: Engineering, procurement and construction cost.

Capture unit equipment	Case A	Case B	Case C	Case D
	kEur 2013	kEur 2013	kEur 2013	kEur 2013
Vessels				
Adsorber columns	15932	25319	22067	32377
H ₂ intermediate storage	320	320	366	366
CO ₂ intermediate storage	1294	1294	898	898
Waste buffer	1799	1838	2039	2101
Vacuum pumps				
LP ₁	1457	1550	1830	1895
LP ₂	103	102	120	117
BD _{vac}	4307	4307	5401	5383
Valves				
Ball valves	4748	11811	7573	15107
Piping				
HP _{in}	55	137	128	158
LP _{1, out}	43	151	118	147
LP _{2, out}	60	109	62	77
Press _{in}	43	107	61	76
Waste _{1+2, out}	55	137	86	107
PE	250	614	353	436
Total EPCC	30466	47796	41100	59245

The TPC obtained represents the cost of the FOAK plant and thus the peak of the learning curve of the considered VPSA based plant. With reference to Figure 4.3, it is clear that the most burdensome expenses are, as expected, the ones related to the adsorption columns and the annexed automatic control valves. The cost of the piping system is almost negligible compared to the evaluated total capital cost; same can be said concerning the cost of the hydrogen intermediate storage tank, due to the fact that it is kept at high pressure and at a temperature which is slightly greater than ambient, thereby leading to rather small dimensions. Concerning the tanks for the storage of carbon dioxide and wastes, they present a higher capital cost with respect to the H₂ tank due to size issues: their design gauge pressure is set close to 1 bar contributing to the need of bigger vessels. Moreover, the vacuum pumps accounts for 10 to 15% of the Bare Erected Cost; this originates from the necessity of having many of them to process large actual flowrates.

The second half of the curve, which goes from the FOAK to the NOAK plant, moving towards higher TRLs, can be drawn applying the following mathematical relation.

$$\text{TPC}_{\text{NOAK}} = \text{TPC}_{\text{FOAK}} \left(\frac{N_{\text{NOAK}}}{N_{\text{FOAK}}} \right)^b$$

Where:

- N is the number of installed plants (5 for the FOAK, 20 for the NOAK) [17]
- b is the learning rate coefficient, calculated from $\text{LR} = 1 - 2^b$
- LR is the learning rate, assumed to be 11% for hydrogen production from SMR [17]

The outcome of the economic assessment is summarized in Table 4.4.

Table 4.4: Learning curve key points.

Cost	Case A	Case B	Case C	Case D
Total EPCC (MEur 2013)	30.5	47.8	41.1	59.2
FOAK TPC (MEur 2013)	59.4	93.2	80.1	115.5
NOAK TPC (MEur 2013)	46.9	73.6	61.1	89.1

Figure 4.4 shows that the most competitive scenarios are represented by CASE A and CASE C, both characterized by a column length of 3.6 m. Although the VPSA units are designed to produce the same amount of hydrogen and carbon

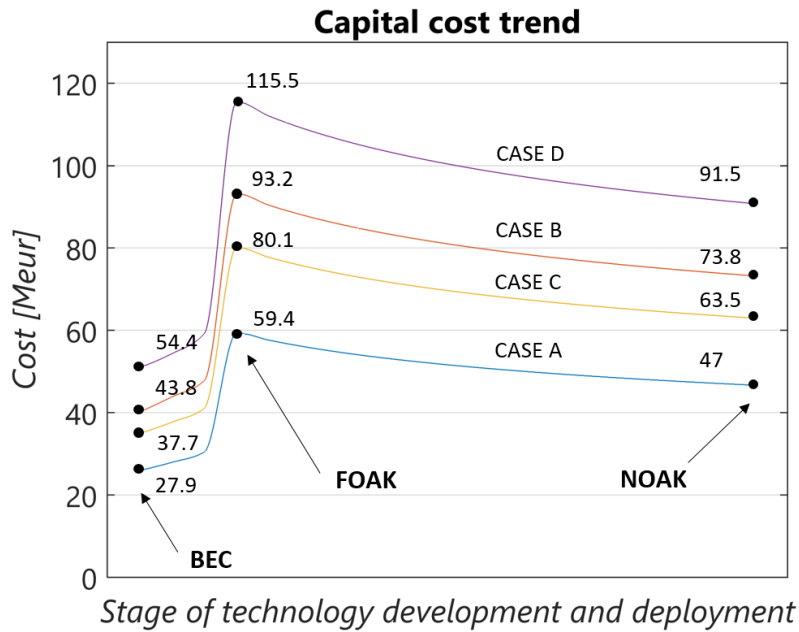


Figure 4.4: Capital cost trend from TRL 3-4 to TRL 8.

dioxide, the effect of a different scheduling must be taken into account when making a comparison. To select the most promising option an analysis on the volume of adsorbent and on the inlet flowrate should be performed.

Table 4.5: Adsorbent material and feed stream comparison.

		Case A	Case C
Adsorbent material	m ³ /column	37.46	29.74
	m ³ /plant	749.25	951.56
Fed syngas	Nm ³ /s	73.91	58.79
	Nm ³ /year	5.5 · 10 ⁵	4.37 · 10 ⁵

Table 4.5 clearly highlights the better efficiency of a 16-columns scheduling. However, to have a precise comparison of the two cases and to estimate the levelized cost of hydrogen (LCOH) and the cost of CO₂ avoided, the VPSA unit should be integrated in an energy production plant.

Chapter 5

Conclusions and outlooks

The project's goal is to understand how the technical and economic performance might progress from the lab stage to a future, commercial state for a vacuum pressure swing adsorption technology. To this end, the pivot of the research is represented by a deep investigation on the challenges of the technical scale-up of a pilot scale VPSA for the production of pure hydrogen and the separation of carbon dioxide within a single cycle.

It is evident that equilibrium theory provides a solid base for simple processes' scale-up, generating simple and useful constraints of fundamental importance for the derivation of the operating envelope.

Being the theoretical approach straightforward and simplified, a comparison with simulation results is made to estimate the reliability of the approach. A similar shape is spotted for the analytical and the modelled operating windows.

It is important to emphasize the importance of selecting a right linearization of the adsorption isotherm to derive a reasonable minimum column length; in fact, when a less effective linearization is chosen, unrealistic values of the adsorption bed length are found. Moreover higher recycle ratios lead to low purities due to heat effects within the column, reason why low productivities and recoveries are seen. This behavior shows a limitation of equilibrium theory that can be overcome by using an analogous method with the first principles software. In fact, when working far from idealities a remarkable rise in temperature is observed and it can be explained by the fact that convergence is reached at higher temperatures when applying simplified assumptions.

Concerning a simple Skarstrom cycle, the scale-up is performed successfully maintaining some dimensionless parameters ms , function of the length of the column, of the time of the steps and of the velocity of the feed stream, constant.

The method proposed by Rota and Wankat is meant for the intensification of processes and therefore it is not exactly suitable for the purpose since it implies a scale-out rather than a scale-up, nevertheless it becomes of crucial importance when more complex cycles are investigated and can be exploited to face pressure drop issues by means of changing the particles' size proportionally to the feed

flowrate.

A simple VPSA is studied as an intermediate step between the simple PSA and the complete VPSA and new constraints are derived based on the most critical steps of the cycle. Since carbon dioxide's purity must be ensured too, the new operating envelope appears to be three-dimensional instead of two-dimensional. Similar functional windows are encountered for simple and full VPSA cycles, whose scale-up undergoes the same approach already adopted for the Skarstrom cycle. As can be logically explained, longer adsorption times lead to opposite hydrogen and carbon dioxide's purity trends; on the one hand H₂ productivity is strongly affected by the time of the feed step and by the light purge recycle ratio, on the other hand CO₂ productivity is consistently influenced by the heavy reflux. The optimal operating point appears to be characterized by as long as possible adsorption times and very little recycle ratios; a previously performed optimization allows for the selection of the most promising point which the scale-up method is applied to.

Very different profiles in concentrations and pressures are encountered when the simple approach is used, demonstrating that the proposed equilibrium theory based method is not sufficient with more complex cycles. These results show that the method used for a simple PSA process presents a clear limitation: when a vacuum step is included in the cycle, the equilibrium theory analogue no longer holds because it neglects issues of pressure drop. Therefore the evacuation pressures are no longer reached when the column is scaled up. Additional modifications are required to bring the technical performance of taller columns to that of the lab scale column, including the use of larger particles to reduce pressure drop issues and the use of longer evacuation steps.

A good design is the link to an accurate cost estimate, therefore process equipment must be precisely listed and sized to guarantee a reliable economic assessment. Once all the plant components' characteristics are defined, an indirect method is applied to evaluate the progression of the capital cost. The reason why a hybrid method is chosen is that it is specifically suitable for low TRL technologies, leaning on a bottom-up approach.

The analysis clearly shows that longer columns can accommodate higher flowrates and are at the same time more competitive from an economic point of view. Once the optimal length is selected, a 16-columns schedule might be preferred to a 10-columns one; in fact, despite showing a higher amount of adsorbent material, it requires a smaller amount of syngas to produce the same quantity of hydrogen due to higher separation efficiencies. Therefore, it might be of great interest to broaden the research integrating the VPSA unit within a more extended hydrogen plant and evaluating the weight which operational costs have on the overall economic estimate. Moreover, the same work could be performed with several other different adsorbent materials to have a clear understanding of which, among all the possible solutions, can be the most interesting and marketable one in terms of technical and economic performances.

Bibliography

- [1] IPCC, 2018: Summary for Policymakers. In: *Global Warming of 1.5 °C. An IPCC Special Report on the impacts of global warming of 1.5 °C above pre-industrial levels and related global greenhouse gas emission pathways, in the context of strengthening the global response to the threat of climate change, sustainable development, and efforts to eradicate poverty* [Masson Delmotte, V., P. Zhai, H. O. Pörtner, D. Roberts, J. Skea, P.R. Shukla, A. Pirani, W. Moufouma Okia, C. Péan, R. Pidcock, S. Connors, J.B.R. Matthews, Y. Chen, X. Zhou, M.I. Gomis, E. Lonnoy, Maycock, M. Tignor, and T. Waterfield (eds.)]. *World Meteorological Organization, Geneva, Switzerland, 32 pp.*
- [2] IPCC, 2014: *Climate Change 2014: Synthesis Report. Contribution of Working Groups I, II and III to the Fifth Assessment Report of the Intergovernmental Panel on Climate Change* [Core Writing Team, R.K. Pachauri and L.A. Meyer (eds.)]. IPCC, Geneva, Switzerland, 151 pp.
- [3] N. Casas, J. Schell, L. Joss and M. Mazzotti, "A parametric study of a PSA process for pre-combustion CO₂ capture", *Separation and Purification Technology*, vol. 104, pp. 183-192, Feb. 2013.
- [4] <https://www.sintef.no/projectweb/elegancy/>
- [5] A. Streb, "Low Carbon Hydrogen Production with VPSA for H₂/CO₂ Separation", GHGT-14 Conference.
- [6] A. Streb, M. van der Spek, M. Gazzani, D. Sutter, C. Antonini and M. Mazzotti, D1.1.1 "Report on new PSA and VPSA cycles for sharp separation of CO₂, H₂ and impurities", WP1-H₂ supply chain and H₂-CO₂ separation, ETHZ, Aug. 2018.
- [7] C. Antonini, M. van der Spek, D. Sutter, A. Streb, M. Gazzani and M. Mazzotti, D1.3.1 "Report on optimal plants for production of low-carbon H₂ with state-of-the-art technologies", WP1, WP5, ETHZ, Aug. 2018.
- [8] M. Mazzotti, HS 2018, "Rate Controlled Separations in Fine Chemistry", Institute of Process Engineering, ETH Zurich.

- [9] R. Rota, P. C. Wankat, "Intensification of Pressure Swing Adsorption Processes", *AIChE Journal*, vol. 36, no. 9, pp. 1299-1312, Sep. 1990.
- [10] Y. Park, Y. Ju, D. Park, C. Lee, "Adsorption equilibria and kinetics of six pure gases on pelletized zeolite 13X up to 1.0 MPa: CO₂, CO, N₂, CH₄, Ar and H₂", *J. Chem. Eng.*, vol. 292, pp. 348-365, Feb. 2016.
- [11] Y.-J. Park, S.-J. Lee, J.-H. Moon, D.-K. Choi, C.-H. Lee, "Adsorption equilibria of O₂, N₂, and Ar on carbon molecular sieve and zeolites 10X, 13X, and LiX", *J. Chem. Eng., Data* 51 (2006) 1001–1008.
- [12] Y. Wang, M.D. LeVan, "Adsorption equilibrium of carbon dioxide and water vapor on zeolites 5A and 13X and silica gel: pure components", *J. Chem. Eng., Data* 54 (2009) 2839–2844.
- [13] S. Cavenati, C.A. Grande, A.E. Rodrigues, "Adsorption equilibrium of methane, carbon dioxide, and nitrogen on zeolite 13X at high pressures", *J. Chem. Eng., Data* 49 (2004) 1095–1101.
- [14] IEAGHG R&D Programme, IEAGHG Technical Report, "Techno-Economic Evaluation of SMR Based Standalone (Merchant) Plant with CCS", February, 2017.
- [15] Chemical Engineering Design, Second Edition. DOI: 10.1016/B978-0-08-096659-5.00016-X © 2013 Elsevier Ltd.
- [16] Quest Carbon Capture and Storage Project, Process Flow Diagram Scotford Upgrader Expansion 1, Hydrogen manufacturing- unit 443, H₂ purification.
- [17] M. van der Spek, A. Ramirez, A. Faaij, "Challenges and uncertainties of ex ante techno-economic analysis of low TRL CO₂ capture technology: Lessons from a case study of an NGCC with exhaust gas recycle and electric swing adsorption", *Applied Energy*, vol. 2018, pp.920-934, Sep. 2017.
- [18] E. S. Rubin, "Seven simple steps to improve cost estimates for advanced carbon capture technologies", Presentation to the DOE transformational carbon capture technology workshop. Pittsburgh, Pa: DOE NETL; 2014.
- [19] E. S. Rubin, "Understanding the pitfalls of CCS cost estimates", *International Journal of Greenhouse Gas Control*, vol. 10, pp.181-190, Jul. 2012.
- [20] E. S. Rubin, C. Short, G. Booras, J. Davison, C. Ekstrom, M. Matuszewski, S. McCoy, "A proposed methodology for CO₂ capture and storage cost estimates", *International Journal of Greenhouse Gas Control*, vol. 17, pp.488-503, Jul. 2013.

- [21] NETL, "*Quality guidelines for energy system studies- Cost estimation methodology for NETL asesments of power plant perormance*" , DOE-NETL, Apr 2011.